Multi-tank Hybrid Energy Storage Using Water and Phase Change Materials in a Direct System

Multi-tank Hybrid Energy Storage Using Water and Phase Change Materials in a Direct System

By

Hebat-Allah Teamah, M.A.Sc., B.Sc., Mechanical Engineering

Alexandria University

A thesis submitted to the

Department of Mechanical Engineering

in partial fulfillment of the requirements for the degree of

Doctor of Philosophy in

Mechanical Engineering

Department of Mechanical Engineering

McMaster University

Hamilton, Ontario, Canada

November, 2017

The undersigned hereby recommends to the

Faculty of Graduate and Postdoctoral Affairs

acceptance of the thesis

Multi-tank Hybrid Energy Storage Using Water and Phase Change Materials in a Direct System

Submitted by **Hebat-Allah Teamah, B.A.Sc., M.A.Sc., Mechanical Engineering**

Alexandria University

in partial fulfillment of the requirements for the degree of

Doctor of Philosophy in

Mechanical Engineering

DOCTOR OF PHILOSOPHY (2017)

MCMASTER UNIVERSITY

MECHANICAL ENGINEERING

HAMILTON, ONTARIO

TITLE: **Multi-tank Hybrid Energy Storage Using Water and Phase Change Materials in a Direct System**

AUTHOR: Hebat-Allah Teamah

SUPERVISOR: Professor\ Marilyn Lightstone

Department of Mechanical Engineering

SUPERVISOR: Professor\ James Cotton

Department of Mechanical Engineering

Number of Pages xxi,

Dr. Marilyn F. Lightstone, Supervisor

Dr. James S. Cotton, Co-supervisor

Dr., Examiner

Dr., Examiner

Department of Mechanical Engineering

McMaster University

October, 2017

Abstract

Novel multi-tank thermal energy storage (TES) containing water and phase change materials (PCMs) was evaluated numerically. The multi-tank storage is based on the interconnection of small volume hot water storage tanks in series configuration. Water enters and exits the system directly and is used as the heat transfer fluid (HTF). PCMs are incorporated in the water tanks to investigate their latent energy storage capability. They are cascaded in a descending order of their melt temperatures to match the operating range of the system. The system was tested for the typical Canadian weather data and demand profiles.

An in-house FORTRAN code was developed to solve the problem computationally. PCMs are placed in vertical cylinders and water flows along them within the tank shell. This is referred to as a hybrid system hereafter. Both component and system level analysis are presented in detail in the thesis. The developed mechanistic model was thoroughly validated and verified with published data with a very good agreement (<5% deviation). The main goal of the current work is to assess the dynamic performance of the proposed system when linked with the solar collector in the Solar Domestic Hot Water system (SDHW) context. Possible storage volume reduction relative to a water only system for the same benefit to the household is the primary objective.

Component level analysis was conducted to understand the behavior of the hybrid system under isothermal charging conditions. It aided in the choice of key parameters when the entire system was modeled. The analysis shows that in narrow temperature operating ranges (around 10^{o}C); the energy density of the hybrid system can be significantly increased to around five times relative to a system containing water only. This is attributed to the latent energy stored during the phase change. The main hindering factor is the low thermal conductivity of the PCM, which can be overcome by encapsulating the materail in small diameter cylinders and thus decrease the imposed thermal resistance on the system.

On the system level, a hybrid single tank model was linked with the collector performance and the system was tested for typical days of Canadian weather with different demand profiles. The solar fraction of the hybrid system was compared to that of an identical system using water-only as the thermal storage medium. Solar fraction is the amount of energy delivered by the solar system relative to the total energy required by the load. The systems approach is critical since it allows for the coupled effects of SDHW components to be incorporated. The analysis clearly shows that incorporation of PCMs into the thermal storage results in enhanced solar fraction at small tank volumes (around 200 liters). In contrast, as the tank volume is increased, the benefit of the PCMs diminishes. An energy balance of the system reveals that, the benefits of the PCMs in small storage volumes are due to the reduction in the collector fluid inlet temperature which increases the pump run time and thus the solar energy collected. This conclusion

presented a clarification for the mixed results from the literature concerned with the incorporation of PCMs in hot water tanks.

Using the key parameters of the system level analysis for the single tank, the analysis was extended to the multi-tank system. The multi-tanks contain PCMs cascaded in a descending order of their melt temperature from the source to the load. The PCM was found to tune the bulk of the tank temperature around its melting temperature. This aided in having better sequential stratification between the tanks. Cooler water returning to collector relative to the single PCM case was maintained. Decreased collector losses and extended the pump activation time were obtained relative to the single PCM case. This resulted in an increase in the time period on the system was able to meet the load demand of hot water and hence augmented solar fraction. It was found that for a multi-residential building of three families, a 630 liter tank containing water only gives the same solar fraction provided by three cascaded 100 liters tank containing 50% PCMs by volume. The melting points of PCMs are (42^{o}C, 32^{o}C and 16^{o}C) respectively. This guarantees more than 50% reduction in volume for the same benefit in the household side.

Dedication

This Thesis is dedicated to the following special people in my life:

To my late mother Esmat Mohamed, Mum, I wish you were here to be proud of your daughter. I miss you each and every day but your endless love, patience and the good you instilled in me continue to bless my life.

To my father Mohamed Teamah, Dad, you gave me the most precious feeling in the world, you BELIEVED in me. You are always my inspiration despite the long distance. You are a great example of hard work, patience and kindness above all. I am truly indebted to you and mum for who I am today.

My sister, Asmaa, I loved texting you across that long distance. My brother, Ahmed, I used to miss arguing with you throughout this period. The apple of my eye, my youngest brother, Abdelfatah, you are ardently loved and missed.

Love You!!

ACKNOWLEDGEMENTS

I would like to express my gratitude towards my supervisors; Dr Lightstone and Dr Cotton. No words can describe my gratitude towards Dr Lightstone. I learned a lot from her extra-ordinary nice personality. Being an extremely modest and extremely talented person at the same time was always impressive to me. Her critical organized way of thinking and revision throughout this program was the key of having the work in the present form. Simply, she is an inspiration to women in engineering. Dr Cotton is a great leader of the Thermal Management Research Lab (TMRL). His suggestions and fruitful discussions were a motivation throughout the course of this work. Being active and always energetic is one of the main things which I learned from him. I am also grateful to my supervisory committee members, Dr Hamed and Dr Ching for their suggestions and comments during our annual meetings, and the precious material I learned when I attended their courses.

I would like to extend my thanks to the members of our TMRL group. They offered lots of helpful comments throughout our meetings. I also thank my present and past colleagues in JHE-215 for their continuous support. I would like to extend my thanks to Florence, Lily and Vania.

My accomplishment wouldn't have been possible without the support and love of my friends. Special thanks is given to my beloved friend and roommate; Reem Zeitoun.

Without her, my stay in Canada would have been impossible. Her jokes and hangouts were always a motivation to keep working well. She is more than a sister. I would like to extend my thanks to Norhan el Saadaway and Aunt Amany Ramzy, It was a blessing for us to have such lovely neighbours. The times we spent together are priceless. Thank you all for giving me the feeling of being at home despite this long distance. A very special thank is given to Dr Alaa Hassan and his family for all what they did to help me especially in the beginning. I don't want to forget anyone who offered me help or welcoming one day. You are all amazing. Lastly, I would like to thank my lifetime friends; Hagar Hamdy and Aya Kassab. Although we don't see each other that much now; your messages, face book wall posts and calls brighten my day. Our undergraduate years' memories are still in my mind as if it was yesterday. Thanks Dalia, Yosra, Menna, Ola, Yassmine, and Alaa for always supporting and motivating me during that entire period.

Finally, thanks my fiancée Mostafa for being in my life recently. May Allah grant us a blessed life ahead.

Table of Contents

LIST OF FIGURES

Appendix B

LIST OF TABLES

Chapter 3:

Chapter 4:

Chapter 5:

Appendix A:

Appendix B:

Nomenclature

Symbols	Definition	Units
A_c	Collector surface area	m^2
C_{pl}	PCM liquid specific heat capacity	J/kg K
C_{ps}	PCM solid specific heat capacity	J/kg K
D	PCM cylinder outer diameter	m
D_h	Hydraulic diameter	m
E	Energy stored	J
$E_{delivered}$	Energy delivered to the load	J
$E_{loss, coll}$	Collector energy loss	J
$E_{loss, tank}$	Tank energy loss	J
E_{mains}	Mains water energy	J
E_{solar}	Solar energy incident to the collector	J
Fo	Fourier number	
F_R	Heat removal factor	
f_s	Solar fraction	

$F_{s,annual}$	Annual solar fraction	
G	Solar irradiation	W/m^2
K	Thermal conductivity W/mK	W/mK
L_c	Length of cylinder	m
$\dot{m}$	Mass flow rate inlet to the tank	kg/s
N_c	Number of cylinders in the tank	
Nu_c	Nusselt number based on hydraulic diameter	
Nu_p	Nusselt number based on Dittus-Boelter correlation	
Q_u	Collector useful heat gain	kW
$R_{c,inn}$	Inner radius of phase change material cylinder	m
$R_{c,out}$	Outer radius of phase change material cylinder	m
Re_c	Reynolds number based on hydraulic diameter	
r_s	Latent heat of fusion	kJ/kg
$\widetilde{Ste}$	Stephan number	
T	Temperature	^oC
T_{amb}	Ambient temperature	^oC

T_{in}	Temperature of incoming fluid	^{o}C
T_m	Melting temperature of PCM	^{o}C
T_{st}	Initial temperature of the tank	^{o}C
$U_{f,mean}$	Mean fluid velocity	m/s
U_L	Collector loss coefficient	W/m^2K
V_{tank}	Tank volume	m^3
ΔF_o	Fourier number	
Δt	Time step	seconds

Latin Symbols

Symbols	Definition	Units
θ	Dimensionless temperature	
μ	Dynamic viscosity	Ns/m^2
ρ	Density	kg/m^3
φ	PCM packing ratio	
$(\tau\alpha)$	Transmittance absorbance product	
η	Solar collector efficiency	

Abbreviations

Symbols	Definition
HTF	Heat transfer fluid
LES	Latent energy storage
PCM	Phase change material
SDHW	Solar domestic hot water
SES	Sensible energy storage
TES	Thermal energy storage

Subscripts

Symbols	Definition
c,inn	Inner surface of cylinder
c,out	Outer surface of cylinder
conv	Convective
eff	Effective
f	Fluid
f,m	Mean for fluid

In	Inlet

CHAPTER 1 Introduction

1.1. The Importance of Thermal Energy Storage

Building energy use in the residential sector currently accounts for 17% of Canada's secondary energy consumption. Secondary energy is defined as the total amount of energy consumed by an end-use, and excludes the energy consumed to convert the energy into a useable form from its primary resource. The breakdown by end-use within the residential sector shows that water and space heating accounts for 80% of the total in that sector. For these two end-uses in Canada, heating is mainly provided by either electricity or natural gas. Reduction in the dependence on fossil fuels has become a must (NRCan 2012). Other relevant yet critical issues are the climate changes and the global warming problems associated with fossil fuel consumption. Residential GHG emissions from space and water heating alone amounted to 54.4 Mt of CO2 in 2009, which is comparable to the 43.3 Mt of CO2 produced by passenger cars in Canada that same year (NRCan 2012). There is thus a need to find alternative renewable resources; one of them is making use of solar radiation to heat water directly and on-site.

Solar energy is characterized by its intermittent nature owing to the day-night cycle and seasonal variation. An idealized solar irradiance with storage over a hypothetical 3-day period shown in Figure 1.1 (Duffie and Beckman 2006). As indicated by the vertical shaded area, the collector useful gain exceeds the load on the 1st and 3rd days. This excess energy is held in the storage subsystem for use at later time. When required, the excess energy is withdrawn from the storage to meet the load (as represented by the horizontal shaded area). If there is not sufficient thermal energy in the storage, the load is met by an auxiliary heater. Proper sizing of the components is critical for minimizing the auxiliary heating.

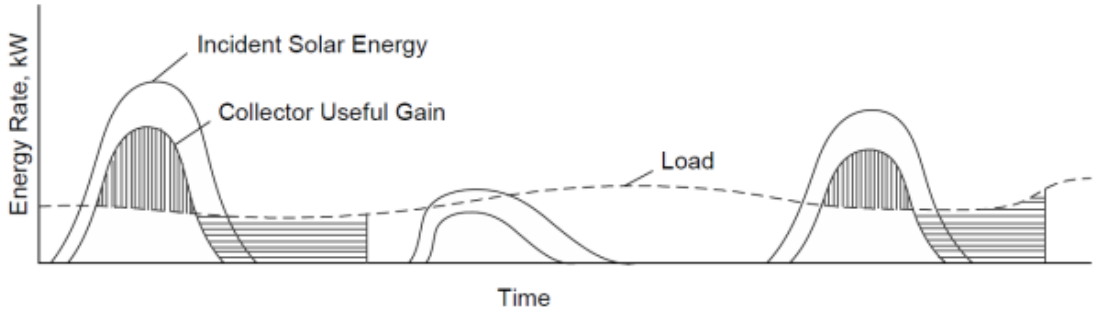

Figure 1.1: Application of thermal storage in a solar heating system (Duffie and Beckman 2006).

Numerous factors influence the proper sizing of a thermal storage including: the time of availability of solar energy; the temperature set point on the load side and the magnitude and distribution of the load throughout the period of interest; the charging and discharging periods; the spatial limitation for the placement of the storage.

Seasonal storage systems are designed to collect solar energy during the summer months and retain the heat in the storage for use during the winter months. They are characterized by their large storage capacity (hundred times the capacity of a daily storage), and much higher costs (Dincer and Rosen, 2002). Seasonal thermal storage systems may take on several physical configurations including underground aquifers or large pools or bore-hole buried earth storage. Large scale thermal storage of this type is not the focus of the current study.

Diurnal or short-term storage is often more suitable for small-scale domestic applications. It is designed to store heat for up to a few days and generally consists of smaller devices that can be installed easily within a building. It typically supplies no more than 70% of the hot water demand of the household (Dincer and Rosen, 2002). Short term storage is the focus of the current work. The considered solar domestic hot water system is described in detail in the following subsection.

1.2. Solar Domestic Hot Water (SDHW) system;

A typical SDHW system consists of one or more tanks, a charging circuit, and a discharging circuit. The heat transfer fluid (HTF) transfers the energy from the source to the storage tank when the supply is available. It carries energy from the tank to the load when there is an energy demand. A typical SDHW system is shown in Figure 1.2. In the charging mode, hot fluid is introduced to the top of the tank and cold fluid is extracted

from the tank bottom. When discharging is activated, the inverse situation takes place. Cold water enters the tank bottom whereas hot water leaves the top to meet the load. When the fluid layers are arranged in a descending order of their temperature, the tank is said to be stratified. Stratification enhances the efficiency of thermal energy storage (TES). It enhances the performance of the collector when cooler water is sent to it. It also ensures that hottest water will be directed to meet the load which minimizes the auxiliary heat required to bring water to its desired set point. As such, it is highly desirable to develop storage systems that promote high levels of thermal stratification. Figure 1.3 shows three different stratification levels within the tank. The left figure shows a highly stratified case where the thickness of thermocline (where the temperature gradient occurs) is small. The middle figure shows a moderately stratified tank where the thermocline region stretches. The last one is the fully mixed tank where the whole body of water is at the same temperature. A number of parameters affect the degree of stratification in a storage tank. These include the volume and configuration of the tank, the size, location and design of the inlets and outlets, the flow rates of the entering and exiting streams, and the duration of the charging, storing and discharging periods. In addition, there are four primary factors contributing to destratification, including: heat losses to the surroundings, heat conduction between hot and cold regions of stored fluid, conduction along the tank wall, and mixing during charging and discharging periods (Lavan and Thompson 1977, Phillips and Dave 1982, Hollands and Lightstone 1989, Cristofari et al. 2003).

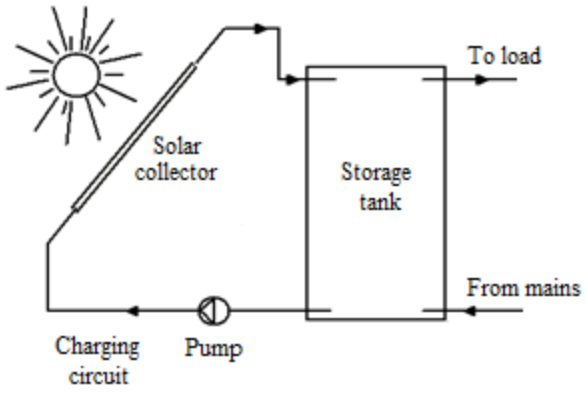

Figure 1.2: sketch of a typical solar energy storage system

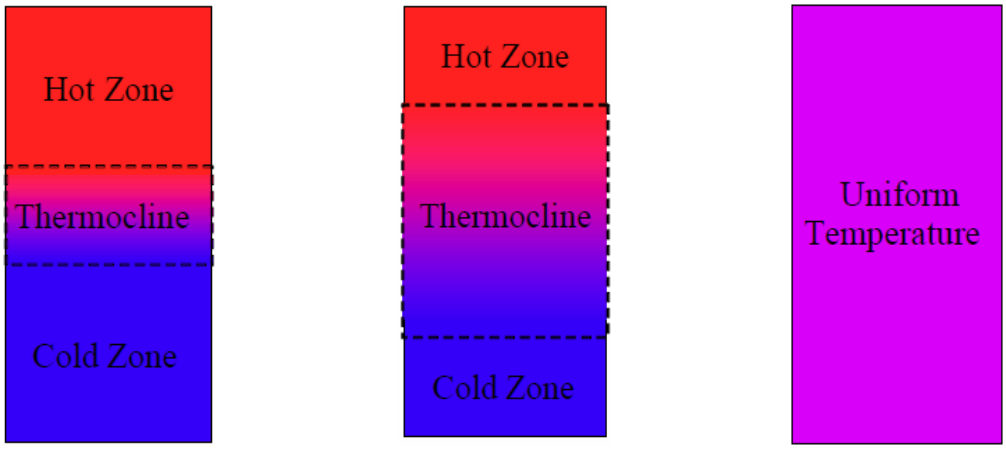

Figure 1.3: Differing levels of stratification within a storage tank (a) highly stratified, (b) moderately stratified and (c) fully mixed storage.

Thermal energy storage systems can either be open-loop or closed loop. With open loop direct storage, the heat transfer fluid (HTF) is the same as the storage media. In contrast

with the closed loop storage, a heat exchanger is employed and HTF may have a different composition from the thermal storage medium. The indirect systems are used when the corrosion of the tank is a concern or when antifreeze is used as the collector heat transfer fluid. Natural convection is their dominant mode of heat transfer which limits their heat transfer rate compared to the open loop direct storage. Figure 1.4 shows the different possible configurations of the system. Figure 1.4(a) and Figure 1.4(b) shows direct charging and indirect charging through the storage tank respectively. When antifreeze separate loop is required in colder climates, the direct and indirect charging modes are shown in figures 1.4(c) and 1.4(d).

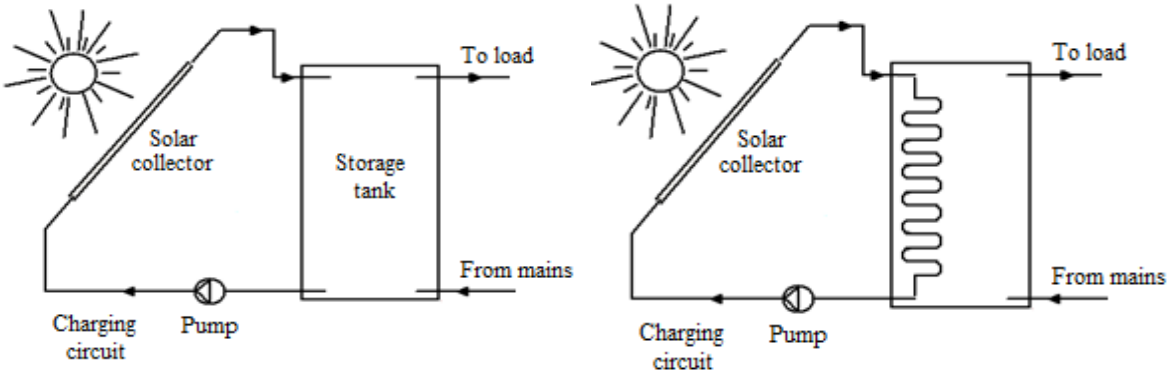

a) Direct charging b) Indirect charging

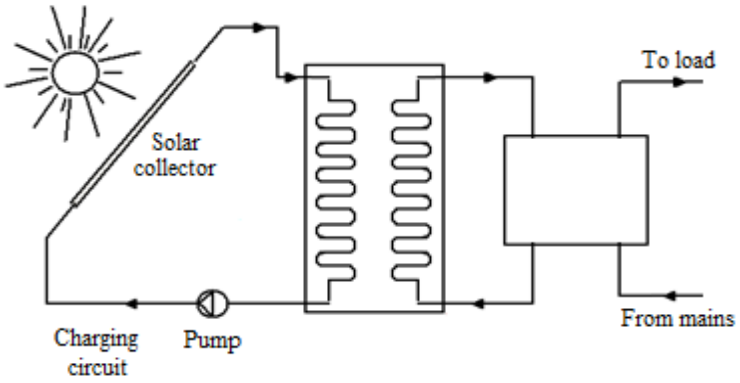

c) Direct charging with antifreeze loop

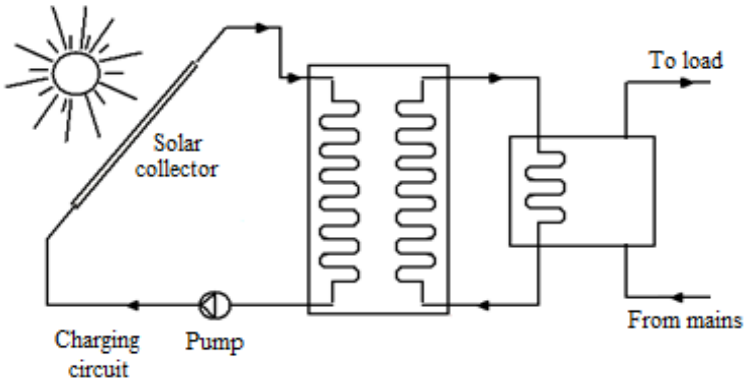

d) Indirect charging with antifreeze loop

Figure 1.4: Different configurations for the charging modes

Storage systems are classified to passive systems and active ones. The passive systems, commonly called thermosyphon systems, use the principal that hotter less dense water rises naturally. Consequently, the storage tank is located above the heat source. Thermosyphon systems are widely used in warm climates and are particularly popular where low cost is important and reliable external power is not available. The active system uses a pump to circulate the heat transfer fluid from the collector to the storage tank. This allows the storage tank to be installed indoors in a heated space (i.e., reducing standby heat losses) and located below the collectors (e.g., in the basement). Active systems are typically used in colder climate. Some systems utilize a combination of the active and passive modes.

1.2.1 Single- versus Multi-Tank Systems

The sizing of a storage tank is strongly dependant on the targeted application. A solar hot water heating system for a typical household consisting of four individuals would have a solar collector array of 4 to 6 m^2 and hot water storage of 150 to 300 L (Cruickshank and Harrison 2009). Hot water demand needed by a multi-residential building can be met through a large single tank (thousand of liters in capacity) or a cascade of small tanks interlinked together. Large tanks are expensive and difficult to fabricate. In addition, they are not well suited to retrofit situations where the storage vessel must be moved into a building space through existing door openings. Consequently, larger storages are often constructed on site, and maintained at low pressure and vented to the atmosphere. The multi-tank configuration is a more practical economical alternative (Mather et al. 2002).

Smaller tanks are readily available in the market. They can be handled through doorways and stacked over each other when needed. The tanks can be connected either in parallel or in series. Figure 1.5 shows the two possible configurations. Researchers have shown that the series multi-tank configuration promotes sequential stratification in the storage system. This reduces entropy production and improves overall system performance (Mather et al 2002, Cruickshank and Harrison 2009).

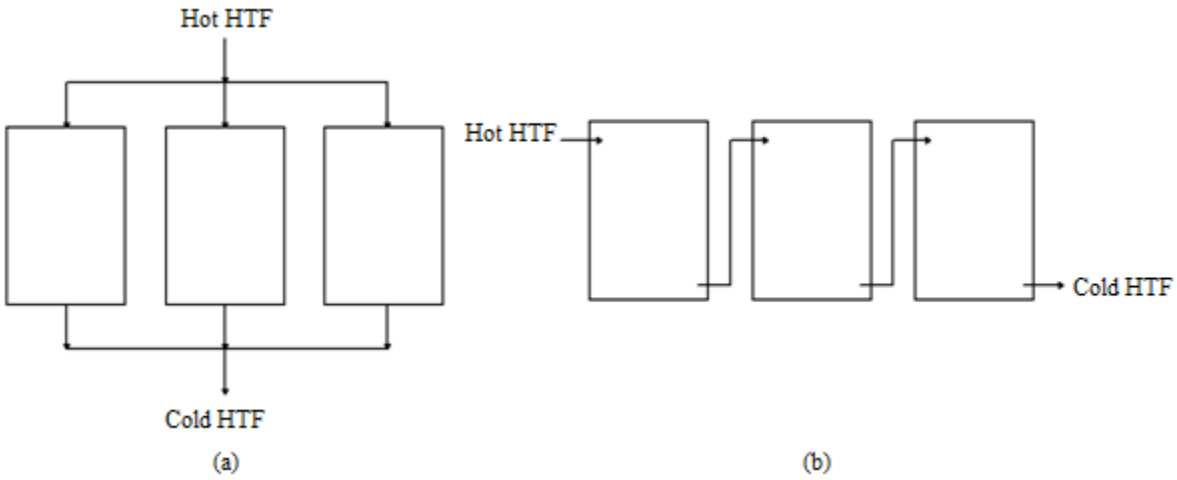

Figure 1.5: Direct charging in a multi-tank system (a) Parallel (b) Series

1.2.2 Types of TES Media

There are two main types of TES systems: (1) Sensible energy and (2) Latent energy storage systems. Sensible energy storage (SES) system stores energy by changing the temperature of the storage medium. The energy stored depends on the amount of storage medium used, its specific heat and the change in temperature. The most common sensible storage medium is water. It is characterized by abundance, low cost and well-known properties. However, its disadvantages are: the continuous increase of their temperature

during the charging process which leads to higher thermal losses and large storage volume needed compared to the latent energy storage systems.

Latent energy storage (LES) systems employ phase change materials (PCMs) and the energy is stored and released in the form of the latent heat of fusion. LES systems have recently captured more attention in various applications owing to their high energy storage density compared to SES systems and their ability to store energy at constant temperature corresponding to the melting temperature (T_m) of the PCM used. Careful selection of the appropriate PCM is required. For example, PCMs should not degrade over large number of cycles, maintain thermal properties in both phases and meet the requirements of low corrosion, toxicity and volume change (Abhat 1983, Zalba et al. 2003, Sharma et al. 2009).

While PCMs have the potential for high energy density, most PCMs are characterized by low specific heat capacity, low thermal conductivity and high cost. Thus, PCM systems need to be designed to have their operating range around melting temperature to minimize sensible storage and the encapsulation design must reduce the thermal resistance of the PCM on the system. Common examples of PCMs used in LES systems are: paraffin, fatty acids, organic eutectics and hydrated salts.

The current study is concerned with sensible and latent energy storage systems and their employment in hybrid systems (containing water as SES medium and phase change materials as LES medium) suited for low temperature applications such as water and space heating for residential and commercial areas.

1.3. Problem definition

The solar domestic hot water market is well-developed, however an unexploited segment exists for small to medium sized systems to supply multi-family or small commercial applications. Few previous works were reported to develop configurations for thermal storage to supply multi-residential building with their hot water demand (Mather et al 2002, Cruickshank et al. 2009, Dickinson et al. 2012).

Mather et al. (2002) studied the water-only multi-tank system shown in figure 1.6. It consists of eight modular 200 liter tanks connected serially. The tanks are heated in series using a coil placed at the bottom of each tank. The discharging is indirectly through coils in the counter direction. The dominant mode of heat transfer is natural convection , this tends to fully mix each tank under different charging and discharging profiles. Although the tanks were found to be fully mixed, tank-to-tank stratification existed. The tanks decrease in bulk temperature from the supply side to the demand side. In addition, this system was observed to benefit from a thermal diode effect. This happens in the late afternoon when cooler water enters the tanks. Due to the density difference, the bulk temperature of the tanks will not be affected by the cooler water which is not the case in direct systems.

The current multi-tank studies have been greatly inspired by the work of Mather et al. 2002 and recent studies Abdelsalam 2015 and Sarafraz 2013 shown in figure 1.7. The hybrid TES storage system comprises a tank filled with water as the SES medium in

which PCM modules, as the LES medium, are submerged. The integration of the PCM modules within the water-filled tanks will lead to the enhancement of the storage capacity of the system due to the latent heat of the PCM. Furthermore, applying this concept to the cascaded system and using PCMs with different melting temperatures in the series of tanks will promote effective stratification especially when the bulk temperature of each tank is controlled around the melting temperature. This concept is described as "tuned storage".

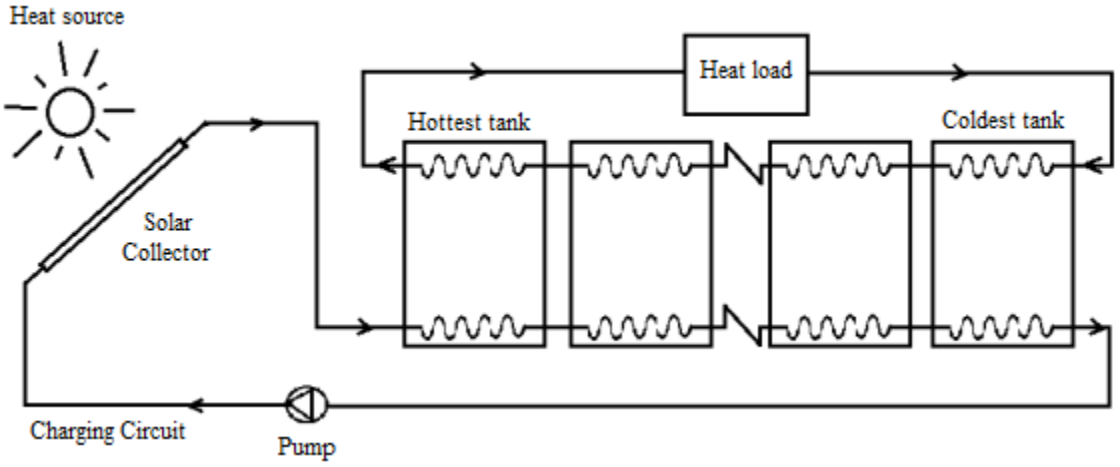

Figure 1.6: Multi-tank system studied by (Mather et al. 2002)

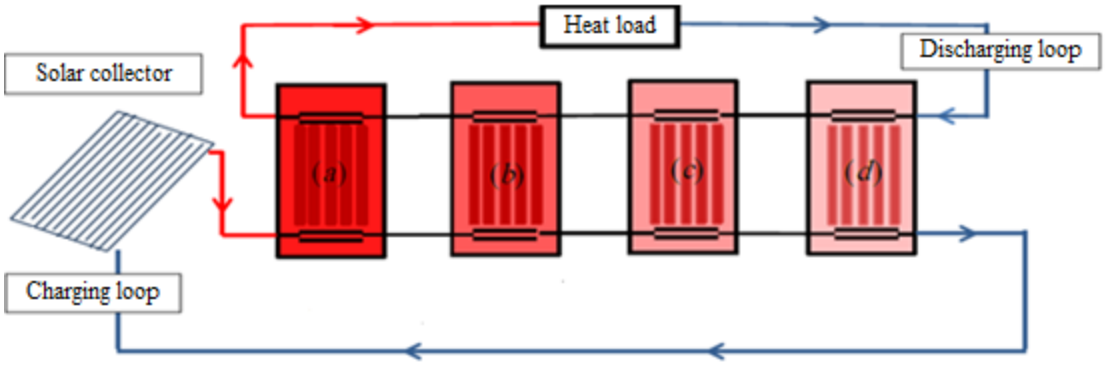

Figure 1.7: Hybrid TES system comprising 4 serially-connected tanks filled with water and PCM modules with different melting temperatures studied by Abdelsalam 2015 and Sarafraz 2013.

Heat transfer inside the tanks is dominated by natural convection which is characterized by lower heat transfer coefficients compared to forced convection. This additional heat transfer resistance limits the rates of charging and discharging. However, this system benefits from the thermal diode effect described by Mather et al 2002. This occurs when water entering the first tank is cooler than the bulk temperature of the tank. This acts to inhibit the natural convection heat transfer at the coil which helps to maintain the existing tank-to-tank stratification. This is beneficial in the late afternoon when the outlet collector temperature drops.

To enhance heat transfer to the PCM modules, the coils are removed in the present study to take advantage of the higher heat transfer coefficient of the direct forced convective mechanism. Figure 1.8 shows the proposed schematic of the multi-tank direct system considered in the present study. The tanks are serially connected and PCMs are arranged in descending order of their melt temperature. The system is

studied in the context of a SDHW application. The main objectives of the current work can be summarized as follows:

1- To explore the dynamic behavior of a hybrid water/PCM tank when subjected to various charging and discharging scenarios.
2- To correlate the key parameters that govern the component behavior and expected energy storage gains compared to water only system.
3- To explore the dynamic behavior of a single hybrid PCM/water tank in the context of SDHW system.
4- To assess the benefit of PCM inclusion in water tanks based on system level analysis to clarify the mixed results pertaining to this issue in the literature.
5- To explore the dynamic behavior of the proposed multi-tank configuration.
6- To develop a mechanistic numerical model to assess the performance of the proposed system under different irradiation and demand profiles.

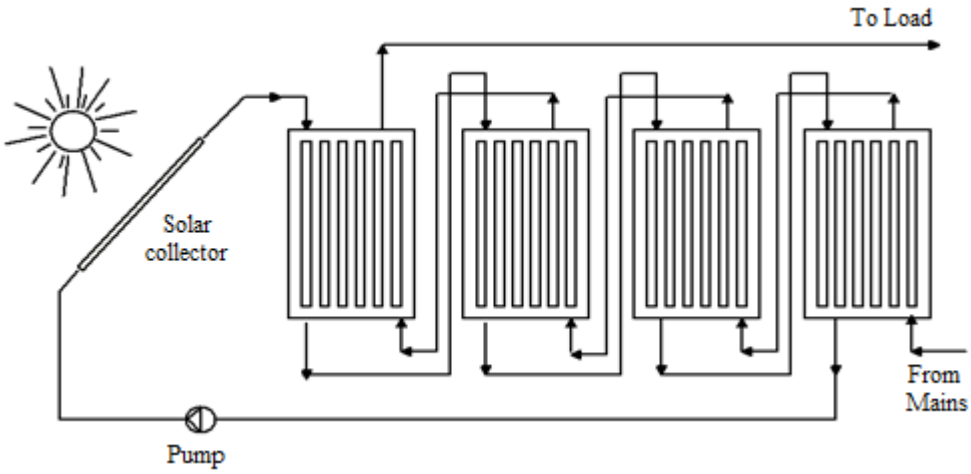

Figure 1.8: Schematic of the proposed multi-tank system.

1.4. Scope of research

The thesis represents a compilation of results presented in three peer reviewed journal They are structured as follows:

1.4.1 Numerical Investigation and Non-Dimensional Analysis of the Dynamic Performance of a Thermal Energy Storage System Containing Phase Change Materials and Liquid Water

In this article, the hybrid water/PCM tank performance is presented in detail for isothermal charging conditions. Gains in energy storage are presented relative to the water-only system. Gains are found to be as high as 179% by using 50% packing ratio and 10^{o}C operating temperature range in water tanks. Gain contours were plotted for a wide range of system operating conditions. The gain is function of the PCM packing ratio, operating range, melt temperature, and the thermal capacity ratio of PCM to HTF. It is a function of the charging time which is prescribed in the analysis as well. A non-dimensional analysis of the energy storage capacity gains as a function of the key non-dimensional parameters (Stefan, Fourier, and Reynolds numbers) as well as PCM melting temperature was performed. The gain was found to be well described by the combination of $(\mathrm{FoRe_c}^{0.8}\theta_m)$ and $\widetilde{\mathrm{Ste}}/(\rho C_P)^*$ for the system. The simulations covered ranges of $0.1<\widetilde{\mathrm{Ste}}<0.4$, $0<\mathrm{Fo}<600$, $20<\mathrm{Re}<4000$, $0.2 < (\rho C_P)^* < 0.8$ and $0.2 < \theta_m < 0.8$. The developed map fits the simulation results with a maximum deviation from the raw data of 5.9%.

1.4.2 An alternative approach for assessing the benefit of phase change materials in solar domestic hot water systems

This article presents the dynamic performance of a single hybrid tank in the context of a solar domestic hot water system. Typical Canadian weather data and demand profiles were considered. This article resolved the contradiction in the results reported in literature on the benefit of incorporating PCMs in water tanks. Energy balance analysis considers the interactions between the thermal storage, the collector performance and the household. It is shown that storage volume plays a key role in influencing the collector performance. It is also demonstrated that PCMs provide a benefit only in comparison to an undersized water based storage system relative to the demand. As the tank volume is increased, the benefit of PCM diminishes. The system energy balance revealed that the benefit of PCM at the undersized storage is due to:

- Reduction in the collector inlet temperature which reduced collector loss and increased collector efficiency.
- Increased pump run time due to cooler tank bottom.
- Increased water delivery temperature to load during early morning and late afternoon.

1.4.3 Potential of multiple Phase Change Materials (PCMs) in enhancing the performance of Solar Domestic Hot Water (SDHW) system

In this article, a multi-tank system containing water and different PCMs cascaded in a descending order of their melt temperature is considered. The solar fraction was found to be enhanced relative to the single PCM case. Sequential stratification between tanks

aided in preserving a cooler collector inlet temperature. This reduced the collector losses and increased the pump activation time and thus increased the delivered energy to the household. A 50% reduction in required storage volume was achieved in the considered case.

This subsection provided a brief overview of the contents of the papers presented in detail in chapters 3, 4 and 5. Those papers followed a logical order for understanding the considered problem. The first paper highlights the key design parameters that enhance the performance of the hybrid tank. Those parameters were used in the second paper when the hybrid tank is considered in the SDHW system context. The results from the second paper were extended to solve for the multi-PCM case and the conclusions were reported in the third paper.

1.5. Contribution of research

This work has:

1. resulted in better understanding of the dynamic performance of multi-tank hybrid configuration for low temperature applications;
2. proved feasibility of using solar energy for multi-family residential and small scale commercial applications; this results in decreasing the dependence on fossil fuels and hence reduction of greenhouse gas emissions
3. demonstrated the operation of a new multi-tank hybrid thermal storage design through numerical simulation;

4. illustrated the key design and operational factors that affect the performance of the investigated hybrid tank and correlated the design and operating parameters;

5. produced a preliminary assessment of the feasibility of PCM incorporation in water tanks installed for multi-family dwellings; and

6. resolved the ongoing debate found in the literature pertaining to the feasibility of PCM inclusion in water tanks.

1.6. Organization of Research and Thesis Document

This thesis is made up of three journal articles that comprise the results section of the thesis along with other supplementary chapters which provide a survey of related literature and context for the research, as well as conclusions and recommendations. The information provided in this study is presented in six chapters:

Chapter 1 presents an introduction to thermal energy storage systems, different configurations of the system, and the scope of this study;

Chapter 2 presents a review of the studies conducted on multi-tank storage systems, PCM based storage systems, multi-PCM storage systems;

Chapter 3 is the first journal article entitled "Numerical Investigation and Non-Dimensional Analysis of the Dynamic Performance of a Thermal Energy Storage System Containing Phase Change Materials and Liquid Water". It presents component level analysis for a hybrid single tank system containing water and PCM under isothermal charging conditions.

Chapter 4 is the second journal article entitled "An alternative approach for assessing the benefit of phase change materials in solar domestic hot water systems". It presents the assessment of the impact of PCM incorporation in a single tank SDHW system.

Chapter 5 is the third journal article entitled "Potential of multiple Phase Change Materials in enhancing the performance of Solar Domestic Hot Water system". It presents the assessment of the impact of PCM incorporation in a multi-tank SDHW system;

Chapter 6 presents conclusions and recommendations for future work.

Appendix A presents parametric analysis results for single hybrid tank in SDHW system context;

Appendix B presents parametric analysis results for multi-tank hybrid SDHW system.

1.7. A note to the Reader

As result of the editorial requirements of publishing a series of separate journal articles, there is some overlap of material contained in this thesis. In particular, the sections of each journal article pertaining to the numerical modelling are repeated. The literature review sections of each article also contain similar material. However, each of these review sections is targeted, and does contain more specific references related to the work presented in each paper.

CHAPTER 2 Literature Review

2.1. Introduction

This section of the thesis provides a comprehensive review of the relevant studies in the literature on PCM incorporation in SDHW systems. The literature reviewed in each journal article contained in this thesis is relatively brief to fit the publication requirement. To provide more insight and greater context to the work performed in this thesis, a more detailed review is presented in this chapter. The chapter begins with a discussion of recent multi-tank systems followed by a review of PCM types and properties and finally hybrid PCM/water systems for solar domestic hot water applications.

2.2. Multi-tank Systems

The practical and economic advantages of using multi-tank systems over large single tank have motivated researchers to investigate and compare the performance of those systems when multi-residential and small commercial applications are considered. There were only few studies done on multi-tank configurations. The current section highlights the key findings of the related research.

Mather et al. (2002) presented an experimental investigation of the performance of a series in-direct charge and discharge multi-tank system with immersed coil heat exchangers. A schematic of the system is shown in Figure 1.4. The system consists of eight modular 200 liter tanks to give an overall storage capacity of 1600 liters. The system was subjected to various charging and discharging scenarios. The temperature evolution in the tanks was monitored with time. As natural convection is the dominant heat transfer mode, tanks were observed to be well mixed. However, there was a high

degree of tank-to-tank stratification. They observed an interesting phenomenon which they called “thermal diode” effect. When water entering the coils is hotter than the tank bulk temperature, natural convection currents arise. However, in the late afternoon periods when cooler fluid flows in the bottom coils natural convection heat transfer from the coils is inhibited and stable stratification is maintained. As a result, the thermal energy in the charging fluid is directed to the tanks that are at a cooler temperature than the charging fluid. This helps to maintain tank-to-tank stratification.

Cruickshank and Harrison (2009) investigated the thermal performance of an indirect charge, direct discharge multi-tank system with side arm heat exchangers in the charge-loop. They conducted both numerical and experimental investigations for the system. The layout of their system is given in Figure 2.1. The system consists of three 270 liter tanks constituting a total volume of 810 liters. They interconnected the tanks in series and in parallel. They tested both constant temperature charging and variable temperature charging by implementing a hypothetical sinusoidal profile. To quantify the relative benefits of the sequentially stratified thermal energy storage, they determined values of exergy stored versus time for the considered test sequences. The Second Law of Thermodynamics provides a mechanism for quantifying any degradation in the “usefulness” of the energy. As a basis of comparison, the series and parallel configurations were also modeled and compared against two theoretical multi-tank configurations, i.e., fully stratified and fully mixed multi-tank storages. Results show that the series-connected configuration closely matched the exergy level of the fully stratified

multi-tank case. At the higher collector flow rate, the exergy levels in both the series and parallel cases are reduced compared to the low flow case.

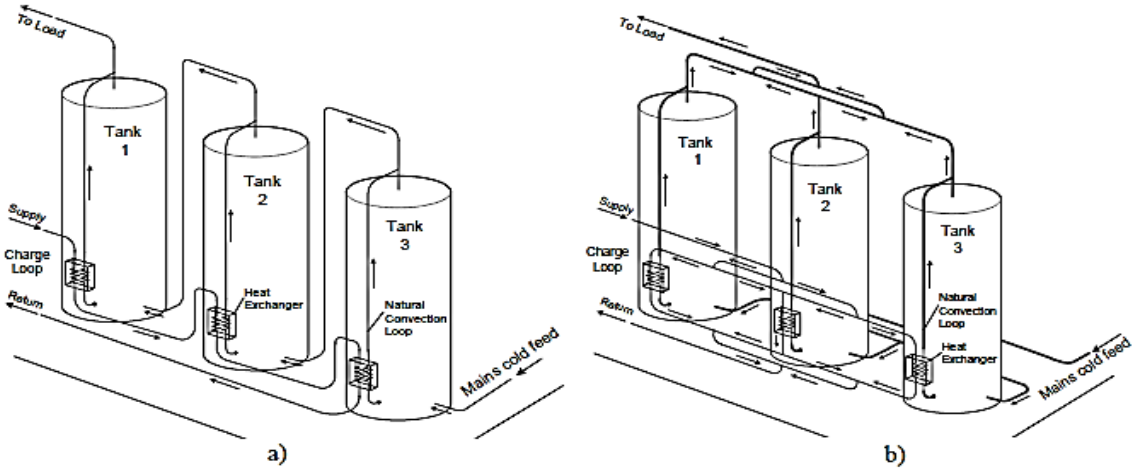

Figure 2.1: The multi-tank system studied by Cruickshank and Harrison 2009.

Dickinson et al. (2012) continued Cruickshank's work by investigating the thermal behavior of the multi-tank system described above. The main focus of the work was the detailed study of the discharging behavior. They subjected the considered system to standard draw profiles. They considered three different configurations: series charge and series discharge, parallel charge and parallel discharge, and series charge and parallel discharge. Significant mixing took place at the bottom of tanks in series discharging. Warm water from the top of the tank entered the cooler region at the bottom of the previous one. However, in the parallel discharging cold water was available at the tank bottom which maintained stratification. They concluded that the series charging and parallel discharging was the best amongst the configurations studied based on both energy and exergy analysis.

From the previous cited work pertaining to multi-tank studied configuration, all the multi-tank studies dealt with water-only systems. No such analysis was performed on tanks containing both water and PCMs. Those works concluded that the sequential stratification is enhanced in the multi-tank configuration relative to the single tank. The incorporation of PCMs into water tanks provides an opportunity for increasing the energy density of the system as well as enhancing stratification by using PCMs of cascaded melt temperatures. This hybrid water/PCM multi-tank configuration will be the focus of the present work.

2.3. PCM-based systems

This subsection summarizes the key research results pertaining to PCM types and properties, single and multi-PCMs systems and inclusion of PCMs in SDHW systems and their role in system performance enhancement.

2.3.1. PCM classification and properties

LES systems have recently captured attention in various applications owing to their high energy storage density compared to SES systems. They also store heat at constant temperature corresponding to the melting temperature (T_m) of the PCM used. To determine the PCM appropriate for a certain application, various factors should be considered. The melting temperature of the chosen PCM must be in the operating range of TES. High specific heat capacity and thermal conductivity are beneficial since that will increase the sensible energy storage and promote higher heat transfer rate to the PCM.

Other desirable PCM properties include: low density variation during the change of phase, minimal super-cooling, chemical stability under large number of cycles, compatibility with container materials, low toxicity and low flammability.

Abhat (1983) classified PCMs into three categories: organic, inorganic and eutectics. Sharma et al. 2009 extended Abhat's division with subcategories classifying the organic into paraffin and non-paraffin compounds, the inorganic into salt hydrate and metallic and finally eutectics into (organic-organic), (inorganic-inorganic) and (inorganic-organic). Paraffin waxes are a family of straight chain alkanes. Their melting temperature and latent heat increase with the hydrocarbon chain length (Zhang and Fang 2006, Kousksou et al. 2010); they are reported to have chemical stability and are non-toxic. However, paraffin waxes are moderately flammable which hinders their application in some industries (Lane 1983).

Non-paraffin organic PCMs consist of fatty acids, esters, alcohols and glycols; among them, fatty acids are promising in solar thermal systems because of their high latent heat of fusion and stable properties (Feldman et al. 1995, Alkan and Sari 2008). The family of fatty acids include: caprylic, capric, lauric, myristic, palmitic and stearic acids. Their melting point ranges from 16°C to 65°C with a heat of fusion between 155 and 180 kJ/kg (Baetens et al. 2010). Differential scanning calorimetry (DSC) curves proved that they are promising candidates for LES owing to their high latent heat of fusion, stable properties and suitable melt temperatures (Desgrosseillier et al. 2011, Sari and Kaygusuz 2002, Sari and Kaygusuz 2003, Sari and Karaipekli 2009).

The experiment presented by Jones et al. (2006) clearly shows the physics of the melting process of the PCM. The schematic of their test facility is shown in figure 2.2. In their experiment, n-eicosane was contained inside a transparent polycarbonate vertical cylinder with an acrylic base and top. The melt temperature of the PCM is 36.4^{o}C. The bottom of the cylinder was maintained at a temperature of 32^{o}C and the exterior of the vertical walls were held at a uniform temperature of 45^{o}C. The top of the cylinder was insulated to reduce the heat losses. The PCM was initially a solid at a subcooled temperature of 23^{o}C. Temperature within the PCM was measured using thermocouple racks. The melt front locations were tracked through digital photography. Figure 2.3 shows the captured melt fronts during different times of the experiment. In the early stage of melting (Figure 2.3a), the melt front is almost vertical as the melting process is dominated by conduction. After that as melt propagates, the melt front becomes tilted due to the effect of natural convection currents in the liquid PCM (Figure 2.3b, Figure 2.3c, and Figure 2.3d).

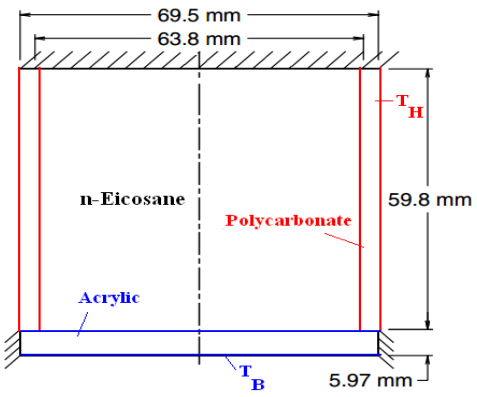

Figure 2.2: Schematic of the experimental facility studied by Jones et al (2006).

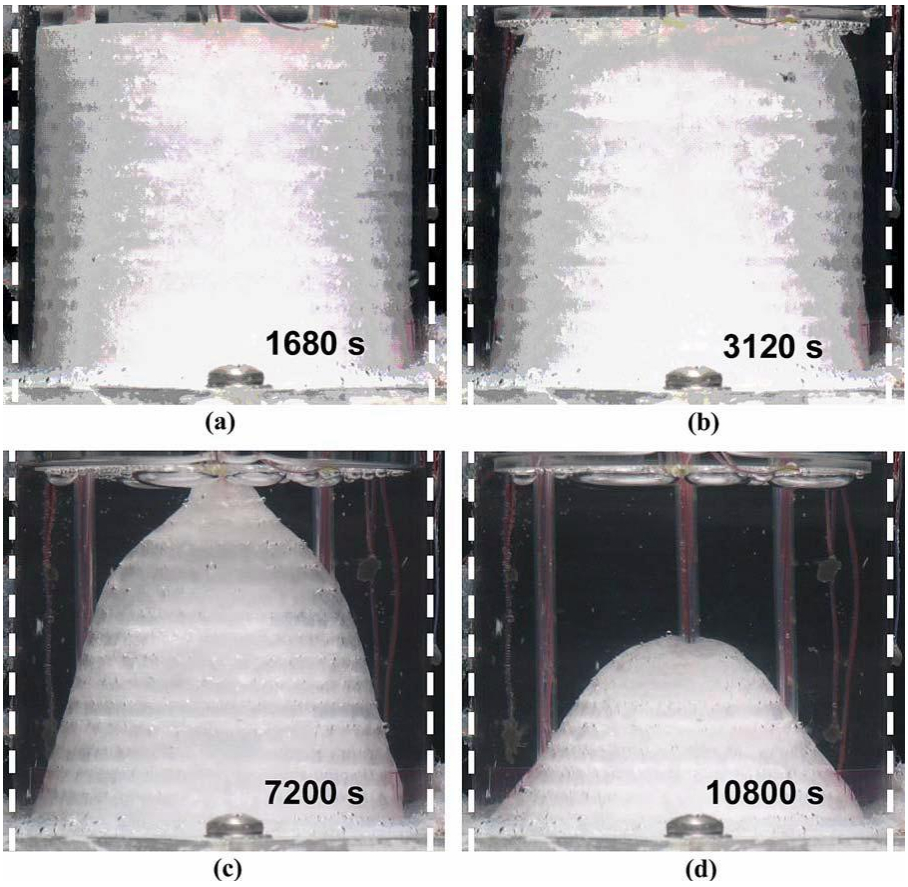

Figure 2.3: Captured melt front locations by Jones et al (2006) at different instances of time (a) 1680 sec, b) 3120 sec, c) 7200 sec, and d) 10800 sec.

The main challenge associated with the PCMs operating in low temperatures is their low thermal conductivity which ranges from 0.1-0.6 [W/m.K]. This leads to slow heat transfer rates from the PCM surface to the core. This implies that the heat transfer rate from the HTF to the PCM will be reduced for a prescribed charging period. Extensive research has been conducted to enhance heat transfer rates in latent heat thermal storage systems. The utilized techniques are categorized into active and passive ones (Nakhla et al. 2015, Bergles 2011). Active techniques include the application of an external source such as

electro-hydrodynamics to enhance the melting rate as studied by Nakhla et al. (2015). Passive techniques include the use of fins, thermal conductivity enhancement by embedding metallic particles, and micro-encapsulation of PCM.

The first passive technique involves the use of extended surfaces such as fins to increase the heat transfer surface area in the thermal system and thus the total rate of heat transfer. Fins vary in shape according to different PCM containments. This approach, however, has adverse impact on the weight and cost of the thermal storage system (Jegadheeswaran and Pohekar 2009, Agyenim et al. 2010).

Thermal conductivity enhancement of the PCM is the second approach. It has been studied by: embedding PCM in a metal or graphite matrix, encapsulating PCM in thin metallic plates or using carbon brushes fibers. The main goal of those techniques is to enhance the effective thermal conductivity of the PCM while maintaining the desired storage capacity. However, loose metal particles tend to agglomerate and the thermo-physical properties of PCMs are altered (Sanusi et al. 2011, Pokhrel et al. 2010, Velraj et al. 1999). Metal foams have been proposed by Tian and Zhao (2013) and they were able to enhance the heat exchange rate by 2-7 times, depending on the properties of metal foam samples (porosity, pore density, and thermal conductivity).

Lastly careful design of PCM geometry, configuration and percentage is required to attain high heat transfer rates from HTF to the PCM. Different encapsulation geometries have been considered including: flat plate, cylindrical and spherical encapsulations. The

spherical containments show higher melting rates followed by the cylindrical modules then the rectangular slabs when comparing the same volume of the PCM. Those encapsulations minimize the thermal resistance imposed by the low conductivity of the PCM on the system (Stritih 2004, Yingqiu et al. 1999, Lacroix and Benmadda 1997).

2.3.2. Single PCM systems

Hybrid tanks containing both water and phase change materials have been studied by a number of researchers. The inclusion of PCM in the tank increases the thermal energy stored compared to a water only tank for isothermal charging conditions due to the latent heat effect (Esen and Ayhan, 1996; Mehling et al., 2003; Nallusamy and Velraj, 2009). The PCM improves the thermal stratification in the tank owing to the temperature modulation effect since it maintains the top layers of the tank at a higher temperature and the bottom ones at lower temperatures (Mehling et al., 2003). The operating conditions and parameters as mass flowrate, PCM volume fraction and module diameter influence the system performance. The mass flow rate was found to have a significant effect on the rate of charging TES as it increases the heat transfer coefficient. Thus, the melting time decreases nonlinearly as the mass flow rate increases. In contrast, the PCM melting time increases with increasing volume fraction due to the additional thermal resistance imposed on the system (Nallusamy and Velraj, 2009). The melting and solidification time was found to be a function of the PCM encapsulation diameter. Increasing the diameter increased the required solidification time due to the increase in PCM material. Up to a

specific diameter the increase was found to be relatively small, at this stage conduction is the dominant mode of heat transfer then convection dominates (Ismail and Moraes 2009).

Agyenim et al. (2010) provided a relatively recent review on thermal performance evaluation of LES systems. They emphasized the need for a unified platform that allows comparison between the behaviors of different proposed systems. Although numerous research have been done in this field, researchers did not present their conclusions in generic dimensionless forms which limit their applicability. Even though few research attempt to non-dimensionalize their data, the variation of employed PCMs made it difficult to cross-correlate the data.

On the system level, the effect of PCM inclusion in the water tank of a SDHW system was investigated by a number of researchers. Realistic supply and draw-off patterns as well as approximated ones were considered (Wang et al. 2015, Al-Hinti et al., 2010; Fazilati and Alemrajabi, 2013; Nabavitabatabayi et al., 2014; Nkwetta et al., 2014; Talmatsky and Kribus, 2008; Kousksou et al., 2011). The PCM increased the exergy efficiency and the storage capacity due to its latent heat and temperature modulation effect (Wang et al., 2015; Al-Hinti et al., 2010; Fazilati and Alemrajabi, 2013). It decreased the delivered temperature swing at night due to the released heat of fusion. This increased the periods of times when the hybrid is able to supply the load with hot water and thus it increased the solar fraction (Al-Hinti et al., 2010; Fazilati and Alemrajabi, 2013). PCM was also found to be beneficial in shifting power demand (Nabavitabatabayi et al., 2014; Nkwetta et al., 2014). The high thermal inertia of the

hybrid system (containing water and PCMs) and system temperature modulation reduced the system temperature variation. This decreased the auxiliary heat required in peak periods (Nabavitabatabayi et al., 2014; Nkwetta et al., 2014).

Talmatsky and Kribus 2008 raised a question that seemed to contradict the ongoing research on the predicted benefit of PCM incorporation in water tanks. They studied numerically the hybrid tank performance throughout the year and compared the predicted solar fraction to a water only system. They reported only a marginal gain in solar fraction (around 1%) when PCM is present inside the tank. They argued that the benefit brought by PCM during the day is penalized by increased heat loss from the tank at night due to the higher bulk temperature level. The two contradicting mechanisms almost cancel each other. This resulted in overall similar performance by the two systems. Kousksou et al. 2011 subsequently determined that the marginal gain reported by Talmatsky and Kribus 2008 was a result of the improper selection of PCM melting temperature. The charging period was not sufficient to fully melt the PCM. This caused the PCM to act as a sensible storage most of the time. In other words, the full latent heat of PCM was not utilized moreover, PCMs have lower sensible storage capability when operating temperature range gets wider. When Kousksou et al. 2011 lowered the PCM melt temperature in Talmatsky's system, a 14% reduction in the annual electricity backup was achieved. A slight increase in the collector efficiency was also noted.

From the previous studies on the systems level, the effects of PCM on solar fraction appear to be mixed. Some researchers found that solar fraction is enhanced with the

presence of PCM (Wang et al., 2015; Al-Hinti et al., 2010; Fazilati and Alemrajabi, 2013; Nabavitabatabayi et al., 2014; Nkwetta et al., 2014; Kousksou et al., 2011) whereas others found only marginal benefits (Talmatsky and Kribus, 2008). In their analyses, the researchers compared PCM thermal storage tanks with water-only tanks at the same volume. The current work aims to clarify the contradiction in those results based on system energy balance. It considers the storage volume as an independent variable.

2.3.3. Multi-PCM systems

PCMs have the potential for high energy storage capacity in small temperature operating ranges. This motivated researchers in concentrated solar power applications to put different PCMs in the LES when wide range of operation is considered.

A number of researchers have explored the use of multiple types of PCMs for energy storage in high temperature applications. They concluded that cascaded LES systems provide high storage potentials compared to both a sensible system and a single PCM system (around 74%) (Michels and Pitz-Paal 2007, Seeniraj and Narasimhan 2008). Multi-PCM system promotes higher charging/discharging rates and leads to reduced fluctuation in the outlet HTF temperature thus improving the exergy efficiency. The optimum melting points of the PCMs can be achieved when the difference between the HTF temperature and the melting point of PCMs is almost constant along the fluid flow direction in the system (Watanabe and Kanzawa 1995).

Attempts were reported to further enhance the charging rates of the considered multi-PCM systems. Researchers used fins to increase the heat transfer area and promote the heat transfer rate (Seeniraj and Narasimhan 2008). They found that the molten fraction increased by 35% in comparison to a single PCM model. In addition, researchers embedded metal foams in the multi-PCM systems (Tian and Zhao 2013). This enhanced heat exchange rate by 2–7 times compared to the ordinary cascaded system when different metal foams were tested.

To the author's knowledge, the cascaded PCM research reported in the literature is for high temperature applications. The PCMs considered in those systems are the hydrated salts whose thermo-physical properties are different from PCMs suitable for low temperature applications. Other than the work performed at McMaster University, no such configuration was reported for the low temperature residential and commercial applications.

2.4. Summary

Thermal energy storage is a critical component in the solar domestic hot water system. The required size of the storage tank in the solar domestic hot water system is a function of the targeted applications. Affordable small tanks of few hundred liters in capacity are readily available in the market. Those tanks are sufficient to supply a single family with their demand of hot water. Those configurations have been thoroughly investigated in the literature. When multi-residential or small commercial applications are considered, large storage volumes are required. This storage can consist of a single large tank or a series of

interconnected small tanks. The economic advantages of small tanks make them more favourable. Moreover, previous research has shown that this configuration promotes sequential stratification between tanks. Sequential stratification arranges water in the tanks in an order of decreasing temperature from the supply side to demand side. This has a positive impact on the solar domestic hot water system as hotter water will be available to the demand and cooler fluid is provided to the collector. The limited number of multi-tank research studies considered either indirect charging (Mather et al. (2002)) or employed natural convection side arm heat exchangers (Cruickshank and Harrison (2009)). There was no previous work conducted on multi-tank direct forced convective configuration.

It has been shown that incorporating phase change materials in water tanks has the potential to enhance system performance. It increases energy density, improves the exergy efficiency and modulates the system temperature around its melt temperature. However, PCMs usually have poor sensible properties compared to water storage solutions. The low specific heat capacity of PCMs has a detrimental effect if storage is subjected to a wide temperature operating range. Also, poor thermal conductivity limits the charging rate of the system. Careful design of those systems is needed to maximize the benefit of PCM incorporation on the system.

Cascading PCMs in a descending order of their melt temperatures is reported to enhance performance of concentrated solar power systems. This arrangement divides the

operating temperature range of the system to narrower bands around the PCMs melting points. It significantly increases exergy efficiency, reduces temperature fluctuations at the outlet, increases energy density, and shows higher charge and discharge rates. No previous research beyond the studies by Abdelsalam (2015) considered a cascaded PCMs solution for low temperature applications.

On the SDHW system level, there is a conflict in the research community as the benefit of the inclusion of PCM in water tanks. Some researchers found enhancement in the solar fraction while others reported marginal benefits. Those studies were performed on a single tank containing water and PCM. The researchers compared tanks of the same volume, one containing water only and other one containing both water and PCM. There is thus a need to develop a framework for a broader assessment of the role of PCM in impacting system performance.

The multi-PCM hybrid active system has not been previously studied. This system is expected to benefit from the tank to tank stratification as well as stratification within the tanks themselves. It will also have a higher energy storage capability owing to the high latent heat of PCMs. Moreover, this system will be assessed in a SDHW system context. A system level analysis including the link of all system components will clarify the role played by PCM in the tanks, thus resolving the mixed results reported in the literature. The analysis presented in this thesis clarifies the role of PCM in influencing solar fraction and resolves the conflict in the research community.

CHAPTER 3

Numerical Investigation and Nondimensional Analysis of the Dynamic Performance of a Thermal Energy Storage System Containing Phase Change Materials and Liquid Water

Complete citation:

Teamah HM, Lightstone MF, Cotton JS. Numerical Investigation and Nondimensional Analysis of the Dynamic Performance of a Thermal Energy Storage System Containing Phase Change Materials and Liquid Water. ASME. I. Sol. Energy Eng. 2016; 139(2):021004-021004-14. doi:10.1115/1.4034642.

Copyright

Relative Contributions:

Teamah HM: Performed all the simulations, interpretation and analysis of the data, wrote the first draft of the manuscript including all figures and text and was responsible for the final draft submittal to the journal.

Lightstone MF: supervisor of Teamah HM, revised and modified the journal paper draft.

Cotton JS: Co-supervisor of Teamah HM, revised and modified the journal paper draft.

Abstract

The dynamic performance of a thermal energy storage tank containing phase change material (PCM) cylinders is investigated computationally. Water flowing along the length of the cylinders is used as the heat transfer fluid. A numerical model based on the enthalpy-porosity method is developed and validated against experimental data from the literature. The performance of this hybrid PCM/water system was assessed based on the gain in energy storage capacity compared to a sensible only system. Gains can reach as high as 179% by using 50% packing ratio and 10^{o}C operating temperature range in water tanks. Gains are highly affected by the choice of PCM module diameter; Gains are almost halved as diameter increases four times. They are also affected by the mass flow rate nonlinearly. A non-dimensional analysis of the energy storage capacity gains as a function of the key non-dimensional parameters (Stefan, Fourier, and Reynolds numbers) as well as PCM melting temperature was performed. The simulations covered ranges of $0.1<\widetilde{Ste}<0.4$, $0<Fo<600$, $20<Re<4000$, $0.2 < (\rho C_P)^* < 0.8$ and $0.2 < \theta_m < 0.8$.

Keywords

Phase Change materials, enthalpy porosity, gain, hybrid system, sensible only system

Nomenclature

C_{pl} Liquid specific heat capacity [J/kg K]

C_{ps} Solid specific heat capacity [J/kg K]

D	PCM cylinder outer diameter [m]
D_h	Hydraulic diameter [m]
E	Energy stored [J]
Fo	Fourier number
Gain	$= \frac{E_{\text{hybrid tank}} - E_{\text{sensible only tank}}}{E_{\text{sensible only tank}}}$
K	Thermal conductivity [W/mK]
L_c	Length of cylinder [m]
$\dot{m}$	Mass flow rate inlet to the tank [kg/s]
N_c	Number of cylinders in the tank
Nu_c	Nusselt number based on hydraulic diameter
Nu_p	Nusselt number based on Dittus-Boelter correlation
$R_{c,inn}$	Inner radius of phase change material cylinder [m]
$R_{c,out}$	Outer radius of phase change material cylinder [m]
Re_c	Reynolds number based on hydraulic diameter
r_s	Latent heat of fusion

$\widetilde{Ste}$ Stephan number

T Temperature [^oC]

T_{in} Temperature of incoming fluid [^oC]

T_m Melting temperature of PCM[^oC]

T_{st} Initial temperature of the tank [^oC]

$U_{f,mean}$ Mean fluid velocity [m/s]

V_{tank} Tank volume [m^3]

ΔF_o Fourier number

Δt Time step [seconds]

Abbreviations

HTF Heat transfer fluid

LES Latent energy storage

PCM Phase change material

TES Thermal energy storage

Latin Symbols

θ	Dimensionless temperature
μ	Dynamic viscosity [Ns/m^2]
ρ	Density [kg/m^3]
φ	PCM packing ratio

Subscripts

c,inn	Inner surface of cylinder
c,out	Outer surface of cylinder
conv	Convective
eff	Effective
f	Fluid
f,m	Mean for fluid
In	Inlet
l	Liquid
m	Melting

st Start

t Transition

3.1. Introduction

Energy use by buildings in the residential sector currently accounts for 17% of Canada's secondary energy consumption. Secondary energy is defined as the total amount of energy consumed by an end-use, and excludes the energy consumed to convert the energy into a useable form from its primary resource (NRCan. 2012). The breakdown by end-use within the residential sector shows that water heating accounts for 17% of the secondary energy consumption, while space heating accounts for 63%. For those two end-uses in Canada, heating is mainly provided by either electricity or natural gas. Assuming 4% annual growth of energy consumption rate, it was found that the Canadian natural gas reserves would only last until 2070. In addition, a reduction in reliance on fossil fuel is also motivated by the need to reduce greenhouse gas emissions. There is thus a need to promote the use of alternative renewable resources such as solar energy. Solar energy is characterized by its intermittent nature. As such, energy storage systems which compensate for the mismatch between the times when the solar energy is available and the times when there is energy demand are required. Thermal energy storage (TES) plays a vital role in many other applications as well; including space refrigeration and air-conditioning, agricultural processes, in addition to waste heat recovery applications (Zalba et al. 2003, Abhat 1983, Sharma et al. 2009). Waste heat recovery has great

potential in industrialized countries, and depending on the temperature at which the waste heat is discharged it can be classified into: (1) Low temperature waste heat (below 100°C), (2) High temperature waste heat (above 400 °C) and (3) Moderate temperature waste heat (between 100°C and 400°C). Our interest throughout this study lies in the low temperature waste heat category which fits into the hot water and space heating applications.

For low temperature applications, energy storage systems typically use water as the storage medium hence storage is in the form of sensible energy. Latent energy storage (LES) systems employ phase change materials (PCMs) and the energy is stored and released in the form of latent heat of fusion. LES systems have recently captured more attention in various applications owing to their high energy storage density compared to SES systems and their ability to store energy at constant temperature corresponding to the melting temperature (T_m) of the PCM used. While PCMs can provide energy density benefits, they are typically characterized by low thermal conductivity, low specific heat capacity and high cost in comparison to liquid water. Common examples of PCMs used in LES systems are: paraffin, fatty acids, organic eutectics and hydrated salts.

Abhat 1983 classified PCMs into three categories: organic, inorganic and eutectics. Sharma et al. 2009 extended Abhat's division with subcategories classifying the organic into paraffin and non-paraffin compounds, the inorganic into salt hydrate and metallic and finally eutectics into (organic-organic), (inorganic-inorganic) and (inorganic-organic). Paraffin waxes are a family of straight chain alkanes, whose melting

temperature and latent heat increase with the hydrocarbon chain length (Zhang and Fang, 2006, Kousksou et al. 2010); they are generally chemically stable, melt congruently and are non-toxic. However, paraffin waxes are moderately flammable with low thermal conductivity which limits its wide application in industry (Lane 1983).

Non-paraffin organic PCMs consist of fatty acids, esters, alcohols and glycols; among them, fatty acids are promising in solar thermal systems because of their high latent heat of fusion and stable properties (Feldman et al. 1995, Alkan and Sari 2008). The most commonly used fatty acids are divided into six groups: caprylic, capric, lauric, myristic, palmitic and stearic with respectively 8 to 18 carbon atoms per molecule. Their melting points are in the range from 16°C to 65°C with a heat of fusion between 155 and 180 kJ/kg which is higher than paraffin waxes (Baetens et al. 2010). Thermal and physical properties of lauric acid were investigated by Desgrosseillier et al. (Desgrosseillier et al. 2011). Differential scanning calorimetry (DSC) curves were obtained and results proved that lauric acid is a promising candidate for LES (Desgrosseillier et al. 2011, Sari and Kaygusuz 2003, Sari and Karaipekli 2009).

The challenge associated with the PCMs operating in low temperatures is their low thermal conductivity which ranges from 0.1-0.6 [W/m.K]. This limits the storage capacity for LES systems for a given charging or discharging time. Extensive research has been carried out to investigate heat transfer enhancements in latent heat thermal storage systems. The techniques can be classified into active and passive ones (Nakhla et al. 2015, Bergles 2011). Active techniques include the application of an external source

such as electro-hydrodynamics to enhance the melting rate as studied by Nakhla et al. 2015. Passive techniques include the use of extended surfaces, thermal conductivity enhancement, and micro-encapsulation (Bergles 2011, Jegadheeswaran and Pohekar 2009, Agyenim et al. 2010).

The use of extended surfaces such as fins increases the heat transfer area in the thermal system and thus the total rate of heat transfer. This approach, however, adversely impacts the weight, volume and cost of the thermal storage system for a given storage energy required (Bergles 2011, Jegadheeswaran and Pohekar 2009, Agyenim et al. 2010). Metallic particles have been proposed to enhance the thermal conductivity of PCM. The main disadvantage of this technique is that metal particles tend to agglomerate and the thermo-physical properties of PCMs are altered (Sanusi et al. 2011, Pokhrel et al. 2010, Velraj et al. 1999). To minimize the resistance imposed by the low thermal conductivity of the PCM, micro-encapsulations are introduced either in the form of thin rectangular slabs or small radii cylindrical containments (Stritih 2004, Yingqiu et al. 1999, Lacroix and Benmadda 1997). Spherical PCM encapsulations in a hybrid system were studied by Nallusamy et al. (Nallusamy et al. 2007). Their results showed that employing PCM in the TES system leads to better control of the heat transfer fluid (HTF) temperature as a result of the constant melting temperature of the PCM. However, the first layer of the spherical capsules receiving the HTF flow showed faster melting than the last layer further downstream. This led to more energy stored in the liquid PCM in the form of sensible energy. This reduces the overall storage capacity since PCMs have low specific

heat in comparison to water. A potential solution to this is the use of cascaded PCMs, in which PCMs having different melt temperatures are arranged in series.

Using multiple PCMs captured the attention of researchers especially for concentrated solar power applications. Michels and Pitz-Paal 2007 experimentally tested on the cascaded latent heat storage system for parabolic trough solar power plants (charging temperature of 390°C and discharging temperature at 285°C) in which three different PCMs were used. They concluded that cascaded LES systems provide high storage potentials compared to the sensible system provided that the PCM thermal conductivity is increased by 4 times. This highlights the limitation of the low thermal conductivity of PCMs. Seeniraj and Narasimhan 2008 used fins to enhance heat transfer in a multi-PCM thermal storage system. They found that the molten fraction increased by 35% in comparison to a single PCM model since the heat transfer fluid temperature drops as it passes through the storage system.

A study of the literature has shown that careful design of TES systems is critical to obtain enhanced utilization of renewable sources as well as the efficient recovery of waste heat. Employing both SES and LES was not well explored in the available literature. This motivated the current research work to study the performance of a hybrid storage system that uses water and organic PCMs to harvest the advantages and minimize the disadvantages of both media. Moreover, the present work introduces dimensionless analysis for the prediction of the gains expected from those systems compared to the sensible only systems.

The paper focuses on tanks that are suitable for residential and commercial applications. Different packing ratios of PCMs are considered in the present study together with different operating conditions of the system (i.e. mass flow rate and operating range of temperature). To justify the incorporation of PCMs in the system, it is compared with the "water only" system in terms of the gain in energy storage capacity or equivalent reduction in storage volume. For example, doubling the energy capacity of the hybrid system compared to the water only system will manifest as a reduction in real estate requirements. This can justify economically the incorporation of PCMs in such systems.

The paper first presents the modelling method used to predict the melting behavior of PCM. Model validation is presented in the appendix. Then the extension of the code to simulate the hybrid system with its verification is presented. A careful discussion and analysis of the dynamic performance of a case study is given. After that, the gain of using the hybrid system compared to the water only system is introduced. A parametric analysis is performed on the system to show how the gain is affected by various key parameters. Finally a non-dimensional analysis to group the results is introduced.

3.2. Numerical modelling of heat transfer in phase change materials

Predicting the thermal behaviour of phase change materials is difficult because of the inherent non-linear nature at moving interfaces. Numerical methods for solving for heat transfer in latent heat energy storage systems were summarized by Dutil et al. 2011: namely fixed grid and adaptive mesh. The essential feature of a fixed grid approach is that the latent heat evolution is accounted for in the governing equation by defining either

an enthalpy, or an effective specific heat, or a heat source (or sink). Consequently, the numerical solution can be carried out on a spatial grid that remains fixed throughout the calculation process.

For the fixed grid enthalpy porosity method, the latent heat evolution is accounted for in the governing equation by defining an enthalpy term. A small transition range on which melting occurs is introduced. The major challenge is in accounting for the zero velocity condition at the interface as the liquid region turns to solid. Morgan 1981 employed the simple approach of fixing the velocities to zero in a computational cell whenever the mean latent heat content reaches some predetermined value between 0 (all solid) and L (all liquid), where L is the latent heat of the phase change. Voller et al. 1987 investigated various ways of dealing with the zero solid velocities in fixed grid enthalpy solutions. Computational cells in which phase change is occurring are modelled as pseudo porous media with the porosity decreasing from 1 to 0 as the latent heat content of the cell decreases from the L to zero.

Another fixed grid method is the "heat capacity method". With this method the latent heat effect is approximated by a large effective heat capacity over a small temperature range (Bonacina et al. 1973, Cornini et al. 1974, Morgan et al. 1978, Lemmon 1981, Pham 1986). This approach is simple in concept and easy to implement. It is, however, sensitive to the choice of the phase change temperature interval and the integration scheme. The sharp change in specific heat at the interface leads to difficulties in obtaining converged solutions.

Due to the stability of the enthalpy porosity method compared to that of heat capacity, this approach is used in the present study. An in-house FORTRAN code was developed to model melting in cylindrical modules. The detailed description of the method and its governing equations is provided in the Appendix. Also the results of validation with an experiment in the literature are presented. A maximum deviation of about 5% is observed at the later stages of melting between the present code and the experiment results.

3.3. Numerical modelling of hybrid tank

The storage tank considered in the present study is a part of a domestic heating system. The PCMs are enclosed in small diameter cylindrical modules to minimize thermal resistance imposed by the low thermal conductivity of the PCM. Water flows parallel to the PCM cylinders as shown in Figure 3.1. During the charging process hot water is introduced to the top of the tank and in discharging the hot water to meet the load it is extracted from the top. Cold water from the mains is introduced at the bottom of the tank.

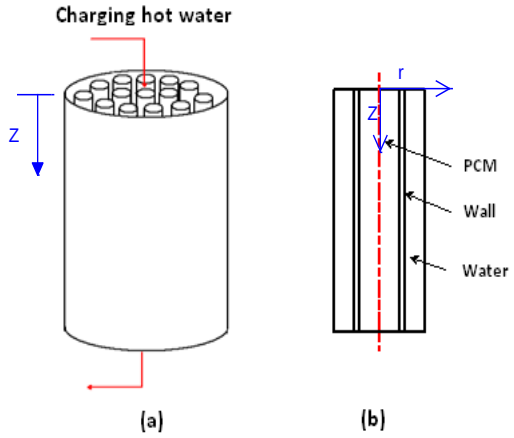

Figure 3.1: The studied domain in the code (a) the whole tank, (b) zoomed view of the cylindrical jacket.

An in-house FORTRAN code was developed to model heat transfer in the hybrid tank. An enthalpy porosity model was invoked to model heat transfer and phase change in the PCM modules. The PCM cylinders are presumed to be uniformly packed into the tank and the flow is treated as a one-dimensional plug flow. As such, the flow around a single module is presumed to be indicative of the 'bundle' of PCM modules. The modelled geometry in the code is shown in Figure 3.1(b). The heat transfer from the fluid can be modelled by considering a water jacket around each module and with heat transfer correlations applied at the outer surface of the module. Heat transfer and energy storage within the encapsulation material is modelled. The tank is considered to be well insulated. Within the module the melting process is presumed to be conduction dominated which is a conservative representation of the heat transfer since natural convection is neglected.

Heat transfer from the fluid adjacent to the PCM modules is calculated from correlations for flow parallel to cylinders developed by Rohsenow et al 1985:

For laminar flow

$$\mathrm{Nu_c} = 3.66 + 4.12\left(\mathrm{D_h}/\mathrm{R_{c,out}} - 0.205\right)^{0.569} \text{ if } \mathrm{Re_c} \leq 2200 \tag{3.1}$$

For turbulent flow

$$\frac{\mathrm{Nu_c}}{\mathrm{Nu_p}} = 1.08 - 0.794\, \mathrm{e}^{-1.62\,\mathrm{D_h}/\mathrm{R_{c,out}}} \text{ if } \mathrm{Re_c} \geq 2200 \tag{3.2}$$

$$\mathrm{Nu_p} = 0.023\ \mathrm{Re_c^{0.8}Pr^{0.4}} \tag{3.3}$$

where

$$\mathrm{Re_c} = \frac{\rho_f \mathrm{U_{f,mean}} \mathrm{D_h}}{\mu_f} \tag{3.4}$$

and

$$\mathrm{D_{h,c}} = \frac{2}{\pi} \frac{\mathrm{V_{tank}}}{\mathrm{N_c R_{c,out} L}} - 2\mathrm{R_{c,out}} \tag{3.5}$$

The means that the velocity can be calculated as follows (assuming uniform flow distribution);

$$U_{f,m} = \frac{\dot{m}}{\rho_f \left({V_{tank}}/{L} - \pi N_c R_{c,out}^2 \right)} \tag{3.6}$$

Applying energy balances on the HTF, wall and PCM control volumes yields a system of algebraic equations which are solved iteratively to meet a predetermined accuracy level.

The simulation of the hybrid tank was verified with the results presented by Esen and Ayhan 1996. They presented numerical predictions of the time for PCMs to fully melt under isothermal charging conditions. The geometry they considered is similar to that shown in Figure 3.1 except that the thermal mass and heat transfer resistance of the encapsulation material was neglected. The results presented focused on prediction of the stored energy when PCM melts under constant temperature charging conditions. A very good agreement is found between the present code and Esen's results as presented in the appendix.

The focus of the current paper is to assess the transient energy storage capability of a hybrid PCM/water storage tank for a range of operating conditions and PCM characteristics. Storage tanks vary from standard, cylindrical 150 L tanks which are produced in large quantities in North America, to various larger sizes (in excess of 10,000 L). A 200 liter tank is considered in the present study to be suitable for residential and commercial applications and to be easily handled through doorways as well. The number of the PCM cylinders varies according to the packing ratio (PCM volume/ total volume). Dimensions and studied parameters are summarized in Table 3.1. The mass flow rate is chosen in the range of residential and commercial applications (Castell et al. 2009,

Hollands and Lightstone 1989, Furbo et al. 2005). Amongst the available PCM data base; fatty acids are chosen due to their stability and promising potentials in TES systems (Desgrosseillier et al. 2011, Sari and Kaygusuz 2002, Sari and Karaipekli 2009). Thermo-physical properties of various fatty acids are listed in Table 3.2.

Table 3.1: Dimensions and studied parameters.

Tank volume	200 litres (0.2 m^3)
Tank length	78 cm
PCM module diameter	From 2 cm to 16 cm
PCM packing ratio	From 10% to 90%
Mass flowrate	From 0.05 kg/s to 0.5 kg/s

Table 3.2: Thermo-physical properties of organic fatty acids (Sharma et al. 2009).

PCM type	T_m [°C]	Density [kg/m^3]	Specific Heat [kJ/kg K]	Heat of Fusion [kJ/kg]	Thermal Conductivity of solid [W/m. k]
Capric Acid	31.5	886	NA*	153	0.149
Lauric Acid	42	870	1.6 (solid), 2.3(liquid)	178	0.147
Myristic Acid	54	844	1.6 (solid), 2.7(liquid)	187	NA*
Palmitic Acid	63	847	NA*	187	0.165

***Not available in the literature**

As a case study, the simulation results for a 200 liter tank with 30% PCM by volume are described in detail. The tank is initially at 40^{o}C and hot water at inlet temperature 52^{o}C is introduced at the top with a rate of 0.05 kg/s. Lauric acid is the selected PCM whose melting point lies in the temperature operating range (T_m= 42^{o}C). The PCM module inner diameter is chosen to be 2 cm for this case. The encapsulation material is copper with a thickness of 0.1 cm. Sensitivity of the solution to the wall material is presented in the appendix and is shown to have a very slight effect on the solution.

A uniform grid was used in both radial and axial directions. The details of the grid are presented in the Appendix. Care was taken to ensure that the simulation results were unaffected by the grid spacing and time step. A grid of 300 nodes in the radial direction and 100 nodes in the axial direction together with 0.005 seconds time step was selected. Using this grid and time step, a solution can be obtained in about 25 minutes of clock time using a 2.4 GHz Quad CPU with 8 GB of RAM.

3.4. Results and discussion

3.4.1. Melting behaviour of PCM in the tank

The melt process is illustrated in Figure 3.2 which shows isotherms at different times in the simulation. Note that the module is initially solid at a uniform temperature of 40^{o}C. There is a short delay of about 0.07 hours to the initiation of melting since the PCM is subcooled. Melting starts from the top of the module and the melt front moves inwards and down with time. The PCM becomes fully molten after 3.2 hours. As expected, there is an axial variation in temperature within the PCM modules; higher levels superheat before lower ones. This occurs because of the reduction in the water temperature as the fluid moves downward along the length of the cylinder and also because of the initial condition in which it is presumed that the water adjacent to the cylinder is initially at the PCM temperature. As such, the initiation of heat transfer to the lower portions of the PCM modules is delayed by the transit time of the fluid. For the current conditions, the transit time for a fluid particle to travel from the top to the bottom of the tank is approximately 0.76 hours. Figure 3.3(a) shows the local molten fraction at different

levels in the PCM module with the origin at the top center of the module. It is observed that the level z/L=0.2 takes around 49% of the time taken by the level z/L=0.8 to be fully molten. Also, the curves are shifted from each other due to the decrease of heat transfer from the water as it flows downwards and as a result of the transit time of the fluid. Figure 3.3(b) presents the local heat transfer rates to those levels. The trends are directly related to the temperature difference between water and PCM surface temperature. Considering z/L=0.8 level as an example; initially the heat transfer rate is zero until the incoming fluid reaches this level (approximately 0.6 hours). The initial increase in the heat transfer is due to the increased temperature of the fluid. The heat transfer then drops as the PCM material responds to the heat addition by the fluid and the PCM temperature rises. Heat transfer increases when the sub-cooling effect is removed and the surface temperature remains close to the melt temperature (between 0.7 and 1.5 hours in Figure 3.3(c)). After that the molten PCM superheats and the surface temperature begins to increase. A sudden decrease in heat transfer rate is observed at around 2.85 hrs. At this time PCM level becomes fully molten and additional heat transfer acts to raise the PCM temperature, thus reducing the heat transfer rate at the wall. The temperature profiles within the PCM at z/L=0.8 and at times of 2.80, 2.85, and 2.90 hours are shown in Figure 3.3(c). The shift in the profile shape indicates the change in the interior heat transfer mechanisms due to the completion of phase change.

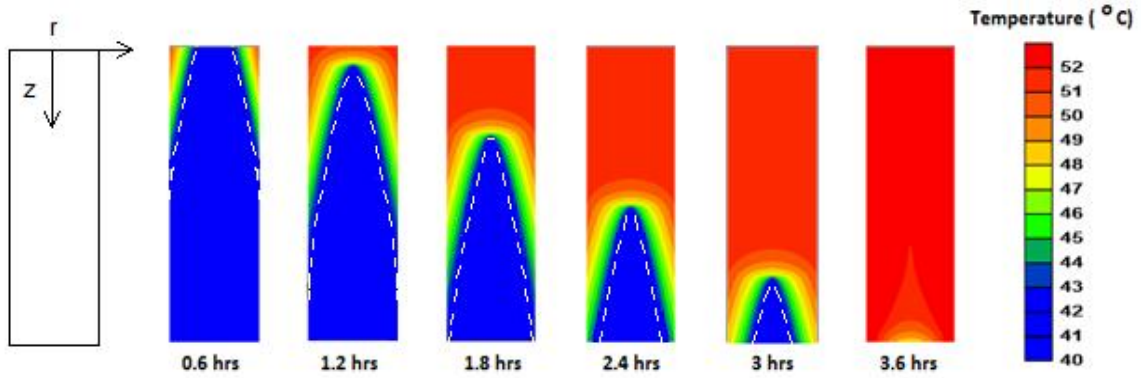

Figure 3.2: Isothermals in PCM modules ($V_{tank} = 0.2\ m^3$, packing ratio $= 30\%$, $T_{st} = 40$ ℃, $T_{in} = 52$ ℃, $T_m = 42$ ℃, $\dot{m} = 0.05\ kg/s$) [melting point is shown in dotted line].

Figure 3.4(a) shows the average molten fraction of the entire PCM module with time. By considering the slope of the curve (Figure 3.4(b)) and the overall heat transfer rate (Figure 3.4(c)), the various heat transfer regimes in this process can be ascertained. The slope initially increases, reaching a peak at about 0.76 hours, which coincides with the peak heat transfer rate as shown in Figure 3.4(c). The slope and heat transfer rates remain high until about 1.64 hours when the melt front reaches the bottom section of the PCM module. Beyond this time, the superheated liquid around the melt front decreases the heat transfer rate as shown in Figure 3.4(c). Moreover, as the melt front progresses towards the

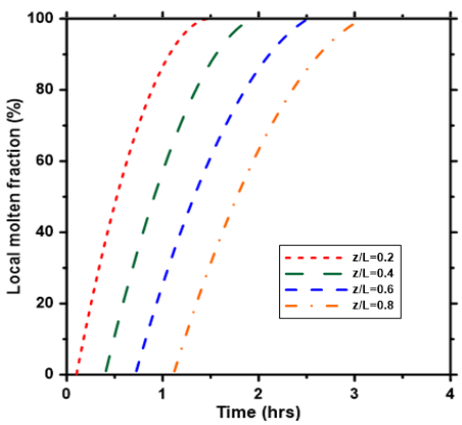

(a) Local molten fraction

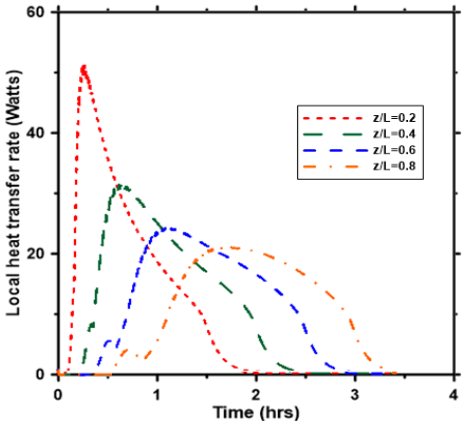

(b) Local heat transfer rate

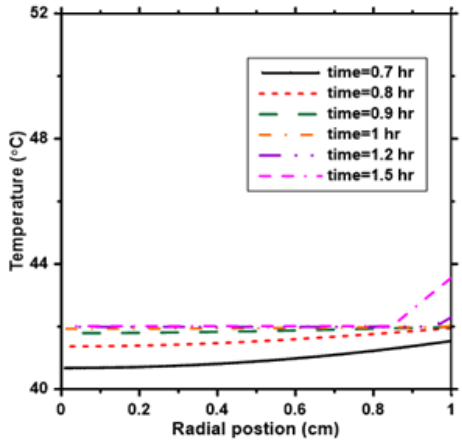

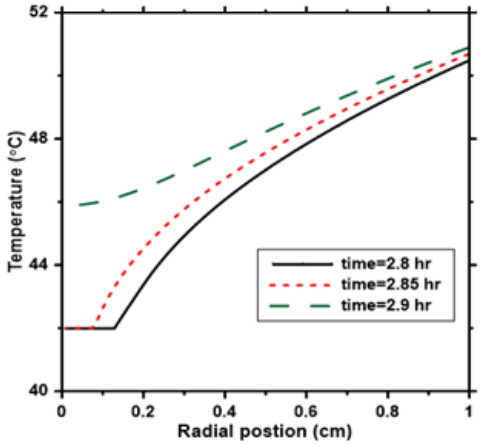

(c) Radial temperature distribution in 4/5 of height of PCM module

Figure 3.3: Local analysis of melting behaviour in PCM modules ($V_{tank} = 0.2\ m^3$, packing ratio $= 30\%$, $T_{st} = 40$ ℃, $T_{in} = 52$ ℃, $T_m = 42$ ℃, $\dot{m} = 0.05\ kg/s$).

centreline, the decrease in area as a result of the cylindrical geometry for the PCM modules acts to reduce the rate of phase change. The effect of incorporating PCM on the water temperature exiting from the bottom of the tank is presented in Figure 3.4(d). Initially, all the water in the tank is at a uniform temperature of 40^{o}C. With the PCM modules, the transit time for the fluid to travel from the top of the tank to the outlet is about 0.76 hours. This coincides with the initial increase in the outlet temperature for the hybrid system. The non-linear plateau in temperature which extends from 1 hour to about 1.6 hours is a result of the high heat transfer during the melting process. This illustrates the capability of the PCM to act to modulate temperature when the phase change is significant. As the PCM superheats, the heat transfer drops thus increasing the temperature of the fluid exiting the bottom of the tank. Without PCM modules present, the fluid essentially moves as a plug and the outlet temperature approaches the inlet temperature at the tank turnover time of about 1.08 hours. The reduced temperatures, and in particular the modulation during phase change with the PCM modules present, are beneficial to solar applications since the heat losses at the collector are reduced (Hollands and Lightstone 1989).

3.4.2. Energy gains in hybrid system

The evolution of the stored energy with time in hybrid tank and the "water only" tank is shown in Figure 3.5(a). The stored energies in the hybrid system components (PCM and water) are also shown. After fully melting the PCM at 3.2 hours, 19.1 MJ of energy will be

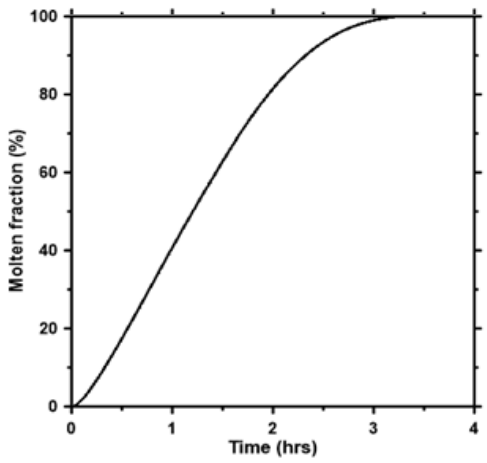

(a) Overall molten fraction

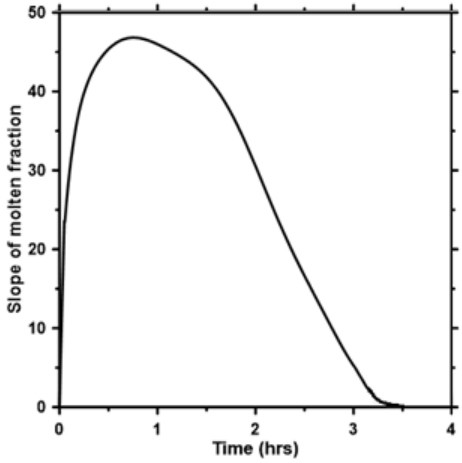

(b) Slope of molten fraction with time

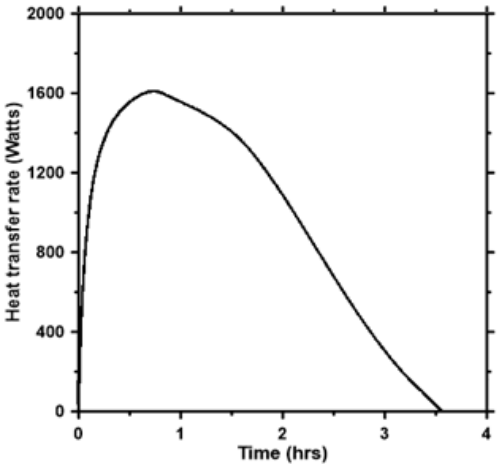

(c) Overall heat transfer rate to PCM

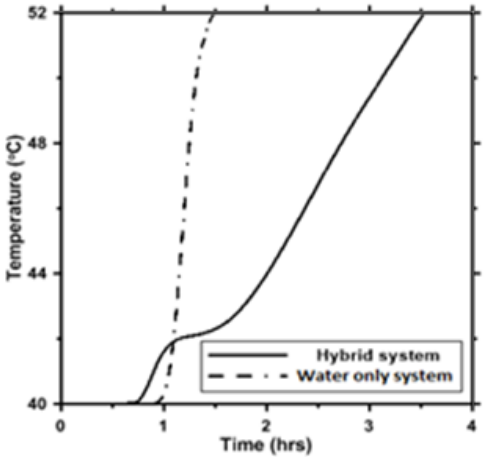

(d) Tank outlet temperature

Figure 3.4: Overall melting performance behaviour ($V_{tank} = 0.2\ m^3$, packing ratio = 30%, $T_{st} = 40\ ℃$, $T_{in} = 52\ ℃$, $T_m = 42\ ℃$, $\dot{m} = 0.05\ kg/s$).

stored in the tank. The energy is stored in both the PCM (62.8%) and the adjacent water (37.2%). In comparison, the same tank containing water only stores about 9.96 MJ. This

corresponds to 93% gain in energy in the hybrid system compared to the water only system, where the gain is defined as:

$$\text{Gain} = \frac{E_{\text{hybrid tank}} - E_{\text{sensible only tank}}}{E_{\text{sensible only tank}}} \tag{3.7}$$

By careful inspection of Figure 3.5(a), it is seen that for the first 0.76 hours the energy of the water only system is the same as the hybrid system. This is because during the initial tank turnover time, both systems have the same fluid exit temperature which is equal to the initial fluid temperature in the tank. This is seen clearly in Figure 3.4(d). For the time period between the turnover times of hybrid system and water only system (0.76 to 1.08 hours respectively), the energy in the water only system slightly exceeds that of the hybrid system (Figure 3.5(a)). This is consistent with the higher outlet temperatures for the hybrid system shown in Figure 3.4(d). After the turnover time of the water only tank (1.08 hours), the energy of the hybrid tank exceeds the water only tank since the water only tank is now fully charged. The instantaneous energy gains as defined in Equation (3.9) are shown in Figure 3.5(b). As seen in the figure, at low times the gains are negligible for the reasons discussed above. Significant gains (up to about 93%) are seen when the PCM has fully melted.

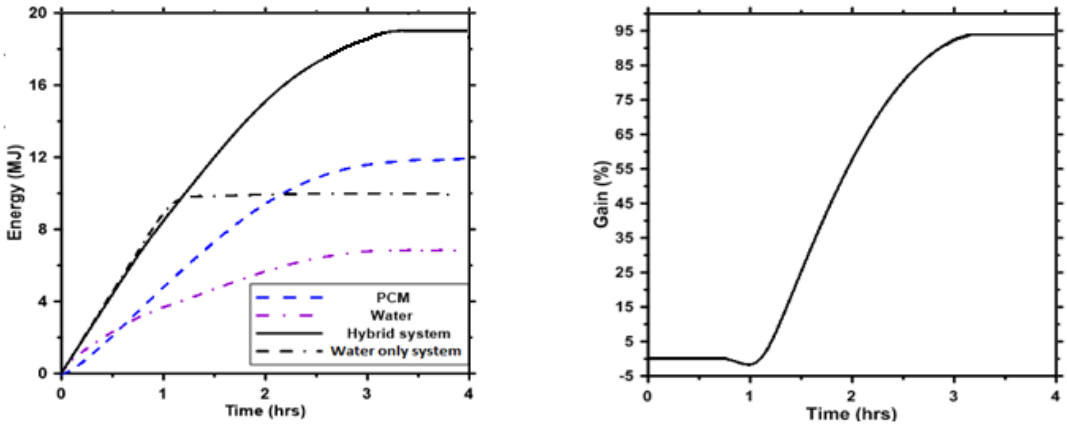

(a) Evolution of energy with time in the system components

(b) Instantaneous gain with time

Figure 3.5: Energy storage gain of hybrid system relative to the only water system ($\mathbf{V_{tank} = 0.2\ m^3}$, packing ratio $= 30\%$, $\mathbf{T_{st}} = 40\ ℃$, $\mathbf{T_{in}} = 52\ ℃$, $\Delta \mathbf{T_{op}} = 12\ ℃$, $\dot{\mathbf{m}} = 0.05\ \mathbf{kg/s}$).

3.4.2.1. Impact of Operating Temperature Range

The previous analysis has shown the potential of a hybrid storage tank for increasing energy density in comparison to a tank containing water only. Figure 3.6 shows the analytical gains of a theoretical hybrid system for different operating temperature ranges. The operating temperature range is the difference between the maximum and the minimum temperature in the system operation. It is chosen to be between 10 ^{o}C and 40 ^{o}C as they are the most common ranges in solar and waste heat recovery applications. Three packing ratios: 30%, 50% and 80% are chosen. The analytical gain corresponds to the gain obtained when sufficient charging time is allowed such that the system becomes

fully charged and can be calculated from Equation (3.10) below. The gains decrease as operating range increases due to the poor sensible properties of PCM compared to water (PCM heat capacity ~1/3 of water heat capacity). Higher packing ratios increase gains especially in the narrow ranges as seen in the spacing between curves. The gain reaches about approximately 250% and 100% in the 10°C range and 20°C range when the packing ratio is 80%. The gains increase in the narrower ranges due to the more pronounced latent heat effect. Also at those ranges the water only system would perform poorly since it is not a favorable operating condition for such system. The reduction in operating temperature range increases the time required to charge the system since the temperature difference is reduced. When operating range increases to 40°C gains drop to only 30% which may not make the usage of the hybrid system justifiable on the economic bases (Sharma et al. 2009).

$$\text{Analytical gain} = \frac{E_{\text{hybrid system}} - E_{\text{sensible only system}}}{E_{\text{sensible only system}}} \tag{3.8}$$

$$E_{\text{hybrid system}} = \varphi \text{ vol } \rho_{PCM}\left(C_{p,s}(T_m - T_{st}) + C_{p,l}(T_{in} - T_m) + r_s\right) + (1-\varphi) * \text{vol} * \rho_{HTF} * C_{P,\,HTF}(T_{in} - T_{st}) \tag{3.9}$$

$$E_{\text{sensible only system}} = \rho_{HTF} * \text{vol} * C_{P,\,HTF}(T_{in} - T_{st}) \tag{3.10}$$

$$\text{Gain} = \frac{\varphi\,\rho_{PCM} C_{p,s}(T_m - T_{st})}{\rho_{HTF} C_{P,\,HTF}(T_{in} - T_{st})} + \frac{\varphi\,\rho_{PCM} C_{p,l}(T_{in} - T_m)}{\rho_{HTF} C_{P,\,HTF}(T_{in} - T_{st})} + \frac{\varphi\,\rho_{PCM} r_s}{\rho_{HTF} C_{P,\,HTF}(T_{in} - T_{st})} - \varphi \tag{3.11}$$

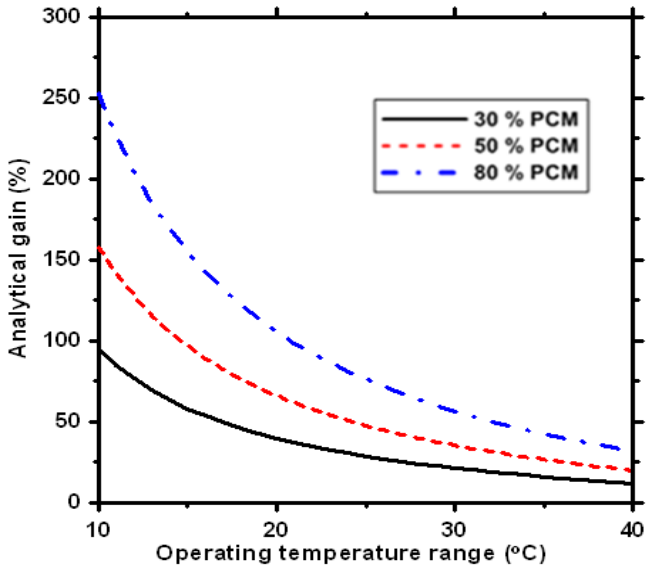

Figure 3.6: Analytical gains for different PCM volume fractions and temperature ranges using lauric acid (Table 3.2).

3.5. Sensitivity analysis of hybrid system

This section presents sensitivity analysis on the hybrid system to assess its performance in a broad range of applications. A maximum charging period of 12 hours was chosen as it is reasonable for solar availability and also commercial applications. An operating temperature range of 10°C to 40°C was chosen to cover most of those applications. Simulations were done on 0.25°C operating temperature range increments to generate molten fraction and gain contour plots. The tested key parameters are summarized in Table 3.3. The properties of the used PCM are stated in Table 3.4.

Table 3.3: Studied parameters in the sensitivity analysis

Parameter	Studied range
Mass flow rate	0.05 kg/s- 0.5 kg/s
PCM module diameter	2 cm – 16 cm
PCM melting temperature	$\frac{4T_{st} + T_{in}}{5} - \frac{T_{st} + 4T_{in}}{5}$
HTF thermal capacity	2000 kJ/ ^{o}C-6000 kJ/ ^{o}C

Table 3.4: Thermo-physical properties of the used PCM

Density (kg/m^3)	Specific heat capacity (kJ/kg ^{o}C)	Latent heat of fusion (kJ/kg)	Thermal conductivity (W/ m K)
870	1.6 (solid), 2.3(liquid)	178	0.147

For a base case, a 200 liter tank with 50% PCM in 2 cm diameter modules was considered. The tank's initial water temperature is 20^{o}C and the inlet water temperature exceeds the initial temperature by the temperature operating range (i.e. varies from 30^{o}C to 60^{o}C). The melt temperature of PCM is taken as the average of the initial and inlet

water temperatures in each operating range. The mass flow rate is 0.05 kg/s. Figure 3.7(a) shows the predicted molten fraction with different combinations of operating temperature ranges and charging times. As expected, as the operating temperature decreases, the time to fully melt PCM increases non-linearly. For example, it takes approximately 2.7 hours to fully melt in the 40^{o}C range, compared to 7.3 hours when the operating range is reduced to 10^{o}C.

Figure 3.7(b) shows the expected gains compared to the water only system. For a fixed operating temperature range, as the charging time increases the gain follows a curve similar to that shown in Figure 3.5(b). That is, the gains are initially zero (during the tank turnover time), followed by slightly negative values. As the charging time increases further, the gains become positive while the PCM is melting and then reach a fixed value when the hybrid tank is fully charged. This coincides with the vertical contours seen in Figure 3.7(b). The horizontal shape of the contours is a result of the fluid transit times (which are independent of operating temperature range).

3.5.1. Effect of mass flowrate

Figure 3.8 shows the effect of doubling mass flow rate on the tank. The two top contour plots show the predicted molten fraction. Increasing the flowrate from 0.05 kg/s to 0.1 kg/s reduces the melting time non-linearly to around 57%. Full melting is achieved at 4.2 hours instead of 7.3 hours for the 10^{o}C range and at 1.6 hours instead of 2.7 hours for the 40^{o}C range. The bottom contour plots show the expected gains compared to the water only system. The higher flowrate causes a reduction of the regions of the negative gains

owing to the lower turnover times. Also the higher gains are reached earlier as the melting time decreases.

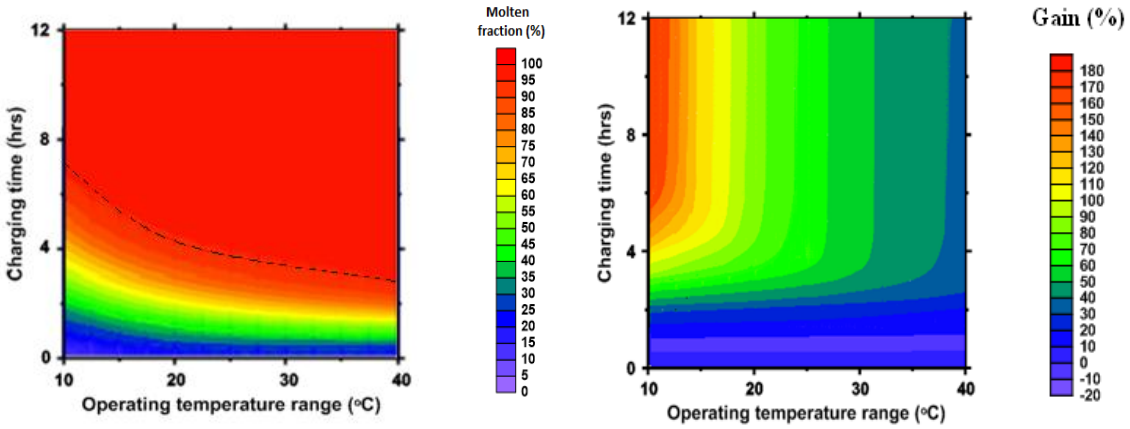

a) Molten fraction b) Gains

Figure 3.7: Melt fraction and gains in a 200 liter tank having 50% PCM (T_{st} = 20℃, $T_m = \frac{T_{st}+T_{in}}{2}$, $\Delta T_{op} = T_{in} - T_{st}$, $\dot{m} = 0.05$ kg/s).

3.5.2. Effect of PCM module diameter and melting temperature choice

Melting times are highly affected by the PCM module diameter as thicker modules increase the internal heat transfer resistance within the PCM. In addition, the heat transfer coefficients at the surface of the modules decreases as the module diameter increases. For example, for module diameters of 2 cm, 4 cm, and 8cm, the corresponding heat transfer coefficients are 387 W/m^{2}K, 182 W/m^{2}K and 84 W/m^{2}K respectively. The combination of higher heat transfer coefficients and surface area for the small diameter modules, leads to a significant impact on melt time. Figure 3.9 shows that, for the 10^{o}C operating range, a charging time of 7.3 hours is sufficient to fully melt PCM in the 2 cm

case. PCM needs 9.8 hours to be fully molten in the 4 cm case. But for the 8 cm case only 72% percent of the

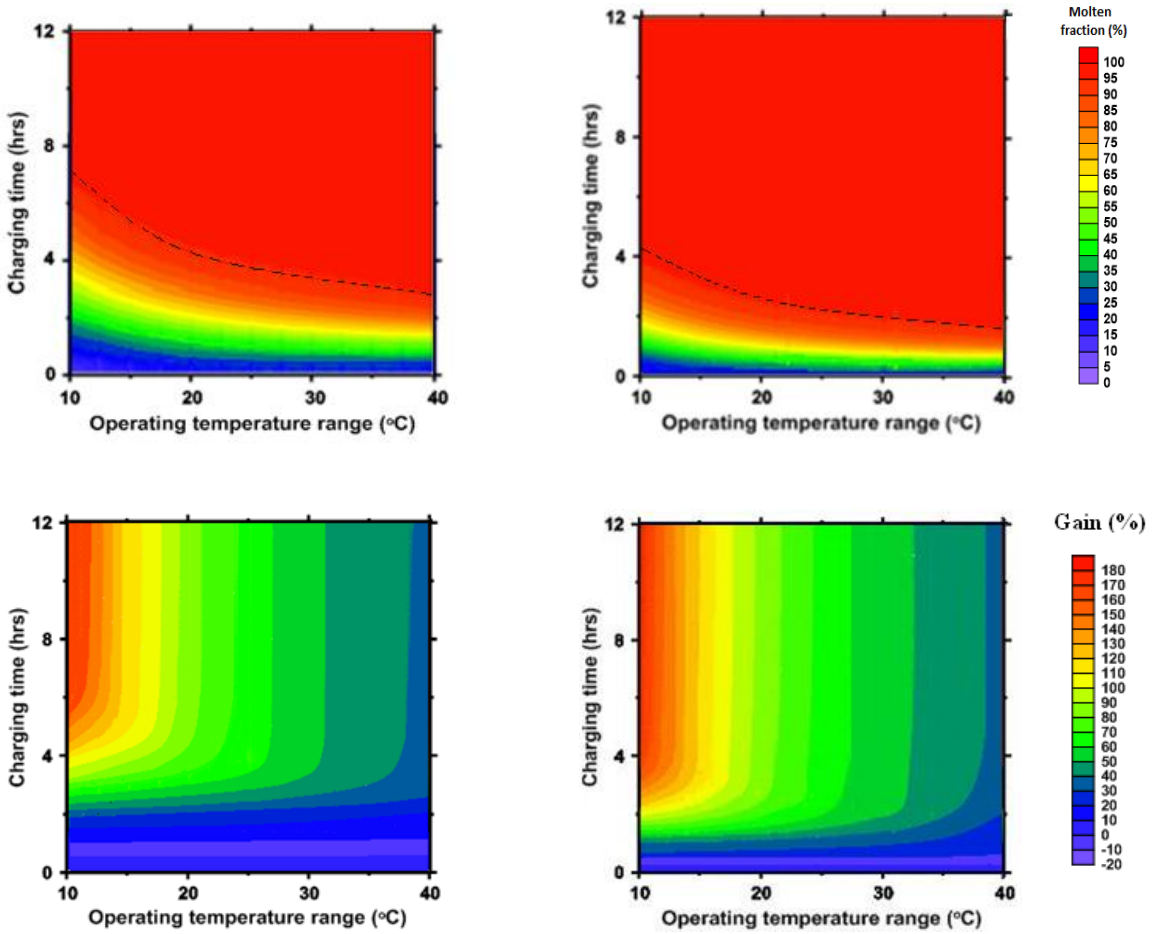

a) $\dot{m}$= 0.05 kg/s (base case)

b) $\dot{m}$= 0.1 kg/s

Figure 3.8: Melt fraction and gains for different mass flowrates in a 200 liter tank having 50% PCM ($T_{st} = 20℃, T_m = \frac{T_{st}+T_{in}}{2}, \Delta T_{op} = T_{in} - T_{st}$).

PCM is molten after the 12 hours charging period. The bottom contours show the adverse effect of increasing module diameter on diminishing the regions of high gains. A maximum gain of 106% can be achieved for the 8 cm compared to 179% in the 2 cm case in the considered range.

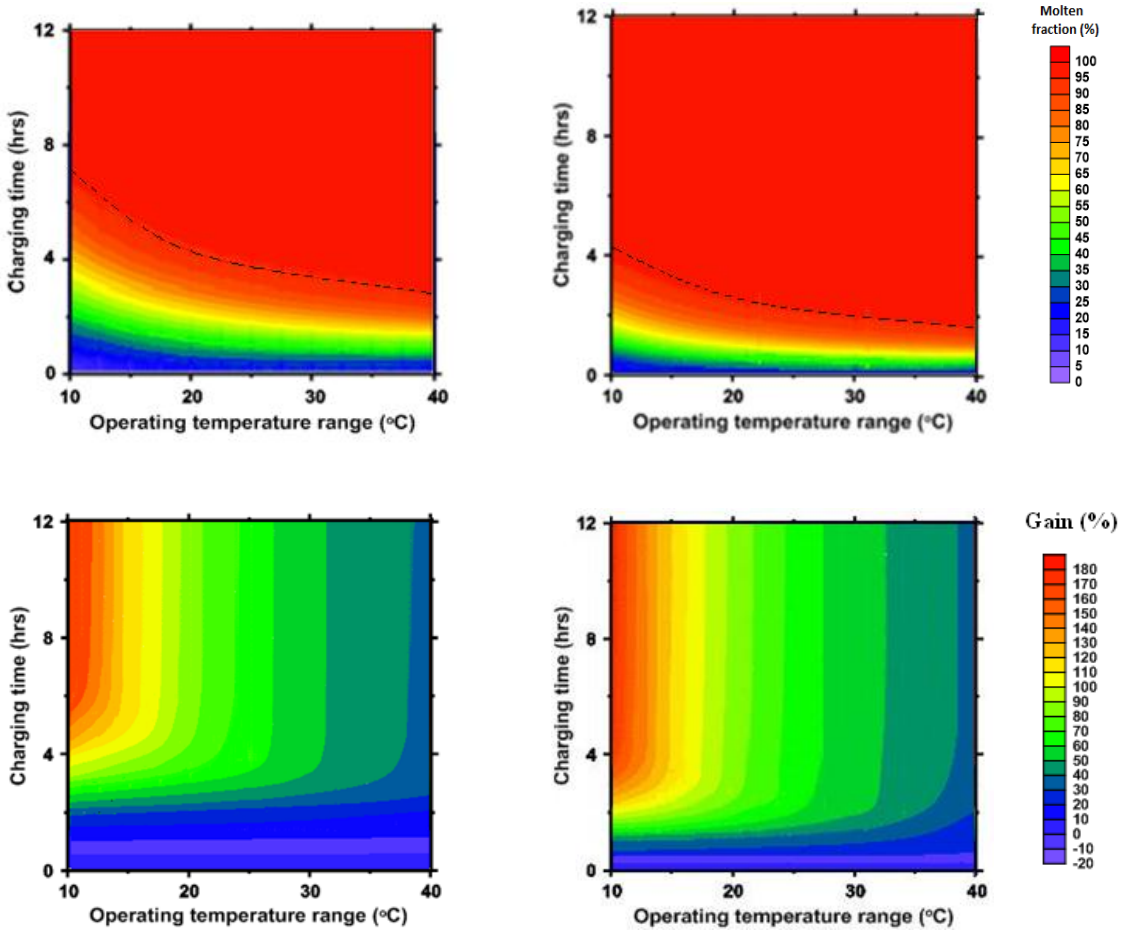

a) $\dot{m}$= 0.05 kg/s (base case)

b) $\dot{m}$= 0.1 kg/s

Figure 3.9: Melt fraction and gains for different module diameters in a 200 liter tank having 50% PCM ($T_{st} = 20℃, T_m = \frac{T_{st}+T_{in}}{2}, \Delta T_{op} = T_{in} - T_{st}, \dot{m} = 0.05\ kg/s$)

The choice of the PCM melting temperature for a given charging period is very critical especially for thicker modules. The effect is shown on the case of 8 cm diameter modules

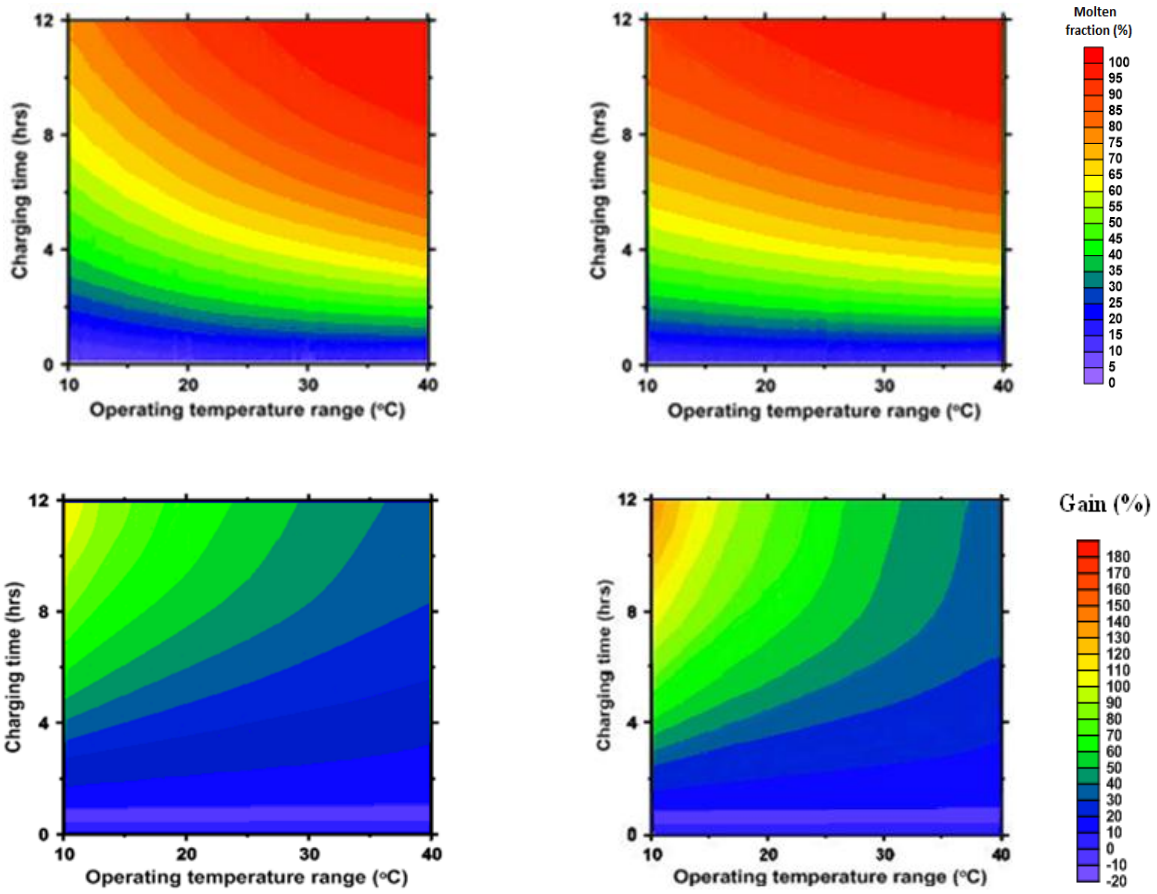

a) $T_m = \frac{T_{st}+T_{in}}{2}$ b) $T_m = \frac{3T_{st}+T_{in}}{4}$

Figure 3.10: Melt fraction and gains for different melting temperature choice in a 200 liter tank having 50% PCM ($T_{st} = 20℃, \dot{m} = 0.05\frac{kg}{s}, \Delta T_{op} = T_{in} - T_{st}$, D = 8cm, $\dot{m} = 0.05$ kg/s).

as the molten fraction was only 72% percent after the 12 hours in the 10°C operating range. The top contours in Figure 3.10 shows that the molten fraction increased from

72% to 86%.when the melting point of PCM is shifted closer to the start temperature ($T_m = \frac{3T_{st}+T_{in}}{4}$ instead of $T_m = \frac{T_{st}+T_{in}}{2}$). This is because of the higher temperature difference between the inlet temperature and melt temperature of the PCM which accelerates melting. The expected gains are shown in the bottom contours. Maximum gain increases from 106% to 137% in the considered operating range.

3.5.3. Effect of HTF thermal capacity

The gain is found to be greatly affected by the thermal capacity of the heat transfer fluid (Equation 3.11). It is seen from the contours in Figure 3.11 that the gains increase dramatically by using HTF with thermal capacity less than water. When the thermal capacity of the HTF is two thirds that of the corresponding water, maximum gains reach 256% instead of 179% in the 10^{o}C operating range. It also increases to 410% when the fluid has half water thermal capacity. This highlights the fact that incorporating PCMs in water tanks is challenging unless the operating temperature range is narrow (water thermal capacity ~3 times PCM thermal capacity). It should be taken into consideration by researchers incorporating PCMs in water tanks to find a smart way to control the operating temperature range for the maximum benefit from the PCM. When the operating temperature range increases to 40 ^{o}C gains drop to around 50% which may not be economically justifiable.

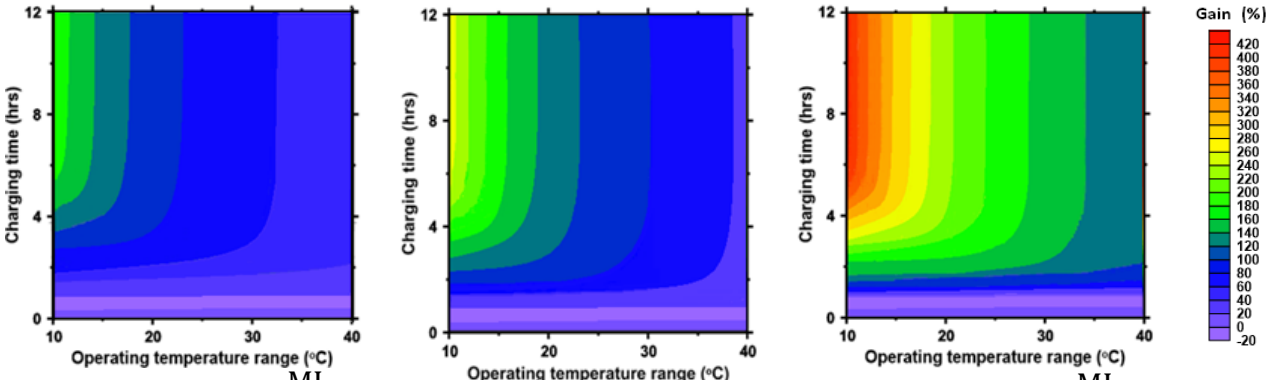

a) $\rho_{HTF}C_{P,\,HTF} = 4.2\ ^{MJ}/_{kg}$ b) $\rho_{HTF}C_{P,\,HTF} = 3.1\ ^{MJ}/_{kg}$ c) $\rho_{HTF}C_{P,\,HTF} = 2.1\ ^{MJ}/_{kg}$

(base case)

Figure 3.11: Gains for different heat transfer fluids in a 200 liter tank having 50% PCM ($\mathbf{T_{st} = 20℃, \dot{m} = 0.05\frac{kg}{s}, \Delta T_{op} = T_{in} - T_{st},\ D = 2cm, , \dot{m} = 0.05\ kg/s}$).

3.6. Non dimensional analysis

By considering the equation for calculating the gain (Equation 3.13), it is seen that the gain is a function of the PCM packing ratio, operating range, melt temperature, and the thermal capacity ratio of PCM to HTF. It is a function of the charging time which is prescribed in the analysis as well.

Due to the scarcity of non-dimensional analysis for the studied system, a way to correlate those key parameters is required. Based on the data of 270 gain contour plots with different combinations of key parameters, a gains map shown in Figure 3.12 is introduced. The dimensionless parameters governing the system performance are as follows:

$$\theta_m = \frac{T_{in} - T_m}{T_{in} - T_{st}} \tag{3.12}$$

θ_m is an indicator of the choice of the melting point relative to the inlet temperature and start (i.e., initial) temperature of the tank.

$$\widetilde{C_{PCM}} = C_{p,s}\,(1 - \theta_m) + C_{p,l}\,\theta_m \tag{3.13}$$

$\widetilde{C_{PCM}}$ is the effective specific heat capacity of the PCM based on the melt temperature choice in the operating range (specific heat capacities of solid and liquid PCM are not always equal).

$$\widetilde{Ste} = \frac{\widetilde{C_{PCM}}(T_{in} - T_{st})}{r_s} \tag{3.14}$$

Stephan number is the ratio of sensible to latent storage capability. It is calculated in terms of the whole operating range and effective specific heat capacity of PCM.

$$(\rho C_P)^* = \frac{\rho_{PCM}\widetilde{C_{PCM}}}{\rho_{HTF} C_{P,\,HTF}} \tag{3.15}$$

$(\rho C_P)^*$ is the ratio between the PCM effective thermal capacity to that of the HTF.

$$Fo = \frac{\alpha t}{\left(\frac{V}{A}\right)^2} \tag{3.16}$$

Fourier number is an indicator of the charging period. The characteristic length in the Fourier number is set to $\frac{V}{A}$ since it is representative of the module diameter ($\frac{D}{4}$).

By combining the key parameters to create two non-dimensional groups, the gain was found to be well described by the combination of ($FoRe_c^{0.8}\theta_m$) and $\widetilde{Ste}/(\rho C_P)^*$. The contour map (Figure 3.12) was obtained through a best-fit using the Eureqa formulize [software]. The map fits the simulation results with a maximum deviation from the raw data of 5.9%. The applicability of this map was tested for the ranges of $0.1<\widetilde{Ste}<0.4$, $0<Fo<600$, $20<Re<4000$, $0.2 < (\rho C_P)^* < 0.8$ and $0.2 < \theta_m < 0.8$.

Figure 3.12 shows that when the Stephan number increases (coinciding for example with an increased operating temperature range), the expected gains from the system decrease. By using a heat transfer fluid whose thermal storage capacity is high compared to that of the PCM, the expected gains decrease as well. Increasing the charge time and/or decreasing the module diameter results in an increase in the Fourier number. This acts to increase the gain in energy storage. The effect of PCM volume fraction is embedded in the Reynolds number through the reduction in flow area and its corresponding impact on fluid velocity. Note that the $Re^{0.8}$ dependence is a result of the heat transfer correlations. Finally, as expected, when the melt temperature is situated nearer to the start temperature it results in higher expected gains at lower charging times.

3.7. Conclusion

A parametric study is conducted on a hybrid tank used for residential applications. Gains are assessed compared to the sensible only system. Gains can reach as high as 179% by using 50% packing ratio and 10^oC operating temperature range in water tanks. The gains are very sensitive to the module diameter; smaller diameters increase the expected gains

because of the higher heat transfer area and reduced internal heat transfer resistance. Gains

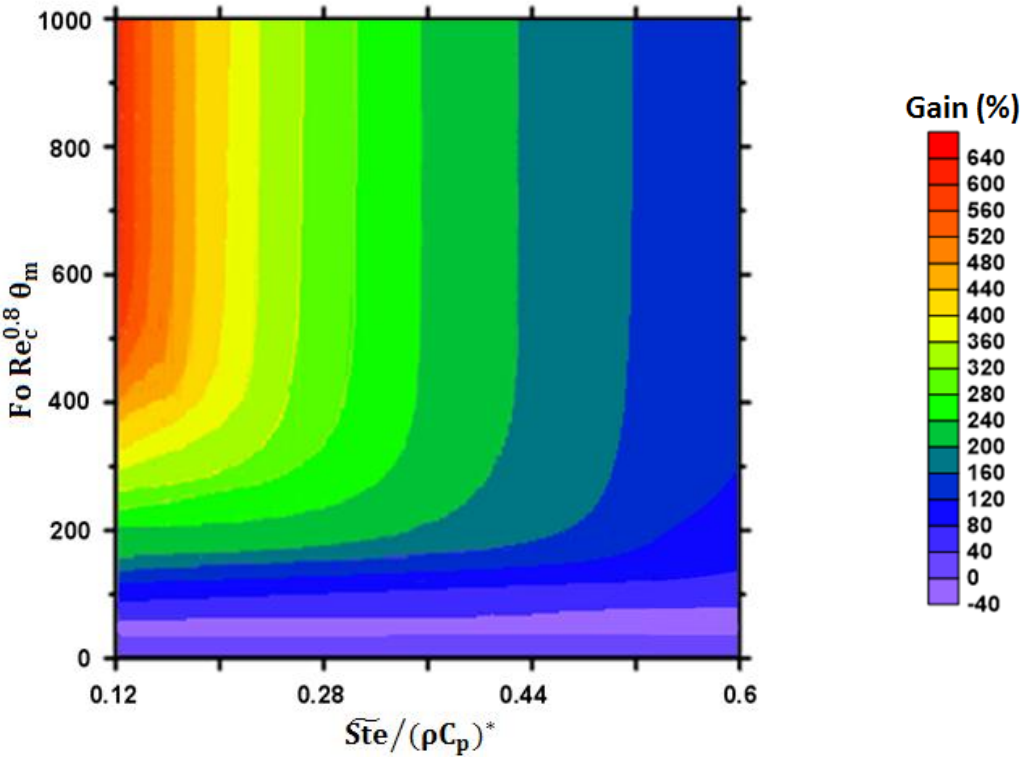

Figure 3.12: Non dimensional map for the expected gains of the system as a combination of key parameters

are almost halved as diameter increases four times. Higher mass flow rates reduce the melting times non-linearly because of the higher heat transfer coefficient. Including PCM in a tank modulates the tank outlet temperature around its melting point due to the high heat transfer during phase change. This is very useful in solar applications as it increases

the collector efficiency by sending colder water to it. When the charging period of the system is between the tank turnover times of the hybrid system and the water only system, incorporation of PCM yields negative gain. A non-dimensional map for the gain is introduced to gather the effects of various key parameters. Its applicability was tested for the ranges of $0.1<\widetilde{Ste}<0.4$, $0<Fo<600$, $20<Re<4000$, $0.2 < (\rho C_P)^* < 0.8$ and $0.2 < \theta_m < 0.8$ with maximum deviation of 5.9%. Note that these results were developed for charging conditions only and energy storage design must also consider discharging conditions.

3.8. Acknowledgement

The authors are grateful to the Natural Sciences and Engineering Research Council of Canada and the Smart Net-Zero Energy Buildings Strategic Research Network (SNEBRN) for their financial support for this work.

3.9. References

[1] NRCan. "Energy Use Data Handbook - 1990 to 2009." Technical report, Office of Energy Efficiency, Natural Resources Canada, Ottawa, ON, Canada. [Online] http://oee.nrcan.gc.ca/Publications/statistics/handbook11/ (2012).

[2] Zalba, B., Marin, J. M., Cabeza, L. F., and Mehling, H., 2003, "Review on thermal energy storage with phase change: materials, heat transfer analysis and applications", Applied Thermal Engineering, 23(3), pp. 251-283.

[3] Abhat, A., 1983,“Low temperature latent heat thermal energy storage: Heat storage materials”, Solar Energy, 30(4), pp. 313-332.

[4] Sharma, A., Tyagi, V.V., Chen, C.R., and Buddhi, D., 2009, “Review on thermal energy storage with phase change materials and applications”, Renewable and Sustainable Energy Reviews, 13(2), pp. 318-345.

[5] Zhang, Z.G., and Fang, X.M., 2006, “Study on paraffin/expanded graphite composite phase change thermal energy storage material”, Energy Conversion and Management, 47, pp. 303-310.

[6] Kousksou, T., Jamil, A., Eirhafiki, T., and Zeraouli, Y. , 2010, “Paraffin wax mixtures as phase change materials”, Solar Energy Materials and Solar Cells, 94, pp. 2158-2165.

[7] Lane, G. A., 1983," Solar heat storage: latent heat materials", vol. I. Boca Raton, FL: CRC Press, Inc.

[8] Feldman, D., Banu, D., and Hawes, D., 1995, “Low chain esters of stearic acid as phase change materials for thermal energy storage in buildings”, Solar Energy Materials and Solar Cells, 36, pp. 311-322.

[9] Feldman, D., Banu, D., and Hawes, D., 1995, “Development and application of organic phase change mixtures in thermal storage gypsum wallboard”, Solar Energy Materials and Solar Cells, 36, pp. 147-157.

[10] Alkan, C., and Sari, A., 2008, “Fatty acid/poly (methyl methacrylate) (PMMA)

blends as form-stable phase change materials for latent heat thermal energy storage", Solar Energy, 82, pp. 118-124.

[11] Baetens, R., Jelle, B., and Gustavsen, A., 2010, "Phase change materials for building applications: A state-of-the-art review", Energy and Buildings, 42, pp. 1361-1368.

[12] Desgrosseillier, L., Murray, R., Safatli, A., Marin, G., Stewart, J., Osbourne, N., White, M.A., Groulx, D. , 2011, "Phase Change Material Selection in the Design of a Latent Heat Energy Storage System Coupled with a Domestic Hot Water Solar Thermal System", ASHRAE Annual Conference, Montreal, Canada.

[13] Sari, A., and Kaygusuz, K., 2002, "Thermal and heat transfer characteristics in a latent heat storage system using lauric acid", Energy Conversion and Management,43, pp. 2493-2507.

[14] Sari, A., and Kaygusuz, K., 2003, "Some fatty acids used for latent heat storage: thermal stability and corrosion of metals with respect to thermal cycling", Renewable Energy, 28, pp. 939-948.

[15] Sari, A., and Karaipekli, A., 2009, "Preparation, thermal properties and thermal reliability of palmitic acid/expanded graphite composite as form-stable PCM for thermal energy storage",Solar Energy Materials and Solar Cells, 93, pp. 571-576.

[16] Nakhla, D., Sadek, H., and Cotton, J. S., 2015,"Melting performance enhancement in latent heat storage module using solid extraction

electrohydrodynamics (EHD) ” International Journal of Heat and Mass Transfer, 81, pp. 695-704.

[17] Bergles, A. E., 2011, "Recent developments in enhanced heat transfer," International Journal of Heat and Mass Transfer, 47(8), pp. 1001-1008.

[18] Jegadheeswaran, S., and Pohekar, S. D. , 2009, "Performance enhancement in latent heat thermal storage system: A review," Renewable and Sustainable Energy Reviews, 13(9), pp. 2225–2244.

[19] Agyenim, F., Hewitt, N., Eames, P. and Smyth, M., 2010,"A review of materials, heat transfer and phase change problem formulation for latent heat thermal energy storage systems (LHTESS)," Renewable and Sustainable Energy Reviews, 14(2), pp. 615–628.

[20] Sanusi, O., Warzoha, R., and Fleischer, A. S. , 2011, "Energy storage and solidification of paraffin phase change material embedded with graphite nano-fibers," International Journal of Heat and Mass Transfer, 54(19), pp. 4429–4436.

[21] Pokhrel, R., Gonzalez, J. E., Hight, T., and Adalsteinsonn,T., 2010, " Analysis and Design of a Paraffin/Graphite Composite PCM Integrated in a Thermal Storage Unit," ASME J. Sol. Energy Eng., 132(4), pp. 041006.

[22] Velraj, R., Seeniraj, R. V., Hafner, B., Faber, C., and Schwarzer, K., 1999, "Heat Transfer Enhancement in a Latent Heat Storage System," Solar Energy, 65(3), pp. 171–180.

[23] Stritih, U., 2004, "An experimental study of enhanced heat transfer in rectangular PCM thermal storage," International Journal of Heat and Mass Transfer, 47 (12), pp. 2841–2847.

[24] Yingqiu, Z.,Yinping, Z., Yi, J., and Yanbing, K., 1999, " Thermal Storage and Heat Transfer in Phase Change Material Outside a Circular Tube with Axial Variation of the Heat Transfer Fluid Temperature", ASME J. Sol. Energy Eng., 121(3), pp. 145-149.

[25] Lacroix, M. and Benmadda, M., 1997, "Numerical Simulation of Natural Convection-Dominated Melting and Solidification From a Finned Vertical Wall," Numerical Heat Transfer, Part A: Applications, 31(1), pp. 71-86.

[26] Nallusamy, N., Sampath, S., Velraj, R., 2007, “Experimental investigation on a combined sensible and latent heat storage system integrated with constant/varying (solar) heat sources”, Renewable Energy, 32(7), pp. 1206-1227.

[27] Michels, H., Pitz-Paal, R.,2007, “Cascaded latent heat storage for parabolic trough solar power plants”, Solar Energy, 81(6), pp. 829-837.

[28] Seeniraj, R.V., Narasimhan, N.L., 2008, “Performance enhancement of a solar dynamic LHTS module having both fins and multiple PCMs”, Solar Energy, 82(6), pp. 535-542.

[29] Dutil, Y., Rousse, D.R., Salah, N.B., Lassue, S., and Zalewski, L., 2011 ,“A review on phase-change materials: Mathematical modeling and simulations”,

Renewable and Sustainable Energy Reviews, 15, pp. 112-130.

[30] Morgan, K., 1981, "A numerical analysis of freezing and melting with convection". Computational methods in applied engineering, 28, pp. 275-284.

[31] Voller, V. R., Markatos, N. C., and Cross, M., 1985 " Techniques for accounting for the moving interface in convection/diffusion phase change". Numerical Methods in Thermal Problems, 4, pp. 595-609.

[32] Voller, V. R. , Markatos, N. C., and Cross, M., 1986, "Solidification in convection and diffusion". Numerical Simulations of Fluid Flow and Heat/Mass Transfer Processes, 24, pp. 425-432.

[33] Voller, V. R., Cross, M., and Markatos, N. C., 1987, "An enthalpy method for convection/diffusion phase changes". International Journal of Numerical Methods in Engineering, 24, pp. 271-284.

[34] Bonacina, C., Cornini, G., Fasano, A, and Primicero, M., 1973, "Numerical Solution of Phase-Change Problems," Int. Journal of Heat and Mass Transfer, 16, pp. 1825- 1832.

[35] Cornini, G., Guidiq, S.D., Lewis, RW., and Zienkiewiq, O.C., 1974, "Finite Element Solution of Non-linear Heat Conduction Problems with Reference to Phase Change," International Journal for Numerical Methods in Engineering., 8, pp. 613-624.

[36] Morgan, K., Lewis, R.W., and Zienkiewicq, O.C., 1978, "An Improved Algorithm for Heat Conduction Problems with Phase Change," International Journal for Numerical Methods in Engineering, 12, pp. 1191 -1195.

[37] Lemmon, E.C., 1981, "Multidimensional Integral Phase Change Approximations for Finite Element Conduction Codes," Numerical Methods in Heat Transfer, Wiley, Chichester, pp. 201-213.

[38] Pham, Q.T., 1986, "The Use of Lumped Capacitance in the Finite-Element Solution of Heat Conduction Problems with Phase Change," International Journal of Heat and Mass Transfer, 29, pp. 285-291.

[39] Jones, B. J., Sun, D., Krishnan, S., and Garimella, S.V. , 2006, " Experimental and numerical study of melting in a cylinder", International Journal of Heat and Mass Transfer, 49 , pp. 2724–2738.

[40] Dhaidan, S. N., and Khodadadi, J. M., 2015, "Melting and convection of phase change materials in different shape containers: A review", Renewable and Sustainable Energy Reviews, 43, pp. 449-477.

[41] Rohsenow, W. M., Hartnett, J.P., and Ganic, E. N.,1985, Handbook of heat transfer fundamentals, 2nd edn, (Eds). New York.

[42] Esen, M., Ayhan, T., 1996, "Development of a model compatible with solar assisted cylindrical energy storage tank and variation of stored energy with time for different phase change materials", Energy Conversion and Management,

37(12), pp. 1775-1785.

[43] Castell, A., Sole, C., Medrano, M., Nogues, N., and Cabeza L.F., 2009,"Comparison of Stratification in a Water Tank and a PCM-Water Tank" ASME J. Sol. Energy Eng., 131(2), pp. 024501-024501-5.

[44] Hollands, K.G.T., and Lightstone, M.F., 1989, "A Review of Low-Flow, Stratified-Tank Solar Water Heating Systems". Solar Energy, 43(2), pp. 97-105.

[45] Furbo, S., Vejen, N., and Shah L., 2005, "Thermal Performance of a Large Low Flow Solar Heating System With a Highly Thermally Stratified Tank", ASME J. Sol. Energy Eng., 127(1), pp.15-20.

[46] Shmidt, M., Lipson,H.,2013, Eureqa[software]. http://www.nutonian.com/products/eureqa/

Appendix

Enthalpy porosity model

According to the enthalpy porosity formulation (Esen and Ayhan 1996)specific enthalpy (enthalpy per unit mass) is defined based on the cell condition (solid, liquid or transition) as follows:

$$i(T) = C_{p,s}T \qquad T < T_{m1} \qquad (A.1)$$

$$i(T) = C_{p,s}T_{m1} + \frac{r_s(T - T_{m1})}{\Delta T_m} \qquad T_{m1} < T < T_{m2} \tag{A. 2}$$

$$i(T) = C_{p,l}(T - T_{m2}) + r_s + C_{p,s}T_{m1} \qquad T > T_{m2} \tag{A. 3}$$

where

r_s is the latent heat, T_{m1} is the lower melting temperature and $T_{m2}$is the upper melting temperature.

The finite difference formulation for conduction dominated melting is given by ;

$$\rho V_{j,k}\left.\frac{\partial i}{\partial t}\right|_{j,k} = -KA_k\left.\frac{\partial T}{\partial R}\right|_k + KA_{k-1}\left.\frac{\partial T}{\partial R}\right|_{k-1} + KA_j\left.\frac{\partial T}{\partial Z}\right|_j - KA_{j-1}\left.\frac{\partial T}{\partial Z}\right|_{j-1} \tag{A. 4}$$

Central differencing is applied to approximate the derivatives above.

The code solves the enthalpy porosity equations together with the conduction dominated melting equation. A uniform grid is applied. The heat transfer to the PCM is calculated using the correlations developed by Rohsenow et al. 1985.

Validation of the melting behavior

The code was validated by comparing predictions of temporal molten fraction to the data presented by Jones et al. 2006. The schematic of their test facility is shown in Figure 3.A.1. The PCM used in the experiment, n-eicosane, was contained inside a transparent

polycarbonate vertical cylinder with an acrylic base and top. The melt temperature of the PCM is 36.4^{o}C. The bottom of the cylinder was maintained at a temperature of 32^{o}C and the exterior of the vertical walls were held at a uniform temperature of 45^{o}C. This experiment has a Stefan number of 0.0836, which was recommended by the authors for numerical benchmarking as it was well controlled. The top of the cylinder was insulated to reduce the heat losses. The PCM was initially a solid at a subcooled temperature of 23^{o}C. Temperature within the PCM was measured using thermocouple racks. The melt front locations were tracked through digital photography. This allowed for the determination of the molten fraction of the PCM as a function of time. They also developed a numerical model and compared its predictions with experiments.

The melting experiment was simulated in the present code. A grid independent solution was obtained. A grid of (250X150) in radial and axial directions is sufficient to solve for melting in the PCM domain. The polycarbonate wall was discretized into (20X150) nodes radially and axially. The acrylic base was discretized to (250X20) in radial and axial directions respectively. A time step of 0.08 seconds was used. Care was taken to ensure that the simulation results were unaffected by further changes in time step.

The effect of natural convection in their simulation was included in the enthalpy porosity model by the effective conductivity method. The effective thermal conductivity in the molten PCM is represented by a correlation as a function of liquid thermal conductivity and Rayleigh number. The empirical correlation used for melting in vertical cylinders provided by Dhaidan and Khodadadi 2015 was used.

$$\frac{K_{eff}}{K_l} = 0.05\ Ra^{0.25} \tag{A.5}$$

$$Ra = \frac{g\beta l^3 (T_w - T_m)}{\nu\alpha} \tag{A.6}$$

Where β is the thermal expansivity, l is the height of the PCM tube, T_w is the wall temperature, T_m is the melting temperature, ν is the kinematic viscosity, and α is the thermal diffusivity.

Figure 3.A.2a shows the comparison of the average molten fraction prediction in the present code and their experimental and numerical results. Good agreement with the experiments is seen with a maximum deviation of about 5% at the later stages of melting. The predicted and experimentally observed melt front at three different times are overlapped in Figures (3.A.2b, 3.A.2c and 3.A.2d) with a very good agreement especially in the first two instances. The slight deviation observed at 10800 seconds was also reported in their numerical prediction which was attributed to the modelling assumption that density differences between the phases were neglible.

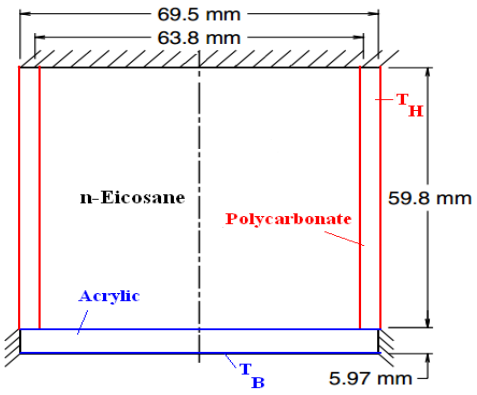

Figure 3.A.1: Schematic of the experimental facility studied by Jones et al 2006.

Verification of hybrid tank model

The simulation of the hybrid tank was verified with the results presented by Esen and Ayhan 1996. They presented numerical predictions of the time for PCMs to fully melt under isothermal charging conditions. The geometry they considered is similar to that shown in Figure 3.1 except that the thermal mass and heat transfer resistance of the encapsulation material was neglected. The results presented focused on prediction of the stored energy when PCM melts under constant temperature charging conditions. Due to the similarities in the geometry studied by Esen et al. and in the current work, the work of Esen et al. represents an excellent case for verification of the present code. The verification case chosen includes a tank of volume 4.25 m^3 and length 3.2 m. The phase change material

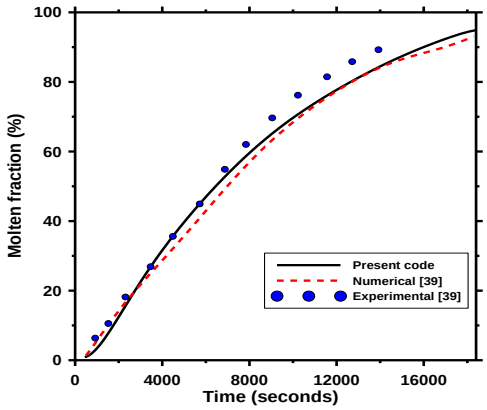

a) Average molten fraction

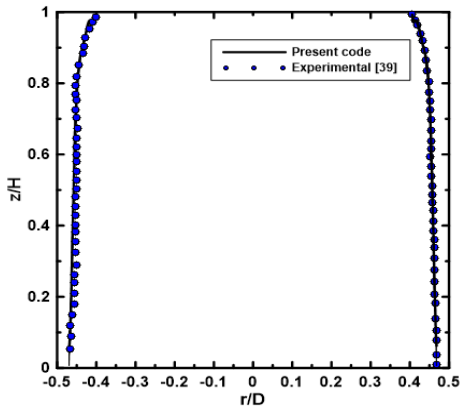

b) Melt front at 3120 seconds

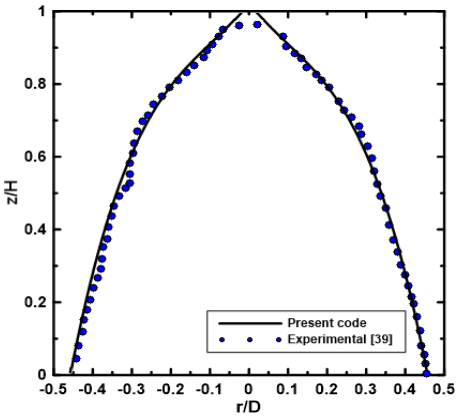

c) Melt front at 7200 seconds

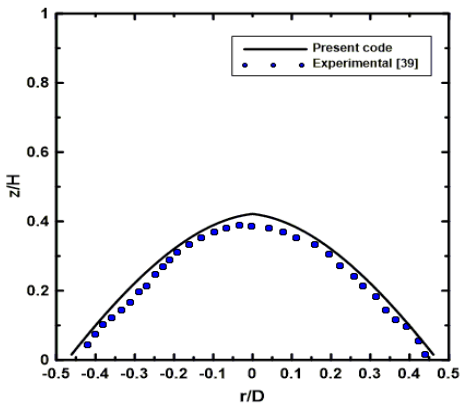

d) Melt front at 10800 seconds

Figure 3.A.2: Comparison of predictions from present code against experimental data of Jones et al. 2006.

occupies 17% by volume and is placed in cylinders of radius 2.4 cm. They considered four different types of PCMs: CCHH, paraffin, SSDH and P-wax, with melting points 29.7^{o}C, 32^{o}C, 39^{o}C and 46.7^{o}C respectively. They changed the inlet water temperature

and flow rate to assess their effect on melting times and stored energy in the tank. Figures 3.A.3a and 3.A.3b show the comparison of stored energy using two different kinds of PCM (P-wax and CCHH) and different inlet temperature conditions (60 ℃ and 50 ℃). Good agreement is found between the present code predictions and their results.

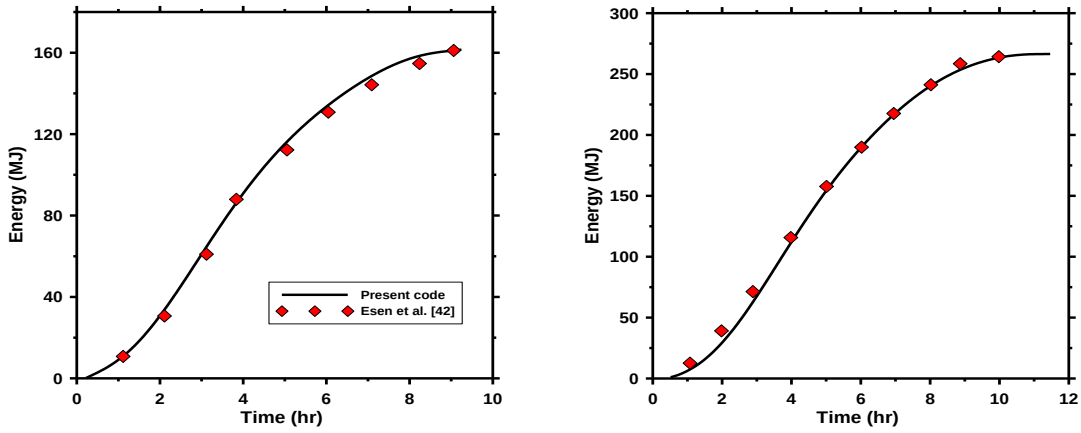

a) Stored energy for P-wax case ($T_{st} = 18\,℃, T_{in} = 60\,℃, T_m = 46.7\,℃, \dot{m} = 0.3055\,\frac{kg}{s}$)

b) Stored energy for CCHH case ($T_{st} = 18\,℃, T_{in} = 50\,℃, T_m = 29.7\,℃, \dot{m} = 0.3055\,\frac{kg}{s}$)

Figure 3.A.3: Comparison of predictions of stored energy from present code and Esen and Ayhan 1996.

Grid and Time step Independence

Grid independence was tested for the base case described in section 3. To assess grid and time step independence, a series of simulations were performed. Figure 3.A.4 shows the predicted molten fraction as a function of time for the various simulations. It was found that a grid of 300 nodes in the radial direction and 100 nodes in the axial direction

together with 0.005 seconds time step was sufficient to solve the problem. The solution did not change with further refinement of the grid and decrease in time step.

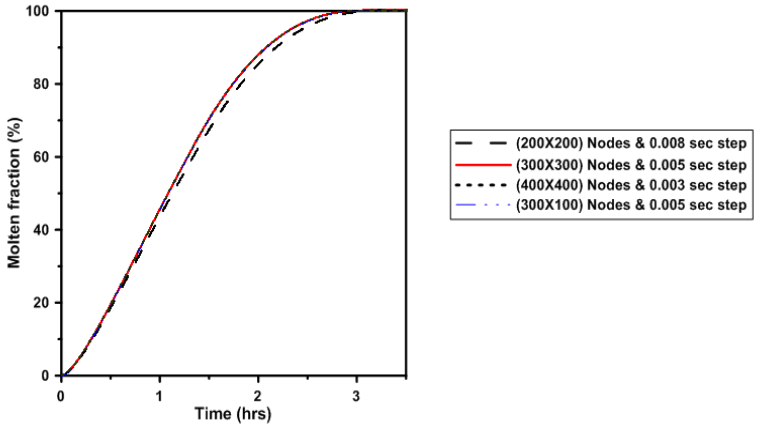

Figure 3.A.4: Grid independence test on average molten fraction ($V_{tank} = 0.2\ m^3$, packing ratio $= 30\%$, $T_{st} = 40$ ℃, $T_{in} = 52$ ℃, $\dot{m} = 0.05\ kg/s$)

Encapsulation material

The impact of the wall material used to encapsulate the PCM was studied by considering three wall materials: copper, aluminum, and plastic. The wall thickness was taken as 1 mm. The total stored energy in the hybrid system for the three cases was compared to a case with zero wall thickness (i.e. the wall thickness is occupied by water instead). Using higher heat capacity materials (copper and aluminum) yields higher storage capacity than the plastic wall case. But overall the three materials give slightly different total stored energy (~3%) as manifested in Figure 3.A.5. Although not shown, the wall material had a negligible impact on the rate of melting of the PCM. This result is expected because

the heat transfer resistance of the PCM, rather than the wall material, dominates the heat transfer process.

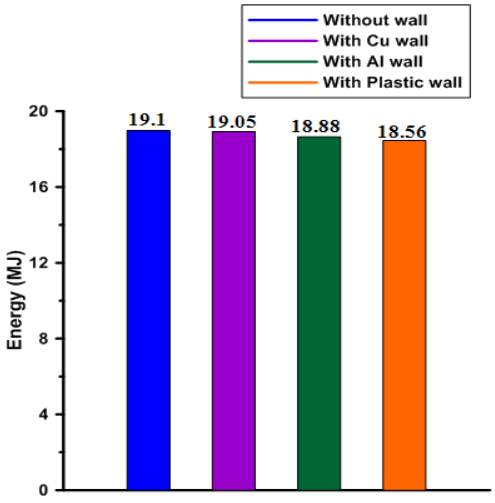

Figure 3.A.5: Effect of wall material on hybrid system total energy ($V_{tank} = 0.2\ m^3, \varphi = 30\%, T_{st} = 40\ ℃, T_{in} = 52\ ℃, \dot{m} = 0.05\ \frac{kg}{s}$, $R_{c,inn}$=1 cm, $R_{c,out} = 1.1$ cm)

CHAPTER 4

An alternative approach for assessing the benefit of phase change materials in solar domestic hot water systems

Complete citation:

H. M. Teamah, M. F. Lightstone, J. S. Cotton , An alternative approach for assessing the benefit of phase change materials in solar domestic hot water systems, Solar Energy- Accepted October 2017.

Relative Contributions:

Teamah HM: Performed all the simulations, interpretation and analysis of the data, wrote the first draft of the manuscript including all figures and text and was responsible for the final draft submittal to the journal.

Lightstone MF: supervisor of Teamah HM, revised and modified the journal paper draft.

Cotton JS: Co-supervisor of Teamah HM, revised and modified the journal paper draft.

Abstract

Phase change materials (PCM) for thermal energy storage in solar energy systems have been the subject of a great deal of research in the literature. Despite this, the research results pertaining to the efficacy of PCMs in enhancing system solar fraction are mixed. The current paper explores this issue numerically within a systems context. A typical solar domestic hot water system is considered. The PCMs are introduced as vertical cylindrical modules contained within the water tank, thus forming a hybrid PCM/water thermal storage. Water flowing along the length of tank is used as the heat transfer fluid. A model was developed based on the enthalpy-porosity method to solve for the phase change process within the PCM modules. The model was thoroughly validated and verified and predictions were in good agreement (less than 5% deviation) with results from the literature. The hybrid tank model was linked with the collector performance and the system was tested for typical days of Canadian weather with a dispersed demand profile. The solar fraction of the hybrid system was compared to that for an identical system using water-only as the thermal storage medium. The system analysis explores the impact of storage volume on solar fraction for systems with and without PCMs included. The systems approach is critical since it allows for the coupled effects of the thermal storage, solar collector, and household load to be incorporated. The analysis clearly shows that incorporation of PCMs into the thermal storage results in enhanced solar fraction at small tank volumes. In contrast, as the tank volume is increased, the benefit of the PCMs diminishes and identical performance is obtained between the two systems at large volumes. An energy balance of the system shows that, despite

marginally increased heat losses from the hybrid tank, the benefits of the hybrid storage at small storage volumes are due to the reduction in the collector fluid inlet temperature which increases the pump run time and thus the solar energy collected.

Keywords

phase change materials, enthalpy porosity, thermal storage, solar fraction, volume reduction

Nomenclature

A_c	Collector surface area [m^2]
C_{pl}	Liquid specific heat capacity [J/kg K]
C_{ps}	Solid specific heat capacity [J/kg K]
D	PCM cylinder outer diameter [m]
$E_{delivered}$	Energy delivered to the load [J]
$E_{loss,\ coll}$	Collector energy loss [J]
$E_{loss,\ tank}$	Tank energy loss [J]
E_{mains}	Mains water energy [J]
E_{solar}	Solar energy incident to the collector [J]
F_R	Heat removal factor
f_s	Solar fraction
$F_{s,annual}$	Annual solar fraction
G	Solar irradiation [W/m^2]

k	Thermal conductivity [W/mK]
L_c	Length of cylinder [m]
	Mass flow rate inlet to the tank [kg/s]
Q_u	Collector useful heat gain [kW]
n	Inner radius of phase change material cylinder [m]
ıt	Outer radius of phase change material cylinder [m]
r_s	Latent heat of fusion [kJ/kg]
T	Temperature [^oC]
T_{amb}	Ambient temperature [^oC]
	Temperature of incoming fluid [^oC]
T_m	Melting temperature of PCM [^oC]
T_{st}	Initial temperature of the tank [^oC]
U_L	Collector loss coefficient [W/m^2K]
V_{tank}	Tank volume [m^3]

Abbreviations

HTF	Heat transfer fluid
LES	Latent energy storage
PCM	Phase change material
SDHW	Solar domestic hot water
SES	Sensible energy storage

TES Thermal energy storage

Latin Symbols

$(\tau\alpha)$ Transmittance absorbance product

η Solar collector efficiency

Subscripts

c,inn Inner surface of cylinder

c,out Outer surface of cylinder

conv Convective

In Inlet

l Liquid

m Melting

st Start

t Transition

4.1. Introduction

Thermal energy storage is an important component of solar domestic hot water systems in order to mitigate the temporal mismatch between solar radiation availability and demand for hot water. For residential applications, energy storage systems typically use

water as a sensible storage medium due to its low cost and high specific heat. Latent energy storage (LES) systems employ phase change materials (PCMs) and the energy is stored and released in the form of latent heat of fusion. This offers higher energy storage density compared to the water only systems. PCMs also modulate the system temperature around its melting temperature (T_m) (Zalba et al. 2003). PCMs are mainly classified as organics, inorganics and eutectics (Abhat 1983). Organic fatty acids have high latent heat of fusion and stable properties and are thus suitable candidates for solar thermal systems (Desgrosseillier et al. 2011, Sari and Kaygusuz 2003, Sari and Karaipekli 2009).

The main challenge associated with PCMs operating at low temperatures (<100^{o}C) is their low specific heat capacity and poor thermal conductivity. The lower heat capacity degrades the energy storage capacity of PCM when the operating temperature range increases. The poor thermal conductivity impacts on the heat transfer rate to the PCMs and thus can limit the storage capacity of the system for a prescribed charging period (Bergles 2011). Extensive research has been conducted to tackle this problem using either active or passive techniques. Active techniques involve an external source such as electro-hydrodynamics to enhance the melting rate (Nakhla et al. 2015). Passive techniques include the use of fins, thermal conductivity enhancement, and micro-encapsulation (Jegadheeswaran and Pohekar 2009, Agyenim et al. 2010, Sanusi et al. 2011, Pokhrel et al. 2010, Velraj et al. 1999, Stritih 2004, Yingqiu et al. 1999, Lacroix and Benmadda 1997). Extended surfaces such as fins increase the heat transfer rate in the thermal system with the increased area (Jegadheeswaran and Pohekar 2009, Agyenim et al. 2010), but result in increased weight and system cost. Embedding metallic particles

enhances the thermal conductivity of PCM, but the particles tend to agglomerate and settle to the bottom of the tank (Sanusi et al. 2011, Pokhrel et al. 2010, Velraj et al. 1999). Alternatively, heat transfer to the PCMs can be enhanced by increasing the surface area of the modules and reducing the conduction distance. This can be accomplished by encapsulating the materials in thin rectangular slabs or small radii cylindrical or spherical containments (Stritih 2004, Yingqiu et al. 1999, Lacroix and Benmadda 1997).

Hybrid tanks containing both water and phase change materials have been studied extensively. The inclusion of PCM in the tank increased the thermal energy stored compared to a water only tank for isothermal charging conditions (Esen and Ayhan 1996, Mehling et al. 2003, Nallusamy and Velraj 2009). The PCM improves the thermal stratification in the tank since it maintains the top layers of the tank at a higher temperature (Mehling et al. 2003). The operating conditions of the system influences its performance. The mass flow rate was found to have a significant effect on the rate of charging TES as it increases the heat transfer coefficient. Thus the melting time decreases as the mass flow rate increases. In contrast, the PCM melting time increases non-linearly with increasing volume fraction due to the additional thermal resistance imposed on the system (Nallusamy, N. N., and Velraj, R. R., 2009).

On the system level, the effect of PCM inclusion in the water tank of a SDHW system was investigated by a number of researchers. Realistic supply and draw-off patterns as well as approximated ones were considered (Wang et al. 2015, Al-Hinti et al. 2010, Fazilati and Alemrajabi 2013, Nabavitabatabayi et al. 2014, Nkwetta et al. 2014,

Talmatsky and Kribus 2008, Kousksou et al. 2011). The PCM increased the exergy efficiency and the storage capacity due to its latent heat and temperature modulation effect (Wang et al. 2015, Al-Hinti et al. 2010, Fazilati and Alemrajabi 2013). It decreased the delivered temperature swing at night due to the released heat of fusion. This increased the periods of times when the PCM is able to supply the load with hot water and thus it increased the amount of energy delivered by the solar system relative to the total energy required by the load, commonly referred to as solar fraction (Al-Hinti et al. 2010, Fazilati and Alemrajabi 2013). PCM was also found to be beneficial in shifting power demand (Nabavitabatabayi et al. 2014, Nkwetta et al. 2014). The high thermal inertia of the hybrid system (containing water and PCMs) reduced the system temperature variation. Thus decreased the auxiliary heat required in peak periods (Nabavitabatabayi et al. 2014, Nkwetta et al. 2014).

Talmatsky and Kribus 2008 raised a question that seemed to contradict the ongoing research on the predicted benefit of PCM incorporation in water tanks. They studied numerically the hybrid tank performance throughout the year and compared the predicted solar fraction to a water only system. They reported only a marginal gain in solar fraction (around 1%) when PCM is present inside the tank. They argued that the benefit brought by PCM during the day is penalized by increased heat loss from the tank at night. This resulted in overall similar performance by the two systems. Kousksou et al. 2011 subsequently determined that the marginal gain reported by Talmatsky and Kribus 2008 was a result of the improper selection of PCM melting temperature. The charging period was not sufficient to fully melt the PCM. This caused the PCM to act as a sensible

storage most of the time. When Kousksou et al. 2011 lowered the PCM melt temperature in Talmatsky's system, a 14% reduction in the annual electricity backup was achieved. A slight increase in the collector efficiency was also noted.

From the previous studies on the systems level, the effects of PCM on solar fraction appear to be mixed. Some researchers found that solar fraction is enhanced with the presence of PCM (Al-Hinti et al. 2010, Fazilati and Alemrajabi 2013, Nabavitabatabayi et al. 2014, Nkwetta et al. 2014, Kousksou et al. 2011) whereas others found only marginal benefits (Talmatsky and Kribus 2008). In their analyses, the researchers compared PCM thermal storage tanks with water-only tanks at the same volume. The current analysis considers the impact of storage volume on system performance for both types of energy storage tanks. The systems approach is critical since it allows for the coupled effects of the thermal storage, solar collector, and household load to be incorporated. Moreover, from an energy balance at the systems level the potential benefits of PCM are clearly seen. While the impact of storage volume is often considered for economic analysis of water-only thermal storage (Beckman and Duffie 1991) and has also been presented for seasonal storage (Morrison and Abdel-khalik 1978), it appears that it has not been studied in the context of hybrid storage tanks with PCMs. The goal of the current paper is to present an analysis methodology that clarifies the role of PCM on the overall solar system performance.

4.2. System modelling

An in-house computer code was written to predict the dynamic performance of a solar energy domestic hot water system for tanks containing PCMs. A schematic of the system is shown in Figure 4.1. The storage tank contains PCMs in cylindrical modules. The components of the system include: collector, pump, controller, storage tank, and auxiliary heater. The system delivers energy to the load. The temperature set point on the load side is set to 55°C. Water from the tank is mixed with cold water whenever its temperature exceeds 55°C. The auxiliary heater is turned on when the inverse situation prevails. The component modelling is described below:

1. Collector: The Hottel-Whillier-Bliss equation is used to model a flat plate collector (Beckman and Duffie 1991) . The useful energy absorbed by the collector is given by:

$$Q_u = \dot{m}\, C_p(T_o - T_{in}) \tag{4.1}$$

This net gain is expressed in terms of incident irradiation and losses as follows:

$$Q_u = F_R A\big((\tau\alpha)G - U_L(T_{in} - T_{amb})\big) \tag{4.2}$$

By equating the previous two equations

$$T_o = T_{in} + \frac{F_R A_c}{\dot{m}\, C_p}\big((\tau\alpha)G - U_L(T_{in} - T_{amb})\big) \tag{4.3}$$

where T_o is the outlet temperature of the collector (=inlet temperature to the storage tank), T_{in} is the inlet temperature to the collector (=outlet temperature from the storage tank), F_R is the heat removal factor that is a function of the mass flow rate, T_{amb} is the ambient temperature and $(\tau\alpha)$ is the transmittance absorbance product and it is taken to be a constant of 0.8.

2. Controller: The pump is turned on when the difference between the collector plate temperature and bottom of the tank reaches 7^{o}C. It is turned off when this difference drops below 2 ^{o}C. This is the same control strategy adopted by Mather 2000.

- Storage tank: The storage tank is presumed to be a water tank containing vertically oriented cylindrical PCM modules. Water flows axially along the length of the modules. The enthalpy porosity model is used to predict the heat transfer and phase change within the PCM modules. With this method the latent heat of fusion is accounted for in the governing equation by defining an enthalpy term (Voller et al. 1985, Cornini et al. 1974). It is reported to have a better stability than other methods (Voller et al. 1987). The model equations are provided in Appendix A. The axial flow of water parallel to the cylinders is presumed to be a one-dimensional plug flow. Thus the flow around one PCM module is a representative for the 'bundle' (Figure 4.2a). The modeled geometry in the code is shown in Figure 4.2b. The heat transfer from the fluid is modeled by considering a water jacket around each module. Heat transfer correlations are applied at the outer surface of the module. The details of the model are previously presented in a published paper (Teamah et al. 2016).

Validation of the enthalpy porosity model was performed using the experimental data of Jones et al. 2006 with good agreement obtained (<5% deviation) (Teamah et al. 2016). The hybrid tank model was verified against results presented by Esen and Ayhan 1996 for isothermal charging. Further validation was conducted for the case of sequential charging and discharging. The results of the code were compared with the experimental results reported by De Gracia et al. 2011. The details of the validation are given in Appendix A. There is a very good agreement between the present code and the reported results with maximum deviation of 3.9% between the results in three tested senarios. On the system level, verification was conducted against TRNSYS [software] predictions for a water only tank. This ensures the robustness of the linked equations to model the system. Excellent agreement was found (the two results overlapped as the same numerical methodology was used) and the details are provided in Appendix A.

The effectiveness of this system is assessed in terms of solar fraction. The solar fraction represents the percentage of the heating load supplied by solar energy and is given by:

$$f_s = \frac{Q_{del}}{Q_{load}} \tag{4.4}$$

The delivered solar load is calculated as:

$$Q_{del} = \int \dot{m}_{tank} C_{pw} \left(T_{top\ of\ tank} - T_{mains}\right) dt \tag{4.5}$$

where $\dot{m}_{tank} = \dot{m}_{demand} = 0.19\ kg/s$ when $T_{top\ of\ tank} < T_{setpoint}$ (4.6)

When $T_{top\ of\ tank} > T_{setpoint}$ the drawn mass flow rate from the tank reduced and is calculated as:

$$\dot{m}_{tank} = \dot{m}_{demand}\left(\frac{T_{setpoint} - T_{mains}}{T_{top\ of\ tank} - T_{mains}}\right) \quad (4.7)$$

Q_{load} represents the energy required by a reference system to meet the heating load with no supply of solar energy (i.e. the energy required to heat the mains water to the delivery set point temperature) and it is calculated according to:

$$Q_{load} = \int \dot{m}_{del} C_{pw}\left(T_{setpoint} - T_{mains}\right)dt \quad (4.8)$$

By using this convention for calculating the solar fraction, the delivered solar energy can be related to the reference energy by:

$$Q_{del} + Q_{aux} = Q_{load} \quad (4.9)$$

where Q_{aux} is the auxiliary power required by the solar system to meet the load requirement.

One representative day for each season of the year was chosen. The irradiation and ambient temperature data were extracted from the Meteonorm [software] for Toronto, Canada. The dispersed draw profile is chosen for a typical family consumption in Canada (Edwards et al. 2015). The profiles are presented in Appendix B. Day-long simulations were repeated until a periodic steady state was achieved. Other load profiles were

assessed and were found to not impact on the conclusions of the study. Annual solar fraction is determined from the summation of the energy delivered to the load divided by the required load energy.

$$F_{s,annual} = \frac{\sum Q_{del}|_{typical\ days}}{\sum Q_{load}|_{typical\ days}} \quad (4.10)$$

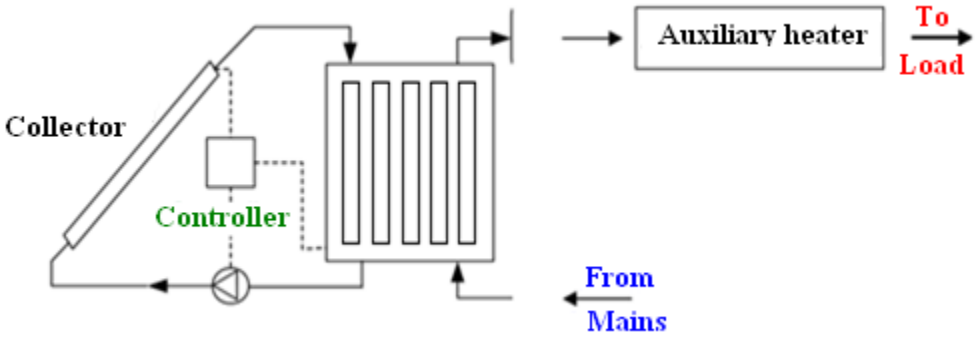

Figure 4.1: Schematic of the studied system

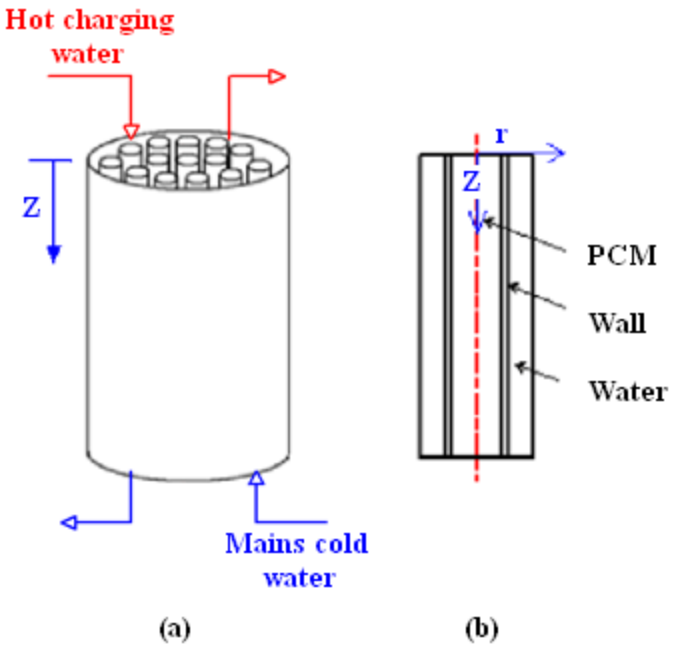

Figure 4.2: Schematic of the studied domain in the code (a) the whole tank, (b) zoomed view of the cylindrical jacket around one of the PCM modules.

4.3. Sample results

4.3.1. Results for a tank volume= 120 liters

This section presents sample results for a case study that compares system performance for a thermal storage system with and without PCM. The system parameters are given in Table 4.1. The PCM properties are given in Table 4.2. Capric acid was chosen because of its appropriate melt temperature, and stable thermo-physical properties (Desgrosseillier et al. 2011, Sari and Kaygusuz 2003, Sari and Karaipekli 2009). The case is taken to be representative of the performance to supply a typical Canadian family with the required

hot water. The weather data and draw off profiles listed in Appendix B were used. Several other cases with different parameters were investigated and were found to yield the same conclusions.

The simulations predict that the hybrid system provides an enhanced annual solar fraction (f=0.65) in comparison to the water only system (f=0.55). The improved performance of the system with the hybrid storage can be explained by considering the pump activation period and the temperatures exiting the storage tank for a typical spring day as shown in

Table 4.1: Parameters for the studied case

Parameter	Value
Collector area	6 m^2
Collector slope	45^o
Azimuth	0^o
Collector loss coefficient	5 W/m^2K
Collector mass flow rate	0.05 kg/s
Storage tank volume	120 liters
Storage tank loss coefficient	0.55 W/m^2K
Tank aspect ratio	2
PCM packing ratio	50%
PCM melting temperature	32^{o}C
PCM module diameter	2 cm
Daily drawn volume of hot water	160 liters
Discharging flow rate	0.19 kg/s

Figure 4.3. Note that zero on the x-axis denote 6:00 a.m.. Figure 4.3a shows the period of pump activation for both systems. The pump is activated at about hour 1.2 and runs continuously until hour 7.6 in the hybrid system and hour 7.2 in the water only system. This extra period of pump operation is attributed to the cooler temperatures exiting the

Table 4.2: Thermo-physical properties of capric acid

Density (kg/m^3)	Specific heat capacity (kJ/kg ^oC)	Latent heat of fusion (kJ/kg)	Thermal conductivity (W/ m K)
870	1.6 (solid), 2.3(liquid)	178	0.147

bottom of the hybrid tank (Figure 4.3c) and entering the solar collector. While the pump is on, the temperatures at the bottom and top of the tank generally increase. The sharp drops in temperature, particularly at the bottom of the tank, are a result of the discharging which is presumed to occur at the start of each hour. During discharging, the bottom temperature of the tank drops to that of the water mains temperature and the top of tank temperature decreases slightly as cooler water layers in the tank shifts upwards. It is seen that the temporal temperature profiles in the hybrid system are modulated in comparison to the water only system. The PCM tunes the temperature around its melting temperature (T_m= 32^{o}C) while melting (from hour 3.9 to hour 5.5) and solidifying (hour 11.9 to hour 14.5). In the periods where the pump is deactivated, the bottoms of both tanks are at the mains temperature. The temperature at the top of the tank decreases slightly due to the losses of tank to environment. The PCM acts as a passive controller in the hybrid system. This is beneficial in increasing the energy supplied to the load in the early morning and night hours. Water supplied from the hybrid tank in hours 0 to 5 and 12 to 24 is hotter compared to the water only system. As a result, the energy delivered to the load for that

spring day is increased from 16.3 MJ for the water only system to 19.1 MJ for the hybrid system. Similar trends were seen in the other typical days. The predicted profiles for the temperatures directed to the load in the four typical days are presented in Appendix B.

The solar fraction enhancement can also be interpreted by analysing the energy balance on the system control volume. Figure 4.4 shows the different modes of energy entering and exiting the studied system: E_{solar} is the solar irradiation on the collector, E_{mains} is the mains energy, E_{Load} is the energy delivered to the load by the system, $E_{loss,\ coll}$ is the energy loss from the collector and $E_{loss,\ tank}$ is the energy loss from the tank. The energy is calculated by integrating the heat transfer rates over the period of interest. E_{solar} and $E_{loss,\ coll}$ are integrated over pump run time.

The energy balance on the system at steady state implies that;

$$E_{solar} + E_{mains} = E_{Load} + E_{loss,\ coll} + E_{loss,\ tank} \quad (4.11)$$

also

$$E_{solar} = E_{delivered} + E_{loss,\ coll} + E_{loss,\ tank} \quad (4.12)$$

where

$$E_{delivered} = E_{Load} - E_{mains} \quad (4.13)$$

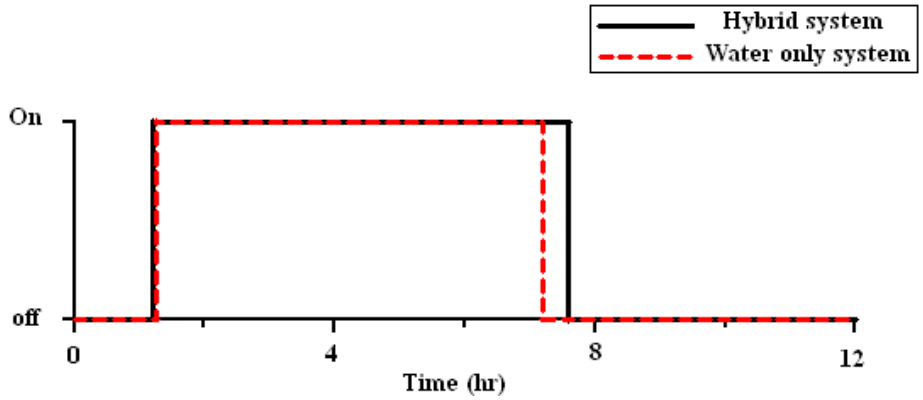

a) Pump activation period (on 12 hr period)

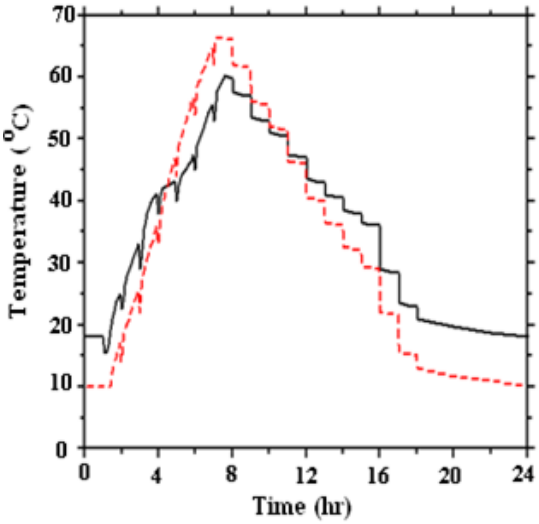

b) Tank temperature on 24 hr period (top)

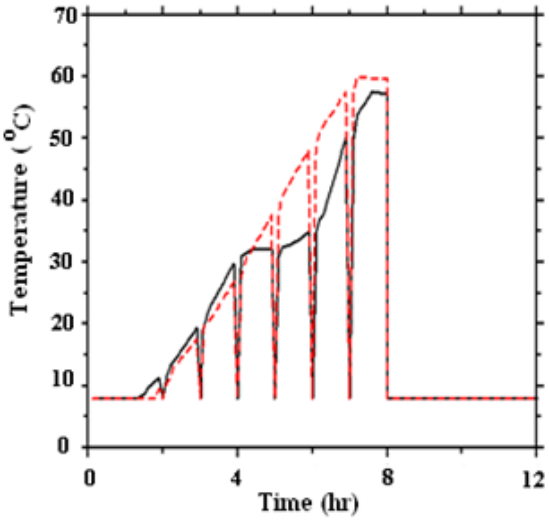

c) Tank temperature on 12 hr period (bottom)

Figure 4.3: Pump activation period and temperatures in a typical spring day (V_{tank}=120 liters)

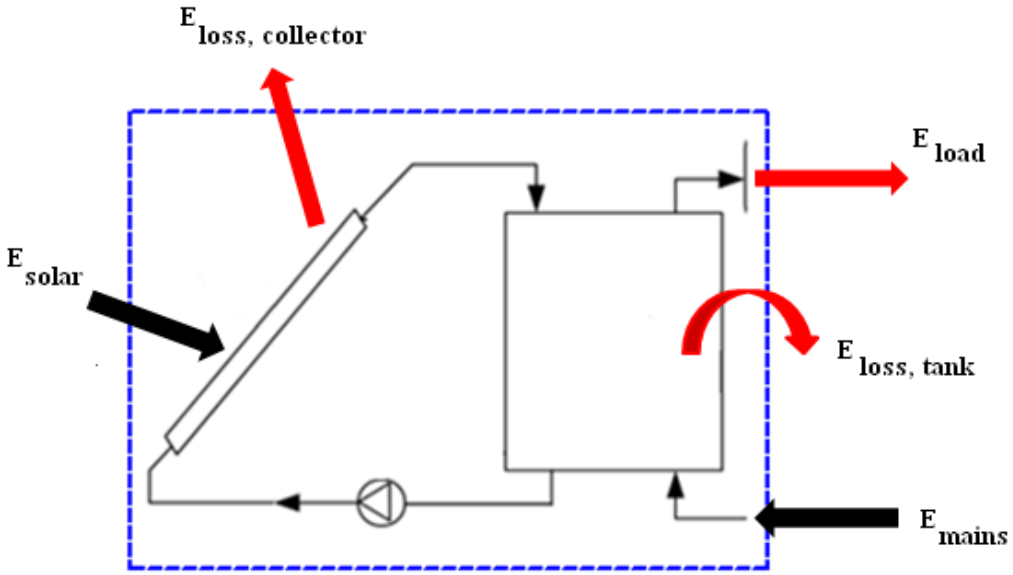

Figure 4.4: Energy entering and exiting the studied system control volume

The energy breakdown for both the hybrid and the water only 120 liter tank in the typical spring day is shown in Table 4.3. The input solar irradiation is higher for the hybrid system owing to the longer pump run time. The collector loss is lower for the hybrid system because of the cooler temperatures entering the collector from the bottom of the tank. The tank loss has a minor effect; it is a bit higher for the hybrid system because of the higher temperature level. The increase in heat losses in hybrid tanks was also reported by Talmatsky and Kribus. The gain in incident solar energy and reduction in collector loss causes the energy supplied to the load from the hybrid system to be higher. The same calculations were performed for the other three typical days.

Table 4.4 provides the predictions for annual system performance. The energy delivered from the solar thermal system to the load increased from 5.73 GJ to 6.85 GJ which is a nearly 20% increase in the energy delivered to the load. Solar fraction correspondingly increases from 0.55 to 0.65.

Table 4.3: Energy breakdown in a typical spring day (120 liter tank)

	Hybrid system	Water only system
E_{solar} (MJ)	55.4	53.5
$E_{loss,\ coll}$ (MJ)	34.7	35.8
$E_{loss,\ tank}$ (MJ)	1.6	1.4
$E_{delivered}$ (MJ)	**19.1**	**16.3**

From this analysis it can be concluded that PCMs act to increase the performance of a solar thermal system. This is due to reduction in the collector inlet temperature which increases the pump run time and decreases the collector losses.

4.3.2. Results for a tank volume= 240 liters

To determine if the statement from the previous simulation is broadly valid, the simulation was repeated with the only change being the storage capacity of the tank. The tank volume was increased from 120 l to 240 l. The volume fraction of PCM was kept constant. All other parameters were the same as presented in Table 4.1. The energy balance results for the larger tank are given in Table 4.5. For this case it is seen that

there is no benefit of introducing PCM on solar fraction since identical solar fractions are obtained.

Table 4.4: Annual breakdown of energy and solar fraction (120 liter tank)

	Hybrid system	Water only system
E_{solar} (GJ)	19.7	18.83
$E_{loss,\ coll}$ (GJ)	12.3	12.59
$E_{loss,\ tank}$ (GJ)	0.55	0.51
$E_{delivered}$ (GJ)	**6.85**	**5.73**
Annual energy required by the load (GJ)	10.5	10.5
Average annual solar fraction	**0.65**	**0.55**

These two simulations illustrate the conflict over the impact of PCM on system performance. Moreover, it indicates the key role that tank volume has on the system solar fraction. The results show that conclusions regarding the impact of PCM on solar fraction are strongly dependent on the chosen energy storage volume. An explanation for this is given in the next section.

Table 4.5: annual breakdown of energy and solar fraction (240 liter tank)

	Hybrid system	Water only system
E_{solar} (GJ)	20.4	20.4
$E_{loss,\ coll}$ (GJ)	12.71	12.71
$E_{loss,\ tank}$ (GJ)	0.629	0.629
$E_{delivered}$ (GJ)	**7.1**	**7.1**
Annual energy required by the load (GJ)	10.5	10.5
Average annual solar fraction	**0.67**	**0.67**

4.4. Effect of Thermal Storage Volume on System Solar Fraction

Based on the annual energy balance on solar system, the solar fraction can be written as:

$$f_s = \frac{E_{\text{delivered to load}}}{E_{\text{required by load}}} \quad (4.14)$$

From the system energy balance (Equation (11)) $E_{\text{solar to load}}$ can be written as:

$$E_{\text{delivered to load}} = E_{\text{solar}} - (E_{\text{loss,collector}} + E_{\text{loss,tank}}) \quad (4.15)$$

This yields that:

$$f_s = \frac{E_{\text{solar}} - (E_{\text{loss,collector}} + E_{\text{loss,tank}})}{E_{\text{required by load}}} \quad (4.16)$$

E_{solar} is strongly influenced by the pump run time since the integration is performed over times when the pump is running. The storage volume influences the pump run time since the pump controller turns on the pump based on the difference between collector temperature and the temperature at the bottom of the tank. $E_{loss,collector}$ is also affected by the volume of the storage tank. An undersized water tank will send hot water to the collector, increasing losses. As the volume increases, hot water is less likely to make it to the bottom of the tank. The heat loss from the tank ($E_{loss,tank}$) depends on the tank surface area (i.e. volume) of the storage and average temperature of the tank. Generally tank losses are much smaller than collector losses since the tank is well insulated. As such, at large tank volumes where cool fluid is consistently sent to the collector inlet, the solar fraction should decrease only slightly with increasing tank volume.

To explore this analysis approach, the system simulations were repeated for a series of tank volumes (both with and without PCM in the tank). Figure 4.5 shows the predicted solar fraction for both systems. The Figure clearly shows that PCM provides an increased solar fraction in comparison to water only tanks at small tank volumes when the tank is essentially undersized for the demand. When the tank is oversized, both tanks will perform similarly. The individual components of the energy balance are shown in Figure 4.6. The input solar radiation for the hybrid system is higher than the water only system until a volume of about 180 liters (Figure 4.6a). After that the two curves approach each other since the pump run time becomes equal when the tank is oversized. Figure 4.6b shows that collector loss for the hybrid system is lower in the smaller volumes (<180 liters) since water only tanks send hotter water to the collector thus deteriorating its

performance. When the tank is oversized this situation will not be encountered and the curves approach each other. The tank loss (Figure 4.6c) is higher for the hybrid system due to higher average temperatures (about 3 ^{o}C), but does not significantly impact system performance since collector losses dominate. The energy from the solar thermal system delivered to the load is shown in Figure 4.6d. The hybrid system delivers more energy to the load in the smaller volumes with the differences diminishing as the tank volume increases. The slight drop in delivered energy at high volumes from both systems is due to increased tank heat losses resulting from larger surface area.

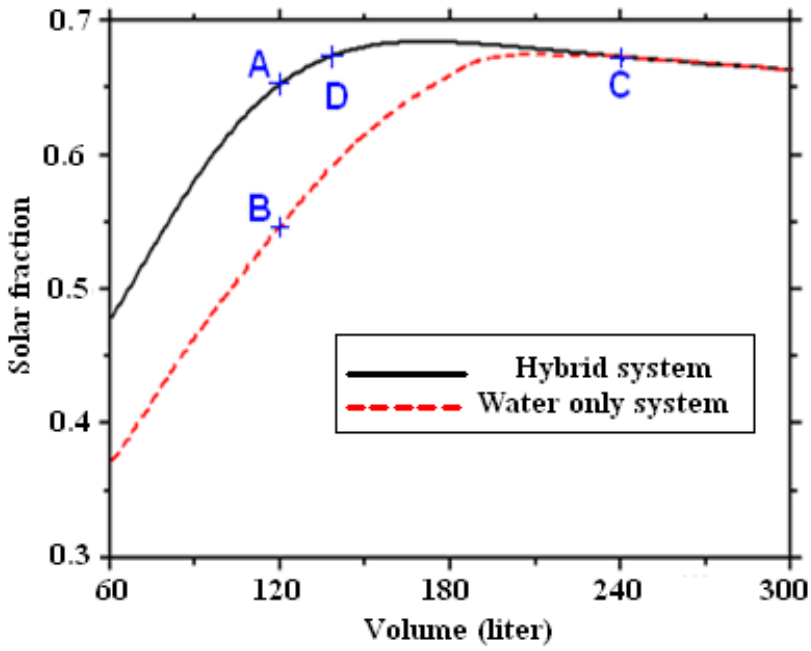

Figure 4.5: Average solar fraction versus volume for hybrid and water only systems

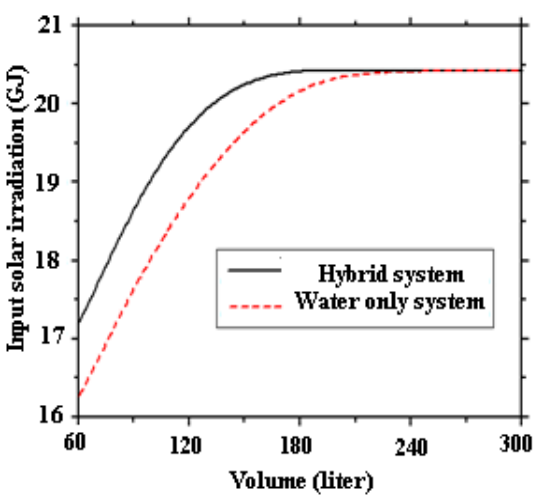

a) Input solar radiation

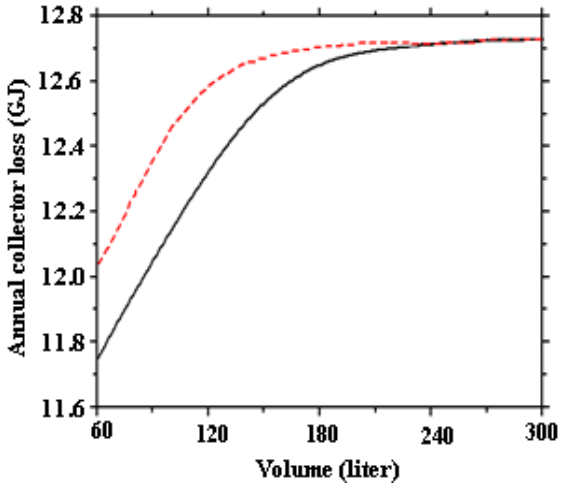

b) Collector loss

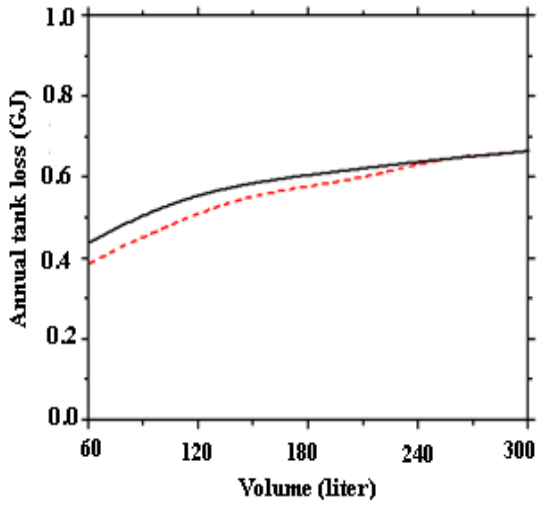

c) Tank loss

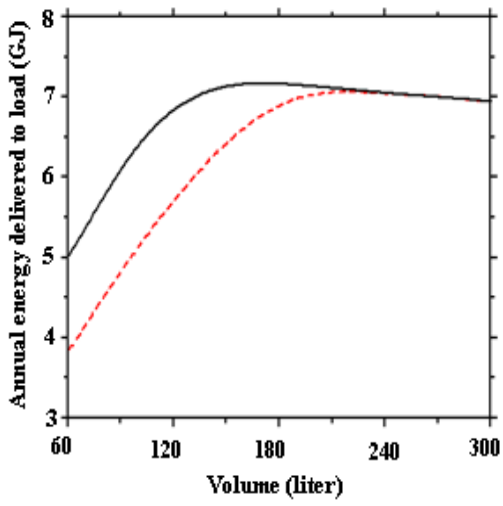

d) Energy delivered to load

Figure 4.6: Breakdown of energies for tanks of different volumes

4.5. Assessment of the impact of PCM on solar system performance – storage volume requirements

Figure 4.5 shows the solar fraction for the two systems as a function of tank volume. For tanks of 120 l, it appears that there is strong benefit to using PCM (i.e. comparison of points A and B on the graph). However, this conclusion is a result of the water-only tank being undersized for the application. As the volume of the tank increases, both curves approach the same behaviour (i.e. point C on the graph). The real benefit of PCM is not in enhancing solar fraction since this could be attained simply by using a larger water tank, but rather in the reduction in volume that is required to give the same peak solar fraction (i.e. comparing points C and D on the graph). For the conditions considered in this work, a 140 l hybrid tank results in the same solar fraction delivered by a 240 l water only tank. This yields a reduction in storage volume of about 40%.

4.6. Summary and Conclusion

The role of PCMs in thermal storage has been subject of a great deal of research in the literature. Despite this, the research results on the value of PCMs in enhancing system performance have been mixed: some researchers have found an enhancement of solar fraction when PCM is introduced into the thermal storage tank whereas others have found a negligible impact. The current paper has provided an explanation for the mixed results found in the literature. It is based on an energy balance that considers the interactions between the thermal storage and the collector performance. It is shown that storage volume plays a key role in influencing the collector performance. It is also demonstrated

that PCMs provide a benefit only in comparison to an undersized water based storage system. As the tank volume is increased, the benefit of PCM diminishes and the two systems eventually converge to the same performance. This paper has shown that the benefit of PCM is in reducing required storage tank volume. PCM does not enhance system performance if the water tank is sized correctly. The system energy balance revealed that the benefit of PCM at low tank volumes is due to:

- Reduction in the collector inlet temperature which reduced collector loss and increased collector efficiency.
- Increased pump run time due to cooler tank bottom.
- Increased water delivery temperature to load during early morning and late afternoon.
- For the hybrid case considered, a reduction in tank volume of about 40% was obtained without compromising the solar fraction.

This analysis was performed using a PCM volume fraction of 50%, T_m= 32^{o}C, and 2 cm diameter modules. There is a potential for further reduction in tank volume (while maintaining the same solar fraction) by exploring the effect of various variables and applying optimization. For example, an increase in PCM volume fraction is expected to result in further reductions in tank volume. This could have significant implications for multi-residential units which would otherwise require very large tanks.

4.7. Acknowledgement

The authors are grateful to the Natural Sciences and Engineering Research Council of Canada and the Smart Net-Zero Energy Buildings Strategic Research Network (SNEBRN) for their financial support for this work.

4.8. References

[1] Zalba, B., Marin, J. M., Cabeza, L. F., and Mehling, H., 2003, "Review on thermal energy storage with phase change: materials, heat transfer analysis and applications", Applied Thermal Engineering, 23(3), pp. 251-283.

[2] Abhat, A., 1983,"Low temperature latent heat thermal energy storage: Heat storage materials", Solar Energy, 30(4), pp. 313-332.

[3] Desgrosseillier, L., Murray, R., Safatli, A., Marin, G., Stewart, J., Osbourne, N., White, M.A., Groulx, D. , 2011, "Phase Change Material Selection in the Design of a Latent Heat Energy Storage System Coupled with a Domestic Hot Water Solar Thermal System", ASHRAE Annual Conference, Montreal, Canada.

[4] Sari, A., and Kaygusuz, K., 2002, "Thermal and heat transfer characteristics in a latent heat storage system using lauric acid", Energy Conversion and Management,43, pp. 2493-2507.

[5] Sari, A., and Kaygusuz, K., 2003, "Some fatty acids used for latent heat storage: thermal stability and corrosion of metals with respect to thermal cycling", Renewable Energy, 28, pp. 939-948.

[6] Sari, A., and Karaipekli, A., 2009, "Preparation, thermal properties and thermal

reliability of palmitic acid/expanded graphite composite as form-stable PCM for thermal energy storage",Solar Energy Materials and Solar Cells, 93, pp. 571-576.

[7] Bergles, A. E., 2011, "Recent developments in enhanced heat transfer," International Journal of Heat and Mass Transfer, 47(8), pp. 1001-1008.

[8] Nakhla, D., Sadek, H., and Cotton, J. S., 2015,"Melting performance enhancement in latent heat storage module using solid extraction electrohydrodynamics (EHD) " International Journal of Heat and Mass Transfer, 81, pp. 695-704.

[9] Jegadheeswaran, S., and Pohekar, S. D. , 2009, "Performance enhancement in latent heat thermal storage system: A review," Renewable and Sustainable Energy Reviews, 13(9), pp. 2225–2244.

[10] Agyenim, F., Hewitt, N., Eames, P. and Smyth, M., 2010,"A review of materials, heat transfer and phase change problem formulation for latent heat thermal energy storage systems (LHTESS)," Renewable and Sustainable Energy Reviews, 14(2), pp. 615–628.

[11] Sanusi, O., Warzoha, R., and Fleischer, A. S. , 2011, "Energy storage and solidification of paraffin phase change material embedded with graphite nano-fibers," International Journal of Heat and Mass Transfer, 54(19), pp. 4429–4436.

[12] Pokhrel, R., Gonzalez, J. E., Hight, T., and Adalsteinsonn,T., 2010, " Analysis and Design of a Paraffin/Graphite Composite PCM Integrated in a Thermal Storage Unit," ASME J. Sol. Energy Eng., 132(4), pp. 041006.

[13] Velraj, R., Seeniraj, R. V., Hafner, B., Faber, C., and Schwarzer, K., 1999, "Heat Transfer Enhancement in a Latent Heat Storage System," Solar Energy, 65(3), pp.

171–180.

[14] Stritih, U., 2004, "An experimental study of enhanced heat transfer in rectangular PCM thermal storage," International Journal of Heat and Mass Transfer, 47 (12), pp. 2841–2847.

[15] Yingqiu, Z.,Yinping, Z., Yi, J., and Yanbing, K., 1999, " Thermal Storage and Heat Transfer in Phase Change Material Outside a Circular Tube with Axial Variation of the Heat Transfer Fluid Temperature", ASME J. Sol. Energy Eng., 121(3), pp. 145-149.

[16] Lacroix, M. and Benmadda, M., 1997, "Numerical Simulation of Natural Convection-Dominated Melting and Solidification From a Finned Vertical Wall," Numerical Heat Transfer, Part A: Applications, 31(1), pp. 71-86.

[17] Esen, M., Ayhan, T., 1996, “Development of a model compatible with solar assisted cylindrical energy storage tank and variation of stored energy with time for different phase change materials”, Energy Conversion and Management, 37(12), pp. 1775-1785.

[18] Mehling, H., Cabeza, L.F., Hippeli, S.,and Hiebler, S., 2003, "PCM-module to improve hot water heat stores with stratification", Renewable Energy, 28, pp. 699-711.

[19] Nallusamy, N. N., and Velraj, R. R., 2009, "Numerical and experimental investigation of a combined sensible and latent heat storage unit integrated with solar water heating system", Journal of Solar Energy engineering, Vol. 131, pp.41002-41002-8.

[20] Wang, Z., Qiu, F., Yang, W., and Zhao, X., 2015, "Applications of solar water heating system with phase change material", Renewable and Sustainable Energy Reviews, 52, pp. 645-652.

[21] Al-Hinti, I., Al-Ghandoor, A., Maaly, A., Abu Naqeera, I., Al-Khateeb, Z., and Al-Sheikh, O., 2010,"Experimental investigation on the use of water-phase change material storage in conventional solar water heating systems", Energy Conversion and Management, 51, pp. 1735-1740.

[22] Fazilati, M. A., and Alemrajabi, A. A., 2013, "Phase change material for enhancing solar water heater, an experimental approach", Energy Conversion and Management, 71, pp. 138-145.

[23] Nabavitabatabayi, M., Haghighat, F., Moreau, A., and Sra, P.,2014, "Numerical analysis of a thermally enhanced domestic hot water tank", Applied Energy, 129, pp. 253-260.

[24] Nkwetta, D. N., Vouillamoz, P., Haghighat, F., El Mankibi, M., Moreau, A., and Desai, K., 2014, "Phase change materials in hot water tank for shifting peak power demand", Solar Energy, 107, pp. 628-635.

[25] Talmatsky, E., and Kribus, A., 2008, "PCM storage for solar DHW: an unfulfilled promise?", Solar energy, 82, pp. 861-869.

[26] Kousksou, T., Bruel, P., Cherreau, G., Leoussoff, V. and El Rhafiki, T. , 2011, “PCM storage for solar DHW: From an unfulfilled promise to a real benefit”, Solar Energy, 85(9), pp. 2033-2040.

[27] Beckman WA, Duffie JA, Solar Engineering of Thermal Processes, Second

Edition, Wiley J. & Sons, Inc, New York, 1991.

[28] Morrison, D. J., and Abdel-khalik, S. I., 1978, " Effects of phase-change energy storage on the performance of air-based and liquid-based solar heating systems", Solar Energy, 20, pp. 57-67.

[29] Mather D. W., "Modular Stratified Thermal Energy Storage for Solar Heating Systems", Department of Mechanical Engineering, University of Waterloo, Waterloo, Ontario, Canada, MASc thesis, 2000.

[30] Voller, V. R., Markatos, N. C., and Cross, M., 1985 " Techniques for accounting for the moving interface in convection/diffusion phase change". Numerical Methods in Thermal Problems, 4, pp. 595-609.

[31] Cornini, G., Guidiq, S.D., Lewis, RW., and Zienkiewiq, O.C., 1974, "Finite Element Solution of Non-linear Heat Conduction Problems with Reference to Phase Change," International Journal for Numerical Methods in Engineering., 8, pp. 613-624.

[32] Voller, V. R., Cross, M., and Markatos, N. C., 1987, "An enthalpy method for convection/diffusion phase changes". International Journal of Numerical Methods in Engineering, 24, pp. 271-284.

[33] Teamah HM, Lightstone MF, Cotton JS. Numerical Investigation and Nondimensional Analysis of the Dynamic Performance of a Thermal Energy Storage System Containing Phase Change Materials and Liquid Water. ASME. I. Sol. Energy Eng. 2016; 139(2):021004-021004-14. doi:10.1115/1.4034642.

[34] Jones, B. J., Sun, D., Krishnan, S., and Garimella, S.V. , 2006, " Experimental

and numerical study of melting in a cylinder", International Journal of Heat and Mass Transfer, 49 , pp. 2724–2738.

[35] De Gracia A., Oró E., Farid M. M., Cabeza L. F., 2011,"Thermal analysis of including phase change material in a domestic hot water cylinder", Applied Thermal Engineering, Vol. 31, pp. 3938-3945.

[36] Klein, S.A. et al, 2010, TRNSYS 17: A Transient System Simulation Program, Solar Energy Laboratory, University of Wisconsin, Madison, USA, http://sel.me.wisc.edu/trnsys.

[37] Meteonorm [software], available from: http://www.meteonorm.com

[38] Edwards S., Beausoleil-Morrison I. and Laperrie`re A., 2015, "Representative Hot Water Draw Profiles at High Temporal Resolution for Simulating the Performance of Solar Thermal Systems," Solar Energy, Volume 111, Pages 43-52, 2015.

[39] Rohsenow, W. M., Hartnett, J.P., and Ganic, E. N.,1985, Handbook of heat transfer fundamentals, 2nd edn, (Eds). New York.

Appendix A

Enthalpy porosity model

According to the enthalpy porosity formulation [17], specific enthalpy (enthalpy per unit mass) is defined based on the cell condition (solid, liquid or transition) as follows:

$$i(T) = C_{p,s}T \qquad T < T_{m1} \qquad (4.A.1)$$

$$i(T) = C_{p,s}T_{m1} + \frac{r_s(T - T_{m1})}{\Delta T_m} \qquad T_{m1} < T < T_{m2} \qquad (4.A.2)$$

$$i(T) = C_{p,l}(T - T_{m2}) + r_s + C_{p,s}T_{m1} \qquad T > T_{m2} \qquad (4.A.3)$$

where

r_s is the latent heat, T_{m1} is the lower melting temperature and $T_{m2}$is the upper melting temperature.

The finite difference formulation for conduction dominated melting is given by:

$$\rho V_{j,k}\left.\frac{\partial i}{\partial t}\right|_{j,k} = -KA_k\left.\frac{\partial T}{\partial R}\right|_k + KA_{k-1}\left.\frac{\partial T}{\partial R}\right|_{k-1} + KA_j\left.\frac{\partial T}{\partial Z}\right|_j - KA_{j-1}\left.\frac{\partial T}{\partial Z}\right|_{j-1} \qquad (4.A.4)$$

Central differencing is applied to approximate the derivatives above.

The code solves the enthalpy porosity equations together with the conduction dominated melting equation. A uniform grid is applied. The heat transfer to the PCM is calculated using the correlations developed by Rohsenow et al. 1985. Those equations are linked to the collector performance equation for the purpose of system modelling

Validation of sequential charging and discharging

The results of the code were compared with the results reported by De Gracia et al. 2011. The geometry considered in their study is shown in Figure 4.A.1. They considered a 180 liter tank of water containing cylinders of PCM that constitutes 22% by volume. The

cylinder can be heated at the bottom by 3 kW electric heaters. During discharging, cold water enters from the bottom of the cylinder and hot water leaves from the top. Seven thermocouples are used to monitor the temperature of water inside the tank. They presented the results of eight cases in which they changed the diameter of the PCM cylinders. They studied one of the cases experimentally as well (module diameter=40 mm). Due to the similarity of their geometry with the present study, this paper represents a good validation case for the present work.

Three scenarios of sequential charging and discharging are considered. Those scenarios begin with a fully charged tank with uniform temperature 80^{o}C. The discharging flowrate is 0.2 kg/s. Discharging is initiated at different times as follows:

i) Scenario 1: Water discharges until outlet water temperature reaches 37^{o}C. First discharge at t=0 and second discharge at t=180 min.

ii) Scenario 2: Water discharges until outlet water temperature reaches 37^{o}C. First discharge at t=0 and second discharge at t=360 min.

iii) Scenario 3: Water discharges of 10 minutes each at different times of 0, 60, 120, 180, 240, 300, 360 min.

The predicted temperature at the top of the tank is overlapped with the present results as shown in Figures 4.A.2, 4.A.3 and 4.A.4. In scenario 1 (Figure 4.A.2), water starts at 80^{o}C and its temperature decreases when the first discharge is initiated. The discharge stops when the water temperature reaches 37^{o}C. At that time there is no flow in the

system but the PCM is hot (T_m=57^{o}C) so it loses its heat to the adjacent water. This increases the water temperature until the initiation of the second discharge. The water temperature begins to decrease again until discharge stops when the temperature reaches 37^{o}C. At that point, the temperature of the water in the tank increases by gaining heat from the molten portion of the PCM. The same trend is observed for scenario 2 (Figure 4.A.3) except for the difference in the time of initiation of the second discharge. For scenario 3 (Figure 4.A.4) water preserves its initial temperature until the end of the first 60 minutes. The water temperature decreases after 60 minutes when discharging is initiated for ten minutes. After that the water temperature decreases due to the heat losses from the tank to the environement (T_{amb}=21^{o}C). After 120 minutes, the discharge is initiated which causes the water temperature to drop for 10 minutes. After the discharge termination, the PCM begins to heat up the adjacent water. This trend is repeated for the following two discharge. By the end of the discharge initiated at the beginning of the fourth hour, the water temperature reaches 37^{o}C and thus there will not be benefit for discharging further (demand set point temperature is 37^{o}C). This causes the temperature of the water to decrease during the remainder of the experiment due to the heat losses from the tank. There is a very good agreement between the present code and the reported results with maximum deviation of 3.9% between the results in the three senarios.

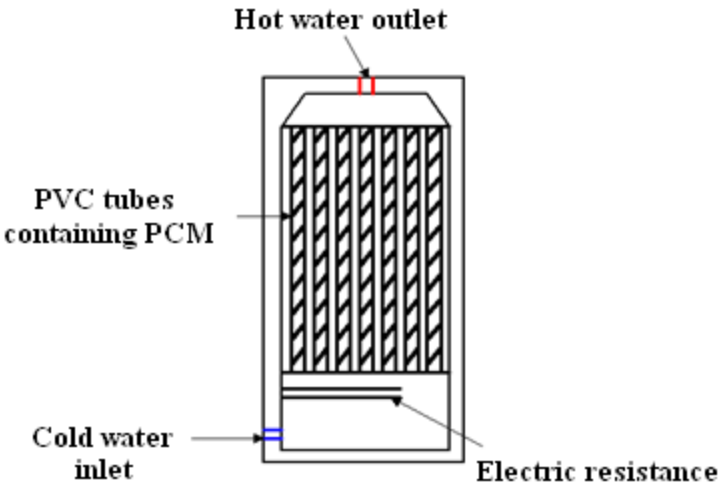

Figure 4.A.1: Schematic of the system studied by De Gracia et al. 2011

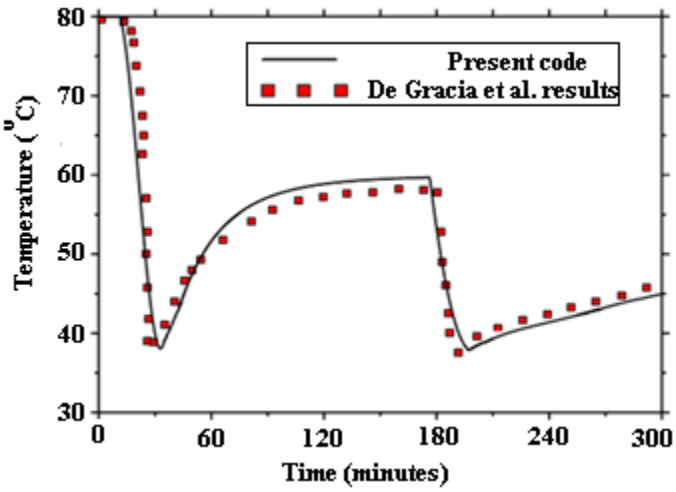

Figure 4.A.2: Comparison of the present code with De Gracia et al 2011 scenario 1 results

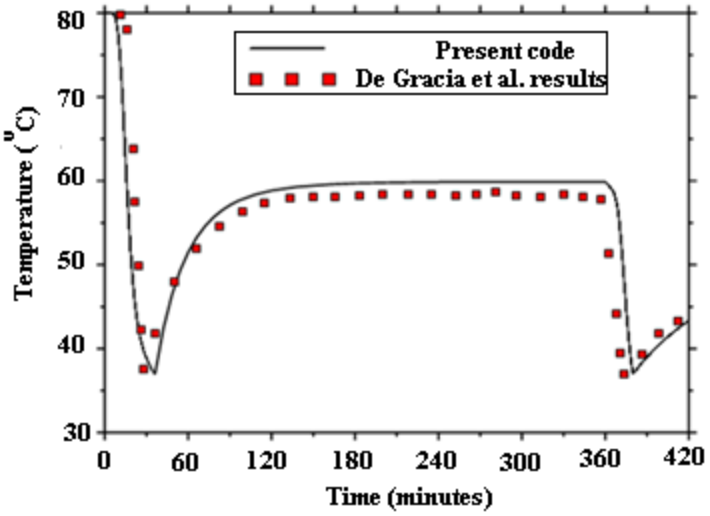

Figure 4.A.3: Comparison of the present code with De Gracia et al 2011 scenario 2 results

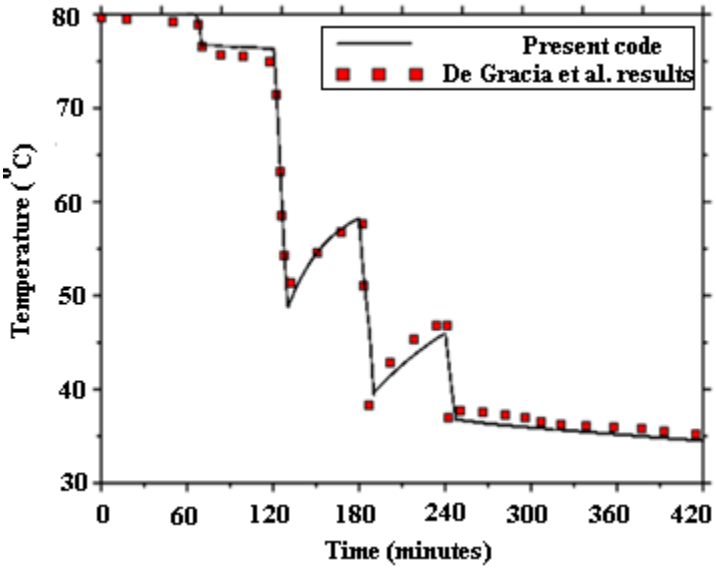

Figure 4.A.4: Comparison of the present code with De Gracia et al 2011 scenario 3 results

Verification for the system code

The system level verification was performed for water only tank which was presented in section 3. Figure 4.A.5 shows the overlapped temperature of tank top and bottom extracted from the code and TRNSYS [36]. There is an excellent agreement between the results as both using the plug flow model for the solution.

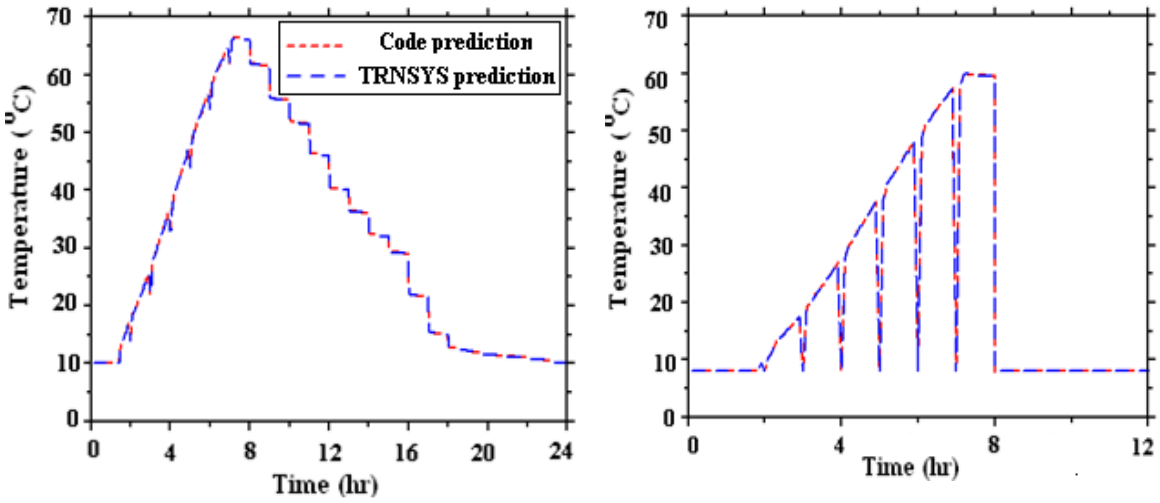

a) Tank temperature on 24 hr period (top) b) Tank temperature on 12 hr period (bottom)

Figure 4.A.5: Temperature profiles in the water only tank in a typical spring day

Appendix B

Weather data and demand profile

Irradiation and ambient temperature profiles were extracted from the Meteonorm [software] for Toronto location. Four typical days representative of the four seasons were selected. Figure 4.B.1 shows the irradiation and ambient temperature profiles for those

days. The profiles used in the code are the polynomial dotted approximations. The dispersed consumption profile for a typical Canadian family was chosen based on the reported results by Edward et al. 2015. The profile is shown in Figure 4.B.2. The consumption is almost steady with a slight peak in the early morning and the late afternoon. The mains temperature in each season is listed in Table 4.B.1.

Supplied temperature to the load in the four typical days

Considering the case study presented in section 3, the predicted profiles for the temperatures directed to the load in the four typical days are presented in Figure 4.B.3. Both summer and autumn days show the same trend previously explained for the spring day. The temperature supplied by the hybrid system is higher than the water only system in the morning and late afternoon. This is due to the heating effect of the released latent heat of fusion in those periods. The winter day shows a different trend (Figure 4.B.3d). This is because the PCM is not molten under this condition and both systems act as sensible storage media.

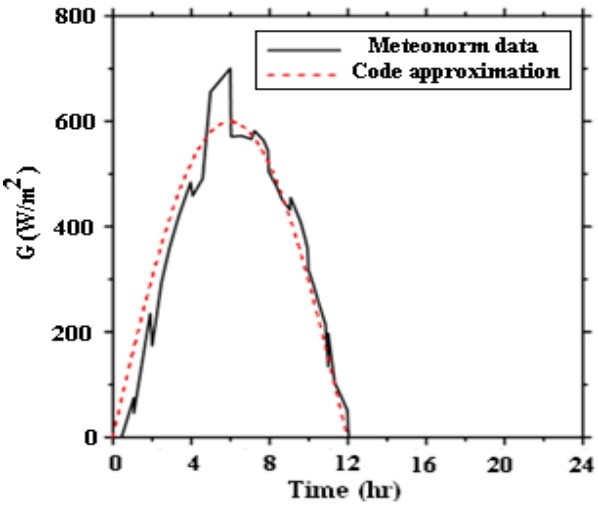

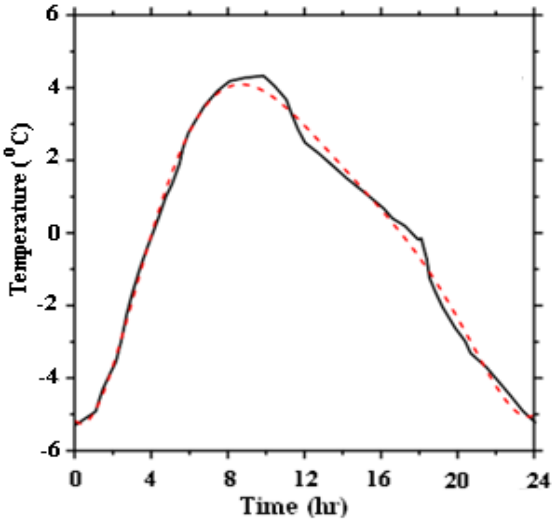

a) Irradiation profile on the horizontal b) Ambient temperature

i) Typical spring day data

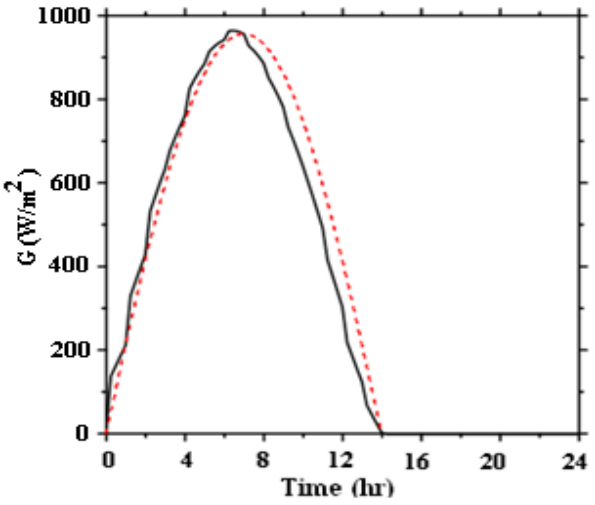

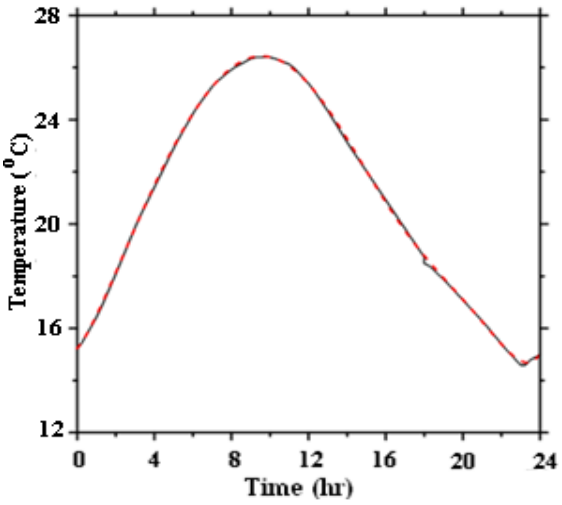

a) Irradiation profile on the horizontal b) Ambient temperature

ii) Typical summer day data

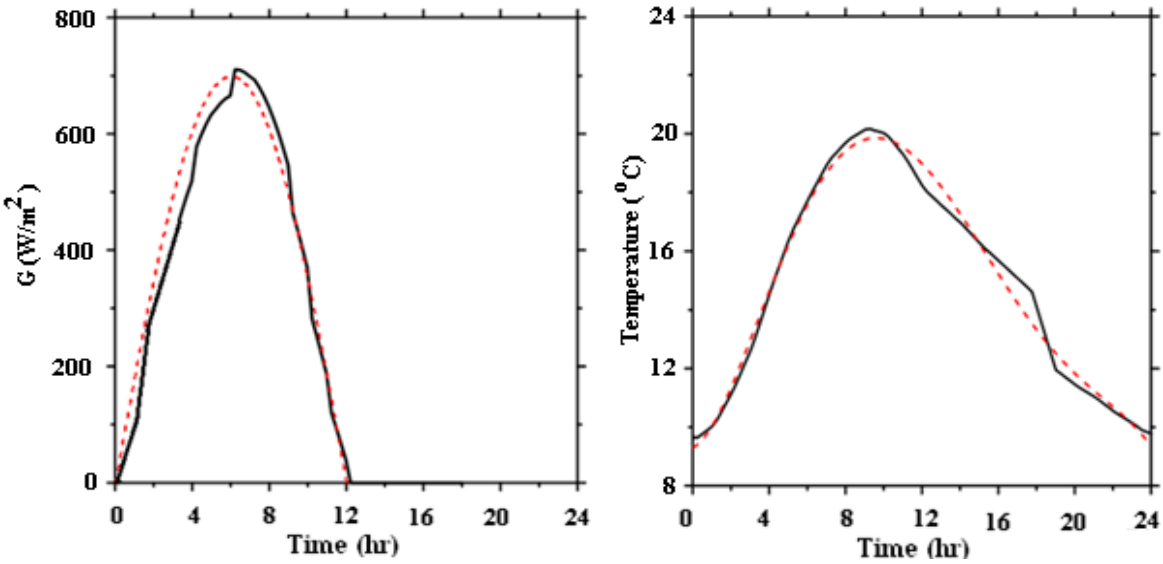

a) Irradiation profile on the horizontal b) Ambient temperature

iii) Typical autumn day data

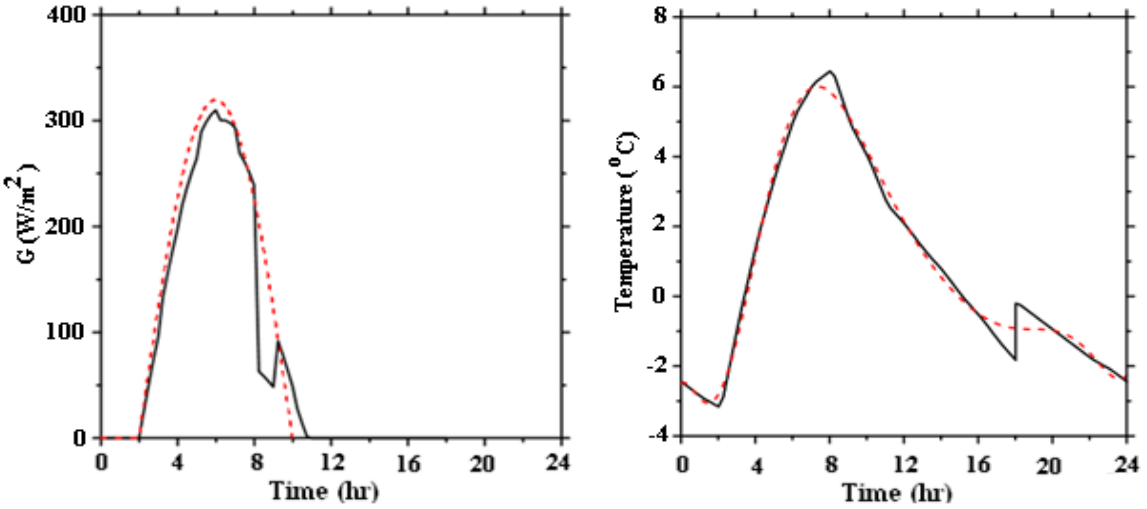

a) Irradiation profile on the horizontal b) Ambient temperature

iv) Typical winter day data

Figure 4.B.1: Typical radiation data for the four seasons

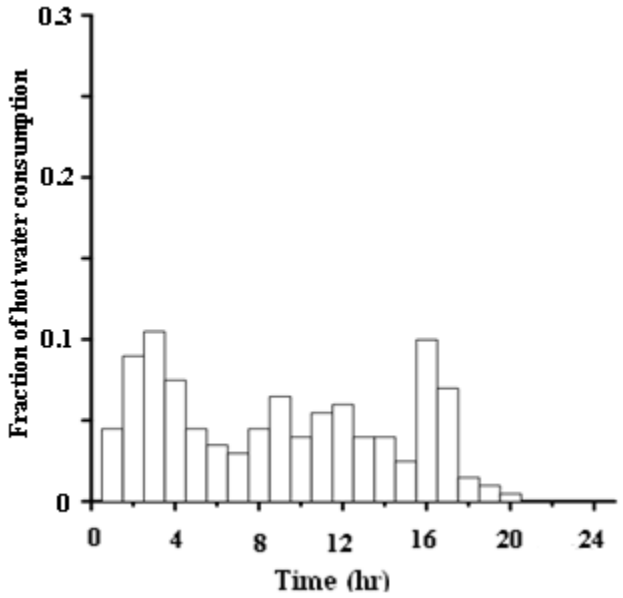

Figure 4.B.2: Dispersed draw profile tested in the code (Edward et al. 2015).

Table 4.B.1: Mains temperature in different seasons (Meteonorm [software])

Spring	summer	autumn	Winter
$8^{o}C$	$18^{o}C$	$11^{o}C$	$2^{o}C$

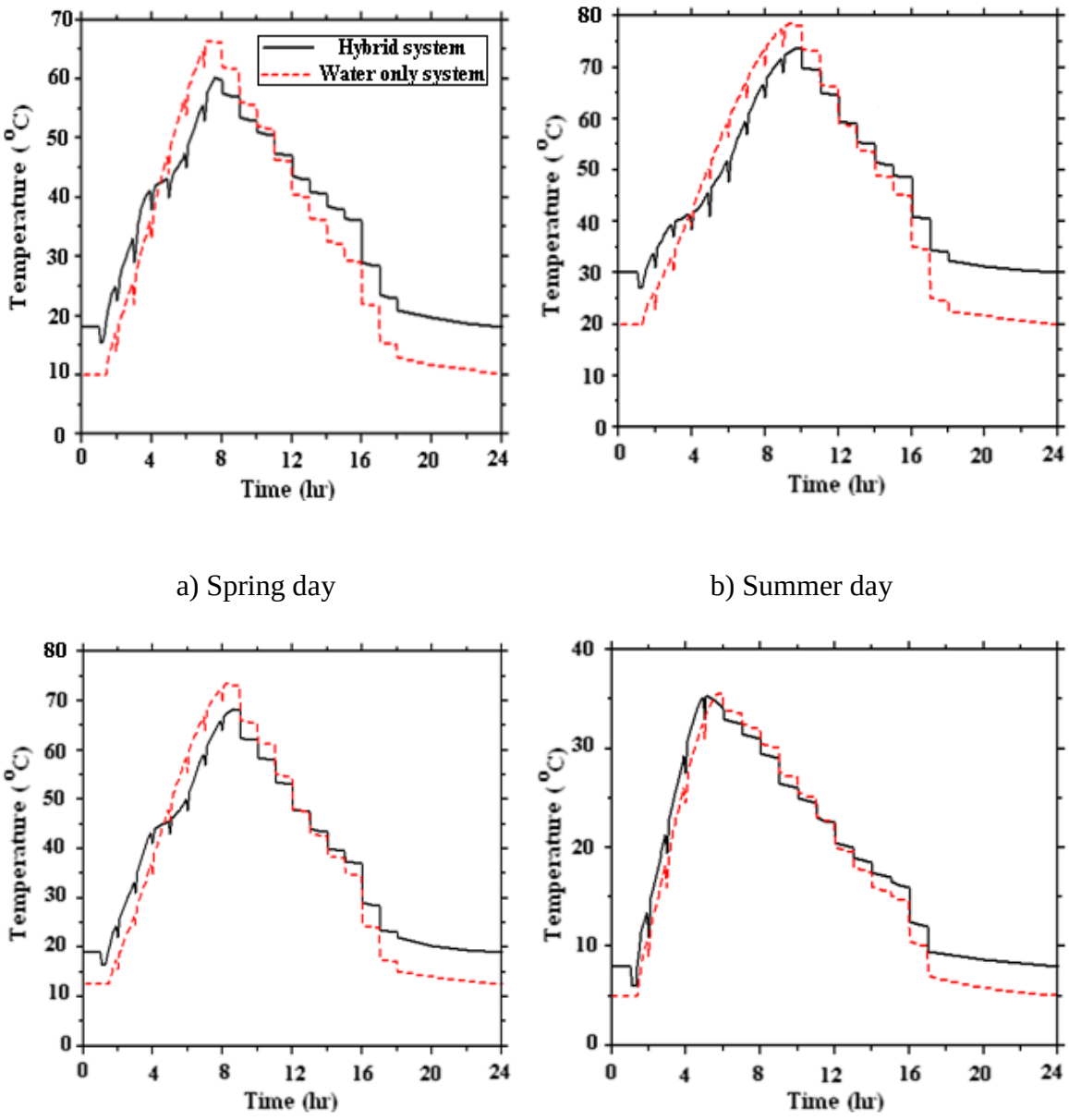

a) Spring day

b) Summer day

c) Autumn day

d) Winter day

Figure 4.B.3: Temperature at the tank top for both hybrid and water only systems (V_{tank}=120 liters)

CHAPTER 5

Potential of multiple Phase Change Materials (PCMs) in enhancing the performance of Solar Domestic Hot Water (SDHW) system

Complete citation:

H. M. Teamah, M. F. Lightstone, J. S. Cotton , Potential of multiple Phase Change Materials (PCMs) in enhancing the performance of Solar Domestic Hot Water (SDHW) system , Solar Energy Engineering-submitted February 2017.

Relative Contributions:

Teamah HM: Performed all the simulations, interpretation and analysis of the data, wrote the first draft of the manuscript including all figures and text and was responsible for the final draft submittal to the journal.

Lightstone MF: supervisor of Teamah HM, revised and modified the journal paper draft.

Cotton JS: Co-supervisor of Teamah HM, revised and modified the journal paper draft.

Abstract

The incorporation of PCMs in the tanks of a solar domestic hot water (SDHW) system has been the focus of the literature in the recent decades. Despite this, all reported modelling was concerned with low scale domestic applications suitable for a single family dwelling as an example. None was found on multi-residential or small commercial applications. Typically those applications require either a large few thousands liter tank or a series of modular tanks interlinked together. The current paper explores a multi-tank system with cascaded PCMs of different melting temperatures incorporated in the tanks. The PCMs are introduced as vertical cylindrical modules and water flowing along the length of tank is used as the heat transfer fluid. An enthalpy porosity model was developed to solve for the phase change process within the PCM modules. The model was validated and verified with previous work and predictions were in good agreement (less than 5% deviation) with the previous results. The hybrid tanks model was linked with the collector performance. Typical Canadian weather data and a dispersed demand profile of a three families' building were considered. The proper cascading of different types of PCM was judged based on the maximum possible volume reduction compared to the water only system with the same benefit to the end user. PCM maintains cooler water temperature leaving the tanks which reflects on reduction of collector losses and extension of pump activation time. According to the system energy balance, this is manifested on increasing the delivered energy to the load and hence solar fraction. It was found that cascading four 75 liter tanks containing PCMs of melting temperatures 54^{o}C,

42°C, 32°C and 16°C gives a nearly similar solar fraction obtained by a 630 liter water only tank. This means more than 50% reduction in the required storage volume.

Keywords

Multi-tank, phase change materials, enthalpy porosity, solar fraction, volume reduction

Nomenclature

A_c	Collector surface area [m^2]
C_{pl}	Liquid specific heat capacity [J/kg K]
C_{ps}	Solid specific heat capacity [J/kg K]
D	PCM cylinder outer diameter [m]
$E_{delivered}$	Energy delivered to the load [J]
$E_{loss, coll}$	Collector energy loss [J]
$E_{loss, tank}$	Tank energy loss [J]
E_{mains}	Mains water energy [J]
E_{solar}	Solar energy incident to the collector [J]
F_R	Heat removal factor
f_s	Solar fraction
$F_{s,annual}$	Annual solar fraction
G	Solar irradiation [W/m^2]
k	Thermal conductivity [W/mK]
L_c	Length of cylinder [m]

	Mass flow rate inlet to the tank [kg/s]
Q_u	Collector useful heat gain [kW]
n	Inner radius of phase change material cylinder [m]
ıt	Outer radius of phase change material cylinder [m]
r_s	Latent heat of fusion [kJ/kg]
T	Temperature [^oC]
T_{amb}	Ambient temperature [^oC]
	Temperature of incoming fluid [^oC]
T_m	Melting temperature of PCM [^oC]
T_{st}	Initial temperature of the tank [^oC]
U_L	Collector loss coefficient [W/m^2K]
V_{tank}	Tank volume [m^3]

Abbreviations

HTF	Heat transfer fluid
LES	Latent energy storage
PCM	Phase change material
SDHW	Solar domestic hot water
SES	Sensible energy storage
TES	Thermal energy storage

Latin Symbols

$(\tau\alpha)$	Transmittance absorbance product
η	Solar collector efficiency

Subscripts

c,inn	Inner surface of cylinder
c,out	Outer surface of cylinder
conv	Convective
In	Inlet
l	Liquid
m	Melting
st	Start
t	Transition

5.1. Introduction

Thermal energy storage is an essential component of solar domestic hot water (SDHW) system. Its proper sizing is crucial to even out the mismatch between the solar supply and residential demand of hot water. Required storage volume is strongly dependent on the targeted application. A solar hot water heating system for a typical household consisting of four individuals would have hot water storage of 150 to 300 L (Cruickshank and Harrison 2009). Hot water demand needed by a multi-residential building can be supplied through a large single tank or a series of small tanks interlinked together. Large volume

tanks are expensive and difficult to fabricate. In addition, they are not well suited to retrofit situations where the storage vessel must be moved into a building space through existing door openings. Consequently, larger storages are often constructed on site. Multi-tank configuration is a more economical alternative. Regular sized tanks are easily available in the market at an affordable price. They can be handled in the doorways and stacked over each other.

These economic advantages have motivated few researchers to compare multi-tank performance to a single tank ((Mather et al. (2002), Cruickshank and Harrison (2009), Dickinson et al. (2012)). They connected the tanks either in series or in parallel. They reported that the multi-tank serial interlinking promotes effective thermal stratification between tanks relative to the single tank configuration. Stratification arranges water layers in the order of their density. Maintaining stratification enhances the solar system performance (Hollands and Lightstone (1989)). Cooler water is sent to the collector which reduces its losses and hotter water is sent to the demand enhancing solar fraction. Solar fraction is the amount of energy delivered by the solar system relative to the total energy required by the load.

Thermal storage tanks either contain water or employ phase change materials besides water in the so-called hybrid system. Phase change materials (PCMs) possess higher energy density when changing its phase. In addition, they modulate the system temperature around their melt temperature (Zalba et al., 2003). PCMs are categorized into three main groups: organics, inorganics and eutectics (Abhat, 1983). Amongst the organic

group, fatty acids were reported to be suitable candidates for the solar system because of their high latent heat of fusion and stable properties (Desgrosseillier et al., 2011; Sari et al., 2009).

Despite their high latent heat storage capability, PCMs have poor sensible properties. Their low specific heat (~ half of water) reduces the energy storage for a wide temperature range of operation. Also, the poor thermal conductivity (~ third of water) adversely impacts the heat transfer rate to the PCMs and thus can limit the storage capacity of the system for a prescribed charging period (Bergles, 2011). Active and passive techniques have been proposed to resolve the low conductivity problem. Active techniques involve an external source such as electro-hydrodynamics to enhance the melting rate (Nakhla et al., 2015). Passive ones includes the usage of extended surfaces, embedding metallic particles to improve conductivity, and micro-encapsulating PCM (Jegadheeswaran and Pohekar, 2009; Agyenim et al., 2010; Sanusi et al., 2011; Pokhrel et al., 2010; Velraj et al., 1999; Stritih, 2004; Yingqiu et al., 1999; Lacroix and Benmadda, 1997).

Fins increase the area of the system which enhances the heat transfer rate, but it increases the overall cost of the system owing to the added material (Jegadheeswaran and Pohekar, 2009,; Agyenim et al., 2010). Embedding high conductive metal particles in the PCM matrix is another technique to enhance thermal conductivity (Sanusi et al., 2011; Pokhrel et al., 2010; Velraj et al., 1999). But those added particles tend to agglomerate and settle to the bottom of the tank. The third passive technique is micro-encapsulating PCM in thin rectangular slabs or small radii cylindrical and spherical containments. Those micro-

encapsulations reduce the conduction resistance imposed by PCM on the system (Stritih, 2004; Yingqiu et al., 1999; Lacroix and Benmadda, 1997).

Phase change materials inclusion in the water tank of a SDHW system has been studied extensively in the recent decades. Researchers tested realistic supply and draw-off patterns as well as approximated ones (Wang et al., 2015; Al-Hinti et al., 2010; Fazilati and Alemrajabi, 2013; Nabavitabatabayi et al., 2014; Nkwetta et al., 2014; Kousksou et al., 2011). PCM increases the storage capacity of the system and increases the exergy efficiency (Wang et al., 2015; Al-Hinti et al., 2010; Fazilati and Alemrajabi, 2013). The modulation of temperature around PCM melting point decreases the delivered temperature swing at night. Therefore, the system can supply the load with hot water for a longer period of time. This increases the predicted solar fraction (Al-Hinti et al., 2010; Fazilati and Alemrajabi, 2013, Kousksou et al. 2011).

From the previous review, PCMs were found to enhance solar system performance. Besides, multi-tank systems were only studied with water only in the tanks. The current paper presents the inclusion of PCM in a multi-tank system to supply hot water for a multi-residential building. To maximize benefit from PCM inclusion, different PCMs are cascaded in the tanks in a descending order of their melting point. This modulates the temperature operating range in each tank around PCM melting point and the effect of latent heat becomes more pronounced. The multi-PCM was found to enhance energy storage capability and exergy efficiency in high temperature concentrated solar power applications (Michels and Pitz-Paal 2007, Seeniraj and Narasimhan 2008, Tian and Zhao

2013). But for the low temperature applications, no similar research was found. In addition this analysis is an extension for the work presented on the single tank dynamic performance in SDHW system (Teamah et al. 2017). It considers the system components interaction to explain the role of PCMs in the tanks. The current paper considers storage volume as an independent variable. This allows for the prediction of possible storage volume reduction when PCMs are cascaded in the tanks relative to the water only tank.

5.2. System modelling

An in-house FORTRAN code was developed to predict the performance of hybrid tanks containing water and PCM. A schematic of the modeled system is shown in Figure 6.1. The storage tanks contain PCMs in thin cylindrical modules. PCMs of different melt temperatures are placed in each tank. The system includes: collector, pump, controller, storage tanks, and auxiliary heater. The system supplies hot water to a three family residential dwelling. The temperature set point on the load side is set to 55^{o}C. Auxiliary heater is turned on if the water from the tank temperature is less than 55^{o}C. It is mixed with the mains cold water when the inverse situation prevails. The component modelling is described below:

3. Collector: The Hottel-Whillier-Bliss equation is used to model a flat plate collector (Duffie and Beckman, 1991). The useful energy collected is given by:

$$Q_u = \dot{m}\, C_p (T_o - T_{in}) \tag{5.1}$$

This net gain can also be expressed in terms of incident irradiation and losses as follows:

$$Q_u = F_R A\big((\tau\alpha)G - U_L(T_{in} - T_{amb})\big) \quad (5.2)$$

By equating the previous two equations it yields;

$$T_o = T_{in} + \frac{F_R A_c}{\dot{m}\, C_p}\big((\tau\alpha)G - U_L(T_{in} - T_{amb})\big) \quad (5.3)$$

where T_o is the outlet temperature of the collector (=inlet temperature to the storage tank), T_{in} is the inlet temperature to the collector (=outlet temperature from the storage tank), F_R is the heat removal factor that is a function of the mass flow rate, T_{amb} is the ambient temperature and $(\tau\alpha)$ is the transmittance absorbance product and it is taken to be a constant of 0.8.

- Controller: The same control strategy reported by (Mather 2002) is considered. In this strategy, the controller activates the pump when the difference between the collector plate temperature and bottom of the tank reaches 7^{o}C. It remains on till this difference drops below 2 ^{o}C.
- Storage tanks: The storage tanks contain PCMs in vertical cylinders and water flows axially along their length. To model the phase change within the modules, the enthalpy porosity model is used. In this method, the latent heat of fusion is accounted for in the governing equation by defining an enthalpy term (Voller et al., 1985; Cornini et al., 1974). It is reported to have better stability than other methods (Voller et al., 1987). The model equations are provided in Appendix A. The axial flow of water parallel to the cylinders is presumed to be a one-dimensional plug flow. Heat exchange between water and PCM is accounted for by correlations that are applied at the outer surface of the

module. The details of the model are previously presented in a published paper (Teamah et al., 2016). Validations and verifications were conducted to ensure the robustness of the code. It showed very good agreement with the literature with maximum deviation of 5%. The details of a sample validation is presented in appendix A. Other validation and verification were presented in a published paper (Teamah et al., 2016).

To assess the performance of this system, solar fraction is computed. The solar fraction represents the percentage of the heating load supplied by solar energy and is given by:

$$f_s = \frac{Q_{del}}{Q_{load}} \tag{5.4}$$

The delivered solar load is calculated as:

$$Q_{del} = \int \dot{m}_{tank} C_{pw} \left(T_{top\ of\ tank} - T_{mains}\right) dt \tag{5.5}$$

where $\dot{m}_{tank} = \dot{m}_{demand} = 0.19\ kg/s$ when $T_{top\ of\ tank} < T_{setpoint}$ (5.6)

When $T_{top\ of\ tank} > T_{setpoint}$ the drawn mass flow rate from the tank reduced and is calculated as:

$$\dot{m}_{tank} = \dot{m}_{demand} \left(\frac{T_{setpoint} - T_{mains}}{T_{top\ of\ tank} - T_{mains}} \right) \tag{5.7}$$

Q_{load} represents the energy required by the system to meet the heating load with no supply of solar energy (i.e. the energy required to heat the mains cold water to the set point temperature) and it is calculated according to:

$$Q_{load} = \int \dot{m}_{del} C_{pw} \left(T_{setpoint} - T_{mains}\right) dt \tag{5.8}$$

By using this convention for calculating the solar fraction, the delivered solar energy can be related to the total energy required to meet the load by:

$$Q_{del} + Q_{aux} = Q_{load} \tag{5.9}$$

where Q_{aux} is the auxiliary power required by the solar system to meet the load requirements.

A representative day for each season of the year was chosen. The irradiation and ambient temperature data were imported from the (Meteonorm [software]) database for Toronto, Canada. A dispersed draw profile is chosen for the three families' consumption (Edwards et al., 2015). The profiles are presented in Appendix B. Day-long simulations were repeated until a periodic steady state was achieved. Other solar and load profiles were assessed and were found to not alter the conclusions of the study. Annual solar fraction is determined from the summation of the energy delivered to the load divided by the required load energy.

$$\mathrm{F_{s,annual}} = \frac{\sum Q_{del}|_{typical\ days}}{\sum Q_{load}|_{typical\ days}} \tag{5.10}$$

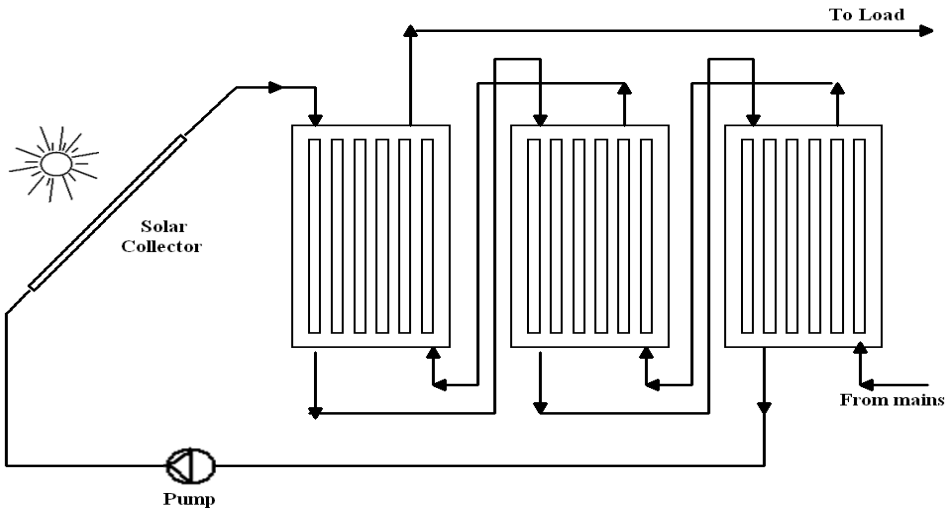

Figure 5.1: Schematic of the studied system

5.3. Sample results

According to the previous work done on the single tank in the SDHW system, PCM shows a promising potential in storage volume reduction without compromising solar fraction (Teamah et al. 2017). This is attributed to the effect of PCM in modulating the system temperature around its melt temperature. This is reflected on the reduction of the collector losses and the extension of pump activation time. According to the system energy balance, this increases the energy delivered to load and hence augments solar fraction. This motivated the current paper to apply this analysis methodology on multi-tank configuration where various PCMs are considered.

5.3.1. Results for a storage total volume= 300 liters

This section presents sample results for a case study that compares system performance of a multi-tank hybrid system to the water only system. A total storage volume of 300

liter is considered. The different configurations of the storage are shown in Figure 5.2. The first one is a 300 liter water only tank. The second one is a 300 liter tank containing capric acid (T_m=32^{o}C) in thin cylindrical containments. The third one consists of two 150 liters tanks with lauric acid (T_m=42^{o}C) placed in the first tank and caprylic acid (T_m=16^{o}C) in the second tank. The last configuration includes three tanks each of 100 liters in capacity containing lauric, capric and caprylic acids respectively.

The dimensions, and considered system parameters are given in Table 5.1. The PCM properties are given in Table 5.2. It includes the family of fatty acids that were chosen for their suitability for the residential application (Desgrosseillier et al., 2011; Sari et al., 2009). The weather data and draw off profiles listed in the Appendix B were used. Several other cases with different parameters were investigated and were found to yield the same conclusions.

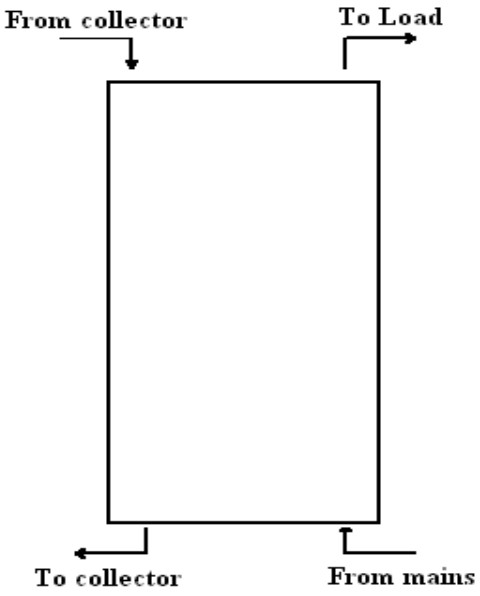

a) Water only 300 liter tank

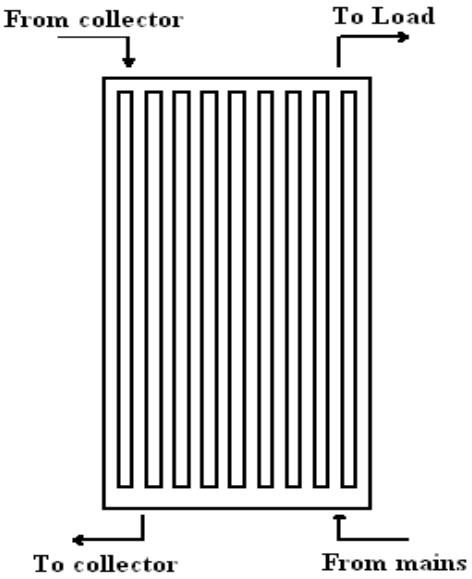

b) 300 liter tank (T_m=32^{o}C)

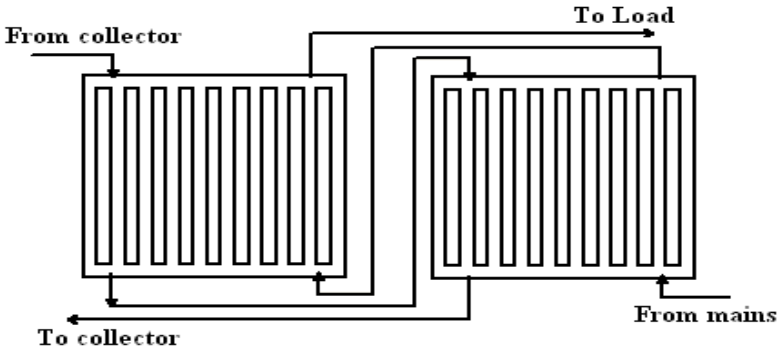

c) two 150 liter tanks (T_{m1}=42^{o}C, T_{m2}=16^{o}C)

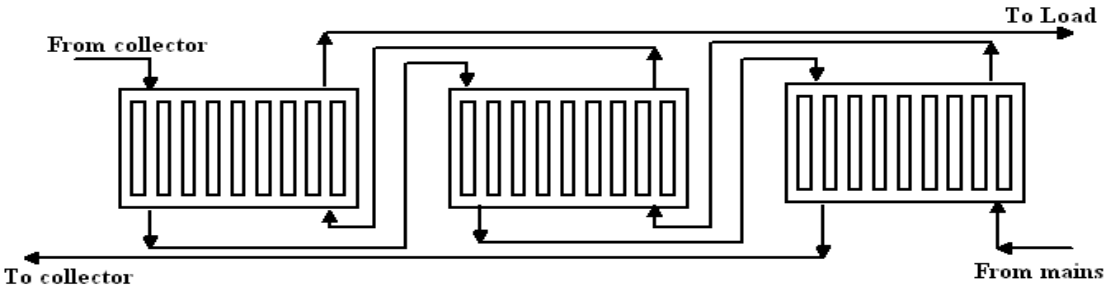

d) three100 liter tanks (T_{m1}=42^{o}C, T_{m2}=32^{o}C, T_{m3}=16^{o}C)

Figure 5.2: Studied storage configurations

Table 5.1: Parameters for the studied case

Parameter	Value
Collector area	16 m^2
Collector slope	45^o
Azimuth	0^o
Collector loss coefficient	5 W/m^2K
Collector mass flow rate	0.05 kg/s
Storage tank loss coefficient	0.55 W/m^2K
storage aspect ratio	2
PCM packing ratio	50%
PCM module diameter	2 cm
Daily drawn volume of hot water	480 liters
Discharging flow rate	0.19 kg/s

The predicted annual solar fractions for the four studied configurations are listed in Table 5.3. It is seen that there is an 8% increase in the annual solar fraction when capric acid was placed in the tank relative to the water only tank. The gain in solar fraction increases by 13% when two tanks containing different PCMs are considered. The gain increases marginally when 3 tanks instead of two tanks were considered (~1.4%). This gain in solar fraction can be interpreted through the energy balance on the studied system. Figure 5.3 shows the energies entering and exiting the system control volume.

Table 5.2: Thermo-physical properties of organic fatty acids

PCM	T_m [°C]	Density [kg/m^3]	Specific Heat [kJ/kg K]	Heat of Fusion [kJ/kg]	Thermal Conductivity of solid [W/m. k]
caprylic acids	16	860	1.7	150	0.15
Capric Acid	32	886	1.7	153	0.149
Lauric Acid	42	870	1.6	178	0.147
Myristic Acid	54	844	1.6 (solid), 2.7(liquid)	187	0.16

Table 5.3: Predicted solar fraction for the studied configurations

	Configuration (a)	Configuration (b)	Configuration (c)	Configuration (d)
$F_{s,annual}$	0.48	0.56	0.61	0.624

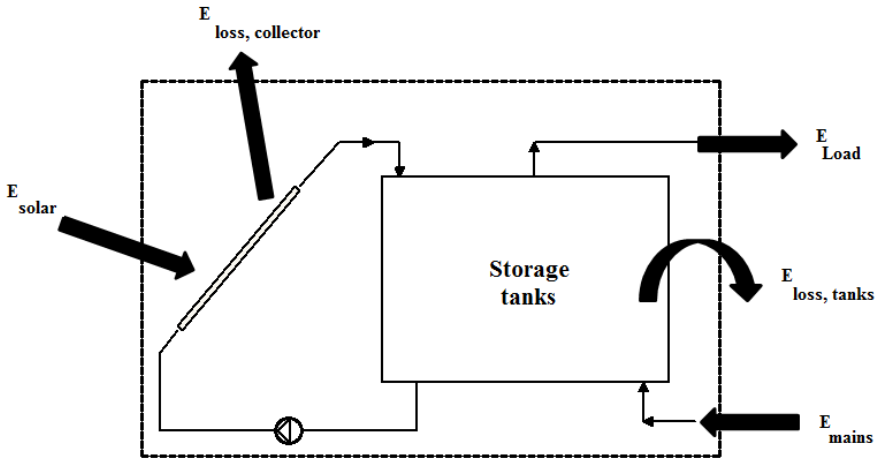

Figure 5.3: Energy entering and exiting the system control volume

According to the steady state energy balance;

$$E_{solar} + E_{mains} = E_{Load} + E_{loss,\ coll} + E_{loss,\ tank} \quad (5.11)$$

Also

$$E_{solar} = E_{delivered} + E_{loss,\ coll} + E_{loss,\ tank} \quad (5.12)$$

where

$$E_{delivered} = E_{Load} - E_{mains} \quad (5.13)$$

The annual energy breakdown for the four studied configurations is shown in Table 5.4. As seen from the numbers, cascading PCMs increases the input solar irradiation into the system. In addition, it reduces the collector losses compared to the water only system. Those two factors contribute to the increase of the energy delivered to the load as tank

losses effect is minor. Thus the solar fraction supplied with the cascaded PCM tanks is higher than the corresponding of the water only system.

Table 5.4: Annual energy breakdown for the studied configurations (total volume= 300 liters)

	Configuration (a)	Configuration (b)	Configuration (c)	Configuration (d)
E_{solar} (GJ)	47.3	49.1	50.6	51
$E_{loss,\ coll}$ (GJ)	28.9	28	27.6	27.47
$E_{loss,\ tank}$ (GJ)	2.43	2.6	2.85	2.95
$E_{delivered}$ (GJ)	15.97	18.5	20.15	20.58
Annual energy required by the load (GJ)	33.1	33.1	33.1	33.1
Average annual solar fraction	0.48	0.56	0.61	0.624

The reduction in collector loss and gain in incident solar radiation can be illustrated by inspecting the performance of the system in the studied spring day as an example. Figure 5.4 shows the pump activation period and the temperature of water returning to the collector. Hour zero indicates 6 a.m. As seen from Figure 5.4a, the period of pump activation is longer for the cascaded PCM systems compared to the water only system. It

is longer by 0.4 hrs for the one PCM case. It is activated an extra 0.6 hrs when 2 PCMs are cascaded. Cascading the 3 tanks yields a marginal extra period of activation relative to the 2 PCMs case (~0.05 hrs). The longer pump activation period is directly related to the cooler water returning to the collector when PCMs are enclosed in the tanks. Figure 4b shows the temperature of water leaving the storage and entering the collector for the four studied configurations. The temperature is preserved at the mains temperature in the beginning of the day. The temperature begins to rise when the controller senses sufficient temperature difference between the collector plate and the tank bottom. When the pump is activated the temperature generally rises in all the configurations. There is a sharp drop in the temperature at the beginning of each hour when the discharge of the household is initiated. The profiles differ in the case of hybrid systems compared to water only system. This is attributed to the modulation of PCMs to the system temperature. This observed around 32^{o}C for the hybrid tank containing capric acid. It occurs around 42 ^{o}C and 16 ^{o}C for the two cascaded tanks. And finally it plateaus around 42 ^{o}C, 32 ^{o}C and 16 ^{o}C for the three cascaded tanks case.

5.3.2. Effect of Thermal Storage Volume on System Solar Fraction

To assess if the PCM inclusion in the system is always beneficial, the effect of storage volume on solar fraction was carefully inspected. The annual solar fraction can be written as:

$$f_s = \frac{E_{\text{delivered to load}}}{E_{\text{required by load}}} \tag{5.14}$$

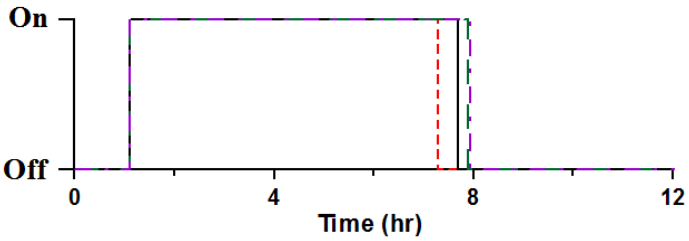

a) Pump activation period

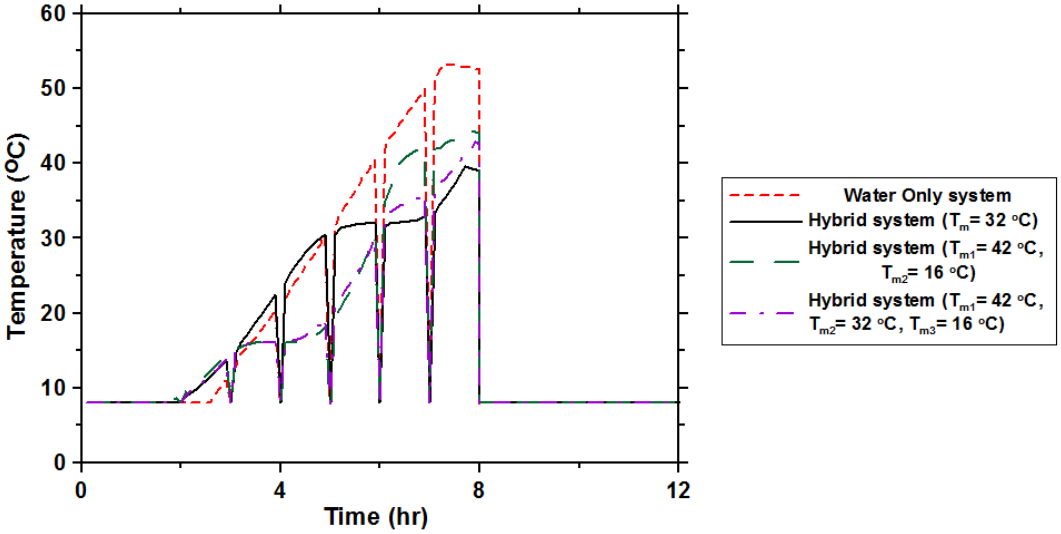

b) Inlet water temperature to the collector

Figure 5.4: Pump activation period and Inlet water temperature to the collector

According to (Equation (5.11)) $E_{\text{delivered to load}}$ can be written as:

$$E_{\text{delivered to load}} = E_{\text{solar}} - (E_{\text{loss,collector}} + E_{\text{loss,tanks}}) \quad (5.15)$$

This yields that:

$$f_s = \frac{E_{\text{solar}} - (E_{\text{loss,collector}} + E_{\text{loss,tanks}})}{E_{\text{required by load}}} \quad (5.16)$$

E_{solar} is a function of the pump activation period as the integration is performed over times when the pump is running. The storage volume influences the pump run time as the

pump activation control strategy turns it on based on the difference between collector temperature and the temperature at the bottom of the storage. $E_{loss,collector}$ is also affected by the volume of the storage. When the water storage is undersized relative to the demand, hot water will be sent to the collector, increasing losses. As the storage volume increases, hot water is less likely to make it to the bottom of the tank. The heat loss from the tanks ($E_{loss,tanks}$) constitute a minor component in the energy balance as the tanks are well insulated. As such, at large tank volumes where cool fluid is consistently sent to the collector inlet, the solar fraction should decrease only slightly with increasing storage volume due to the storage loss.

To assess the effect of the storage volume, the system simulations were repeated for a series of tank volumes. Water only tank and cascaded multi-tanks with different PCMs were considered. Figure 5.5 shows the predicted solar fraction for the considered systems. To avoid the confusion, each cascaded system with a certain tank volume is shown separately (Figures 5.5b, 5.5c, 5.5d, 5.5e, 5.5f and 5.5g). The legend shown in Figure 5.5a shows the cascading of the different PCMs in all figures. The dotted red line represents the water only system. For example Figure 5.5b shows the cascaded 300 liter hybrid tanks relative to the water only system predicted solar fraction. The (+) symbol indicates the solar fraction when a 300 liter tank containing PCM of melt temperature 32^{o}C was considered. The (▲) symbol shows the predicted solar fraction for two cascaded 300 liter tanks the first contains PCM of melt temperature 42^{o}C and the second contains PCM of melt temperature 16^{o}C. Finally the (✕) symbol shows the predicted solar fraction for three cascaded 300 liter tanks the first contains PCM of melt

temperature 42^{o}C and the second contains PCM of melt temperature 32^{o}C and the last contains PCM of melt temperature 16^{o}C. When comparing those symbols to the water only dotted red lines, it is found that PCM enhances the solar fraction in the undersized storage volume (300 liters). For the 600 liters and the 900 liters, the hybrid systems and the water only system behaves nearly the same. By the same methodology of interpretation, Figures 5.5c, 5.5d, 5.5e, 5.5f and 5.5g can be explained. It is seen that PCMs offers benefit in augmenting solar fraction for undersized tanks (<600 liters). For the oversized storage volume all the systems perform similarly. Figure 5.5h shows all the studied cascaded hybrid systems together with the water only system. Cascading smaller tanks enhances the solar fraction. The virtual lines connecting the symbols shows that when volume of cascaded tanks decreases below 100 liters there is a marginal benefit (i.e the cascaded 100 liter tanks and the cascaded 75 liter tanks). Approximately the same solar fraction is obtained by 3 cascaded 100 liter tanks or 4 cascaded 75 liter tanks. This is attributed to the fact that the considered system benefits from tank to tank stratification and stratifications in the tanks themselves. So when lots of tanks are cascaded, the stratification within the tanks will not be improved that much and a marginal gain in solar fraction results.

The individual components of the energy balance for one of the cases (cascaded hybrid 200 liter tanks) are shown in Figure 5.6. The input solar radiation for the hybrid configurations is higher than the water only system until a volume of about 600 liters (Figure 5.6b). After that the two curves approach each other since the pump run time becomes equal when the storage is oversized. Figure 5.6c shows that collector loss for the

hybrid configurations is lower in the smaller storage volumes since water only tanks send hotter water to the collector thus deteriorating its performance. When the storage is oversized this situation will not happen and the curves overlap. The tanks loss (Figure 5.6d) is higher for the hybrid configurations due to higher average temperatures (about 3 ^{o}C), but it has a negligible impact on the system energy balance. The energy from the solar thermal system delivered to the load is shown in Figure 5.6e. The cascaded PCM configuration deliver more energy to the load in the smaller storage volumes with the differences diminishing as the storage volume increases. The slight drop in delivered energy at high volumes from both systems is due to increased storage heat losses resulting from larger surface area.

5.4. Storage volume requirements of the multi-tank hybrid system relative to the water only system

Figure 5.5 shows the solar fraction for the multi-tanks hybrid system and water only system as a function of storage volume. PCMs show noticeable enhancement in undersized storage volumes. However, this conclusion is a result of the water-only tank being undersized for the application. As the storage volume of the tank increases, both curves approach the same behaviour (Storage volume ~ 600 liters). The benefit of PCM inclusion is the reduction in volume that is required without compromising the peak solar fraction. For the conditions considered in this work, a cascaded four 75 liter tanks system results in approximately similar solar fraction delivered by 630 l water only tank. Those values are

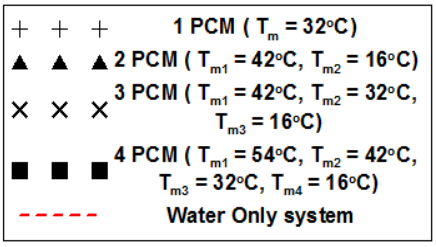

a) Legend for the PCM cascade

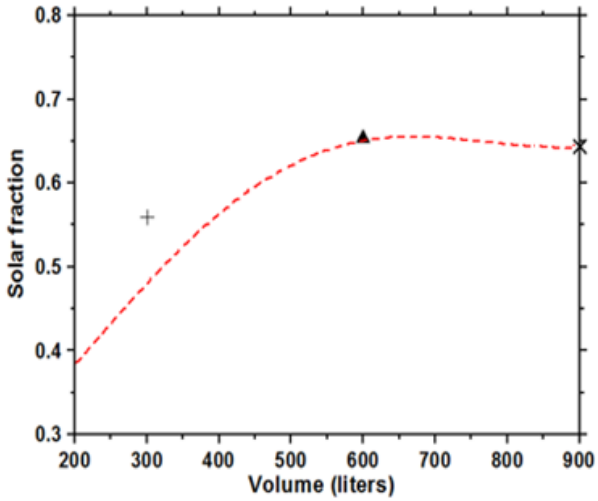

b) Solar fraction of cascaded hybrid system (V_{tank} = 300 liters) versus water only system

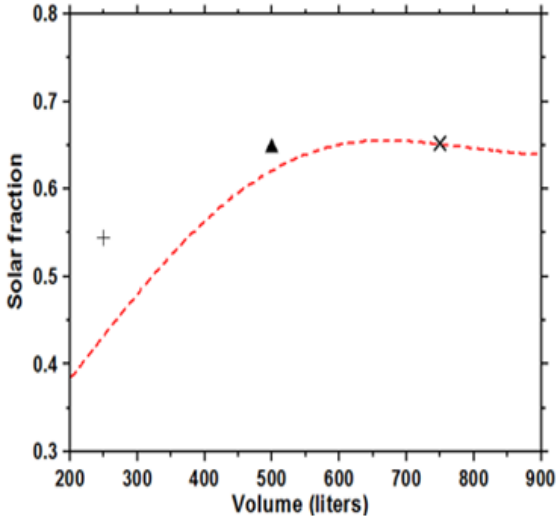

c) Solar fraction of cascaded hybrid system (V_{tank} = 250 liters) versus water only system

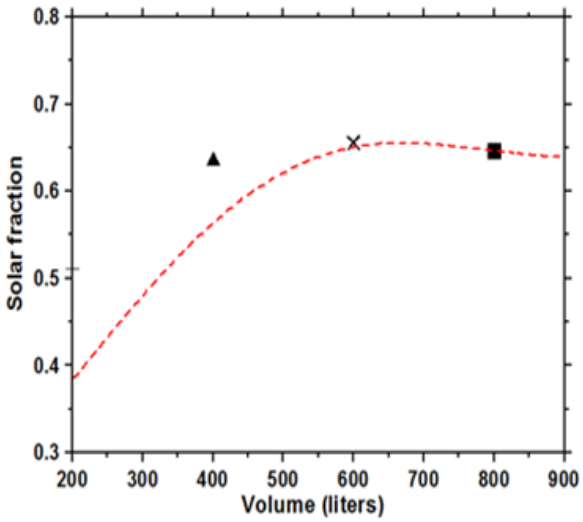

d) Solar fraction of cascaded hybrid system (V_{tank} = 200 liters) versus water only system

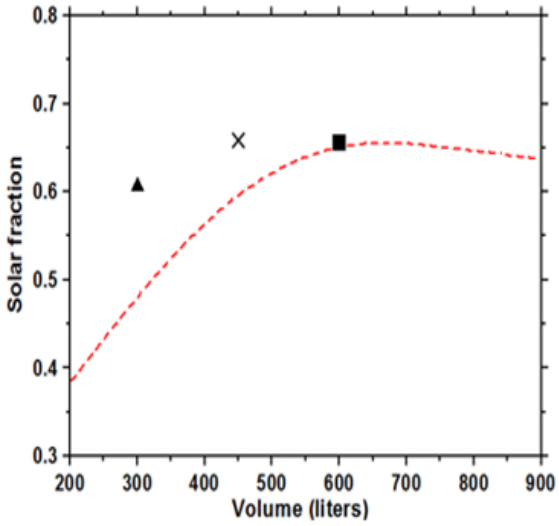

e) Solar fraction of cascaded hybrid system (V_{tank} = 150 liters) versus water only system

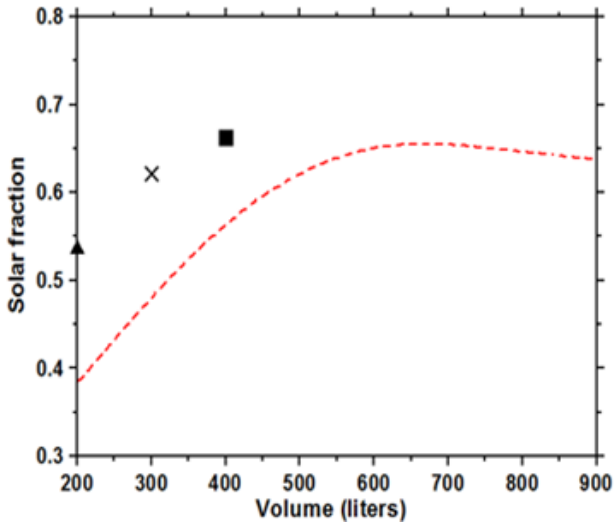

f) Solar fraction of cascaded hybrid system (V_{tank} = 100 liters) versus water only system

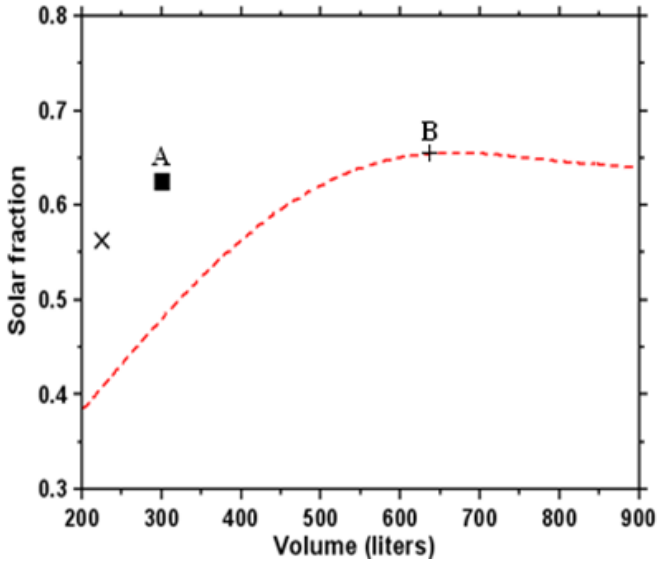

g) Solar fraction of cascaded hybrid system (V_{tank} = 75 liters) versus water only system

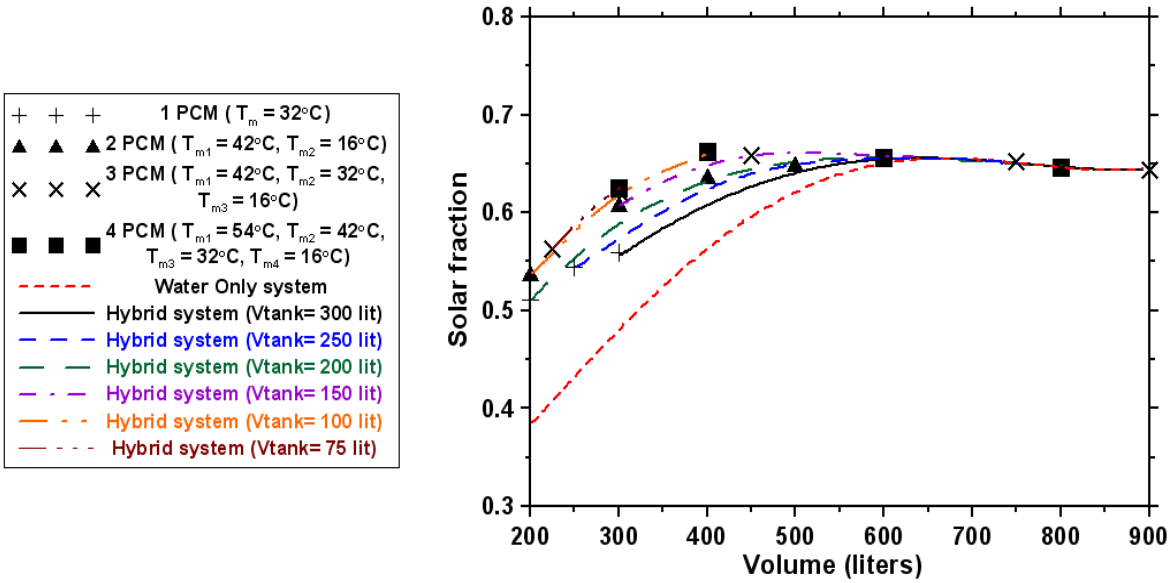

h) Grouped solar fraction of cascaded hybrid system versus water only system.

Figure 5.5: Average solar fraction versus volume for hybrid and water only systems

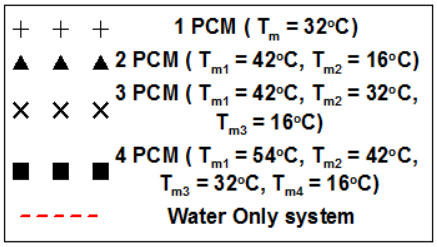

a) legend

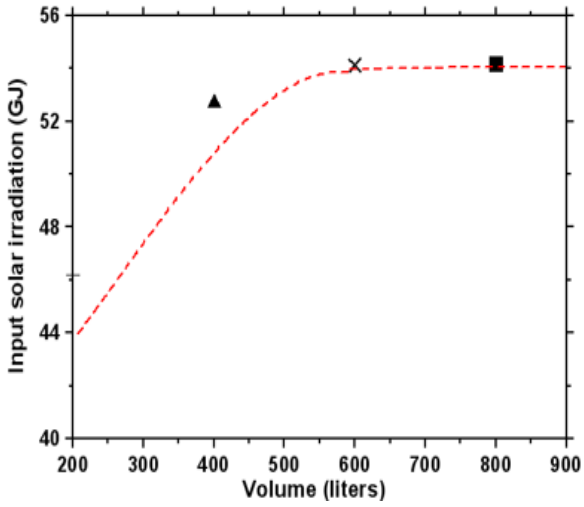

b) Input solar irradiation for the hybrid cascaded and water only systems (V_{tank} = 200 liters)

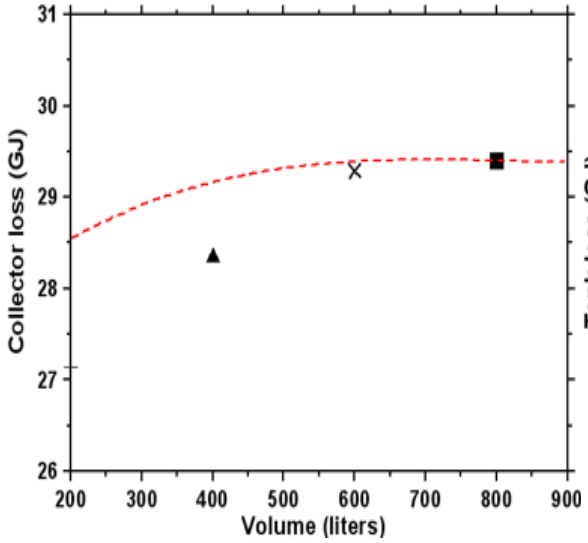

c) Collector loss for the hybrid cascaded and water only systems (V_{tank} = 200 liters)

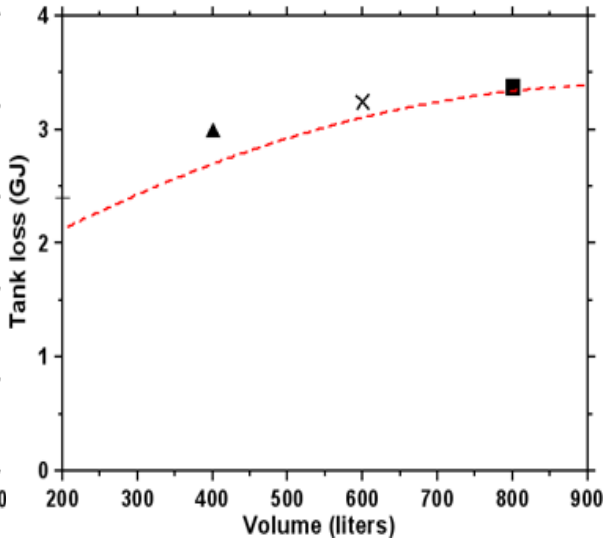

d) Tank loss for the hybrid cascaded and water only systems (V_{tank} = 200 liters)

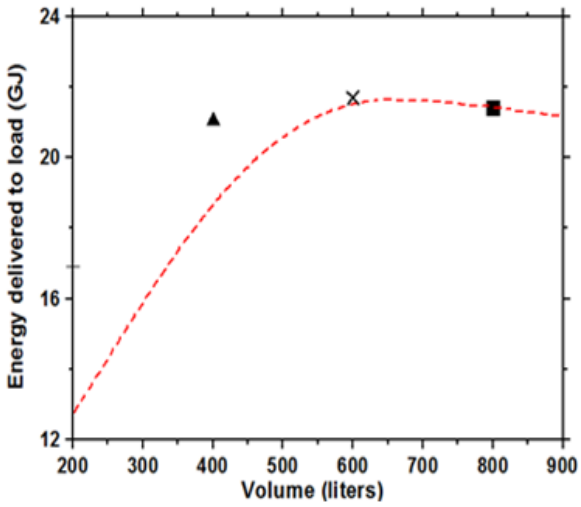

e) Energy delivered for the hybrid cascaded and water only systems (V_{tank} = 200 liters)

Figure 5.6: Energy balance components for the hybrid cascaded and water only systems (V_{tank} = 200 liters)

shown by points A and B in Figure 5.5g. This yields a reduction in storage volume of about 52%.

5.5. Summary and Conclusion

The incorporation of PCMs in thermal storage tanks has been a subject of the ongoing research. However, those studies were oriented to single tank system to supply a typical family with hot water. The current work deals with multi-residential applications. The current paper explains the potential of cascaded PCMs in the reduction of required storage volume to yield the same peak solar fraction. It is based on an energy balance that considers the interactions between storage system components. It is concluded that PCMs provide a benefit only in comparison to an undersized water based storage system. As the storage volume is increased, the benefit of PCM diminishes and the systems

eventually converge to the same performance. The system energy balance revealed that the benefit of cascading PCMs at low storage volumes is due to: the increase in pump activation time and reduction of the collector loss. The best case can be achieved by putting PCM of the least melting temperature in the last tank of the cascaded assembly. This insures that the water inlet to the collector is as cool as possible which maximizes the predicted benefits.

The case study presented herein considered a PCM volume fraction of 50%, and 2 cm diameter modules. There is a potential for further reduction in tank volume without compromising solar fraction by exploring the effect of various parameters. The main idea of the presented results is to assess the potential of cascaded PCM to enhance solar domestic hot water system performance which has not been reported before.

Acknowledgement

The authors are grateful to the Natural Sciences and Engineering Research Council of Canada and the Smart Net-Zero Energy Buildings Strategic Research Network (SNEBRN) for their financial support for this work.

5.6. References

[1] Cruickshank, C.A., and Harrison, S.J., 2009, "Characterization of a Thermosyphon Heat Exchanger for Solar Domestic Hot Water Systems", Journal of Solar Energy Engineering 131(2), 024502-024502-4**.**

[2] Mather, D.W., Hollands, K.G.T., and Wright, J.L., 2002, "Single- and Multi-tank

Energy Storage for Solar Heating Systems: Fundamentals", Solar Energy 73 (1), 3–13.

[3] Dickinson, R. M., Cruickshank, C. A., and Harrison., S. J., 2012, "The Effect of Discharge Configurations on the Thermal Behavior of a Multi-tank Storage System", Energy Procedia 30, 215-224.

[4] Hollands, K.G.T., and Lightstone, M.F., 1989, "A Review of Low-Flow, Stratified-Tank Solar Water Heating Systems", Solar Energy 43(2), 97-105.

[5] Zalba, B., Marin, J. M., Cabeza, L. F., and Mehling, H., 2003, "Review on thermal energy storage with phase change: materials, heat transfer analysis and applications", Applied Thermal Engineering 23(3), 251-283.

[6] Abhat, A., 1983, "Low temperature latent heat thermal energy storage: Heat storage materials", Solar Energy 30(4), 313-332.

[7] Desgrosseillier, L., Murray, R., Safatli, A., Marin, G., Stewart, J., Osbourne, N., White, M.A., Groulx, D. , 2011, "Phase Change Material Selection in the Design of a Latent Heat Energy Storage System Coupled with a Domestic Hot Water Solar Thermal System", ASHRAE Annual Conference, Montreal, Canada.

[8] Sari, A., and Karaipekli, A., 2009, "Preparation, thermal properties and thermal reliability of palmitic acid/expanded graphite composite as form-stable PCM for thermal energy storage",Solar Energy Materials and Solar Cells 93, 571-576.

[9] Bergles, A. E., 2011, "Recent developments in enhanced heat transfer," International Journal of Heat and Mass Transfer 47(8), 1001-1008.

[10] Nakhla, D., Sadek, H., and Cotton, J. S., 2015,"Melting performance

enhancement in latent heat storage module using solid extraction electrohydrodynamics (EHD) ” International Journal of Heat and Mass Transfer 81, 695-704.

[11] Jegadheeswaran, S., and Pohekar, S. D. , 2009, "Performance enhancement in latent heat thermal storage system: A review," Renewable and Sustainable Energy Reviews 13(9), 2225–2244.

[12] Agyenim, F., Hewitt, N., Eames, P. and Smyth, M., 2010,"A review of materials, heat transfer and phase change problem formulation for latent heat thermal energy storage systems (LHTESS)," Renewable and Sustainable Energy Reviews 14(2), 615–628.

[13] Sanusi, O., Warzoha, R., and Fleischer, A. S., 2011, "Energy storage and solidification of paraffin phase change material embedded with graphite nano-fibers," International Journal of Heat and Mass Transfer 54(19), 4429–4436.

[14] Pokhrel, R., Gonzalez, J. E., Hight, T., and Adalsteinsonn,T., 2010, " Analysis and Design of a Paraffin/Graphite Composite PCM Integrated in a Thermal Storage Unit," ASME J. Sol. Energy Eng. 132(4), 041006.

[15] Velraj, R., Seeniraj, R. V., Hafner, B., Faber, C., and Schwarzer, K., 1999, "Heat Transfer Enhancement in a Latent Heat Storage System," Solar Energy 65(3), 171–180.

[16] Stritih, U., 2004, "An experimental study of enhanced heat transfer in rectangular PCM thermal storage," International Journal of Heat and Mass Transfer 47 (12), 2841–2847.

[17] Yingqiu, Z.,Yinping, Z., Yi, J., and Yanbing, K., 1999, " Thermal Storage and Heat Transfer in Phase Change Material Outside a Circular Tube with Axial Variation of the Heat Transfer Fluid Temperature", ASME J. Sol. Energy Eng. 121(3), 145-149.

[18] Lacroix, M. and Benmadda, M., 1997, "Numerical Simulation of Natural Convection-Dominated Melting and Solidification From a Finned Vertical Wall," Numerical Heat Transfer, Part A: Applications 31(1), 71-86.

[19] Wang, Z., Qiu, F., Yang, W., and Zhao, X., 2015, "Applications of solar water heating system with phase change material", Renewable and Sustainable Energy Reviews 52, 645-652.

[20] Al-Hinti, I., Al-Ghandoor, A., Maaly, A., Abu Naqeera, I., Al-Khateeb, Z., and Al-Sheikh, O., 2010,"Experimental investigation on the use of water-phase change material storage in conventional solar water heating systems", Energy Conversion and Management 51, 1735-1740.

[21] Fazilati, M. A., and Alemrajabi, A. A., 2013, "Phase change material for enhancing solar water heater, an experimental approach", Energy Conversion and Management 71, 138-145.

[22] Nabavitabatabayi, M., Haghighat, F., Moreau, A., and Sra, P., 2014, "Numerical analysis of a thermally enhanced domestic hot water tank", Applied Energy 129, 253-260.

[23] Nkwetta, D. N., Vouillamoz, P., Haghighat, F., El Mankibi, M., Moreau, A., and Desai, K., 2014, "Phase change materials in hot water tank for shifting peak

power demand", Solar Energy 107, 628-635.

[24] Kousksou, T., Bruel, P., Cherreau, G., Leoussoff, V. and El Rhafiki, T., 2011, "PCM storage for solar DHW: From an unfulfilled promise to a real benefit", Solar Energy 85(9), 2033-2040.

[25] Michels, H., and, Pitz-Paal, R, 2007, "Cascaded latent heat storage for parabolic trough solar power plants", Solar Energy 8(6), 829-837.

[26] Seeniraj, R.V., and, Narasimhan, N.L., 2008, "Performance enhancement of a solar dynamic LHTS module having both fins and multiple PCMs", Solar Energy 82(6), 535-542.

[27] Tian, Y., and Zhao, C.Y., 2013, "Thermal and exergetic analysis of Metal Foam-enhanced Cascaded Thermal Energy Storage (MF-CTES)", International Journal of Heat and Mass Transfer 58 (1–2), 86-96.

[28] Duffie JA, and Beckman WA, Solar Engineering of Thermal Processes, Second Edition, Wiley J. & Sons, Inc, New York, 1991.

[29] Voller, V. R., Markatos, N. C., and Cross, M., 1985 " Techniques for accounting for the moving interface in convection/diffusion phase change". Numerical Methods in Thermal Problems 4, 595-609.

[30] Cornini, G., Guidiq, S.D., Lewis, RW., and Zienkiewiq, O.C., 1974, "Finite Element Solution of Non-linear Heat Conduction Problems with Reference to Phase Change," International Journal for Numerical Methods in Engineering 8, 613-624.

[31] Voller, V. R., Cross, M., and Markatos, N. C., 1987, "An enthalpy method for convection/diffusion phase changes". International Journal of Numerical Methods in Engineering 24, 271-284.

[32] Teamah HM, Lightstone MF, Cotton JS. Numerical Investigation and Non dimensional Analysis of the Dynamic Performance of a Thermal Energy Storage System Containing Phase Change Materials and Liquid Water. ASME. I. Sol. Energy Eng. 2016; 139(2):021004-021004-14. doi:10.1115/1.4034642.

[33] Teamah H. M., Lightstone M. F., Cotton J.S. , 2017, "An alternative approach for assessing the benefit of phase change materials in solar domestic hot water systems". Submitted to the Solar Energy journal.

[34] Meteonorm [software], available from: http://www.meteonorm.com

[35] Edwards S., Beausoleil-Morrison I. and Laperrie`re A., 2015, "Representative Hot Water Draw Profiles at High Temporal Resolution for Simulating the Performance of Solar Thermal Systems," Solar Energy 111, 43-52.

[36] Esen, M., Ayhan, T., 1996, "Development of a model compatible with solar assisted cylindrical energy storage tank and variation of stored energy with time for different phase change materials", Energy Conversion and Management 37(12), 1775-1785.

[37] Rohsenow, W. M., Hartnett, J.P., and Ganic, E. N., 1985, Handbook of heat transfer fundamentals, 2nd edn, (Eds). New York.

[38] De Gracia A., Oró E., Farid M. M., Cabeza L. F., 2011,"Thermal analysis of including phase change material in a domestic hot water cylinder", Applied Thermal Engineering, Vol. 31, pp. 3938-3945.

Appendix A

According to the enthalpy porosity formulation (Esen and Ayhan, 1996) specific enthalpy (enthalpy per unit mass) can be defined based on the PCM phase (solid, liquid or transition) as follows:

$$i(T) = C_{p,s}T \qquad T < T_{m1} \qquad (A.1)$$

$$i(T) = C_{p,s}T_{m1} + \frac{r_s(T - T_{m1})}{\Delta T_m} \qquad T_{m1} < T < T_{m2} \qquad (A.2)$$

$$i(T) = C_{p,l}(T - T_{m2}) + r_s + C_{p,s}T_{m1} \qquad T > T_{m2} \qquad (A.3)$$

Where r_s is the latent heat, T_{m1} is the lower melting temperature and $T_{m2}$is the upper melting temperature.

The discretized conduction dominated melting equation is given by:

$$\rho V_{j,k}\left.\frac{\partial i}{\partial t}\right|_{j,k} = -KA_k\left.\frac{\partial T}{\partial R}\right|_k + KA_{k-1}\left.\frac{\partial T}{\partial R}\right|_{k-1} + KA_j\left.\frac{\partial T}{\partial Z}\right|_j - KA_{j-1}\left.\frac{\partial T}{\partial Z}\right|_{j-1} \qquad (A.4)$$

Central differencing is applied to approximate the derivatives above.

The code solves the enthalpy porosity equations together with the conduction dominated melting equation. A uniform grid is applied. The heat transfer to the PCM is calculated using the correlations developed by (Rohsenow et al., 1985).

Validation of sequential charging and discharging

The results of the code were compared with the results reported by (De Gracia et al., 2011). The geometry they considered is illustrated in Figure 5.A.1. It consists of a 180 liter tank of water containing PCM cylinders that constitutes 22% by volume. The cylinder can be heated at the bottom by electric heaters. When discharging is initiated, cold water enters from the bottom of the tank and hot water leaves from the top. They used seven thermocouples to monitor the water temperature in the tank at different levels. They conducted a parametric analysis by varying the diameter of the PCM cylinders. They studied one of the diameters experimentally as well (40 mm). As the geometry resembles the one considered here, the experimental studied case was performed to validate the present results.

They presented the results for three scenarios of sequential charging and discharging. One of them is compared with the present code results. In this scenario, the tank is initially at a uniform temperature 80^{o}C. The discharging flowrate is 0.2 kg/s. Water discharges of 10 minutes each are initiated at different times of 0, 60, 120, 180, 240, 300, 360 min.

The predicted temperature at the top of the tank is overlapped with the present results as shown in Figure 5.A.2. As shown from the curves, water remains at its initial temperature until the end of the first hour. Water temperature decreases when discharging is initiated for a period of ten minutes. After that water temperature decreases due to the heat losses from the tank to the environement (T_{amb}=21^{o}C). After 120 minutes, the third discharge is

initiated and water temperature drops for 10 minutes. After the discharge end, the PCM begins to heat up the adjacent water as PCM is still hot (T_m=57^{o}C). This trend is repeated for the consequent two discharges. By the end of the discharge initiated at the beginning of the fourth hour, the water temperature reaches 37^{o}C and thus no benefit for discharging further (demand set point temperature is 37^{o}C). This causes the temperature of water to decrease during the rest of the experiment due to the heat losses from the tank. There is a very good agreement between the present code and the reported results with maximum deviation of 3.9% between the results.

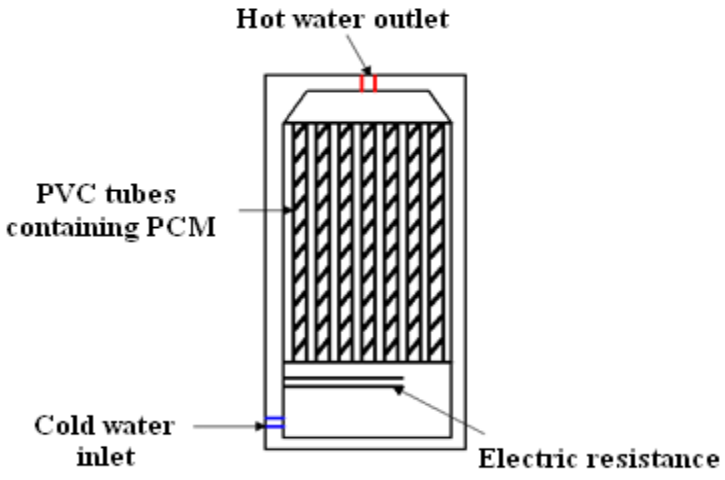

Figure 5.A.1: Schematic of the system studied by (De Gracia et al., 2011).

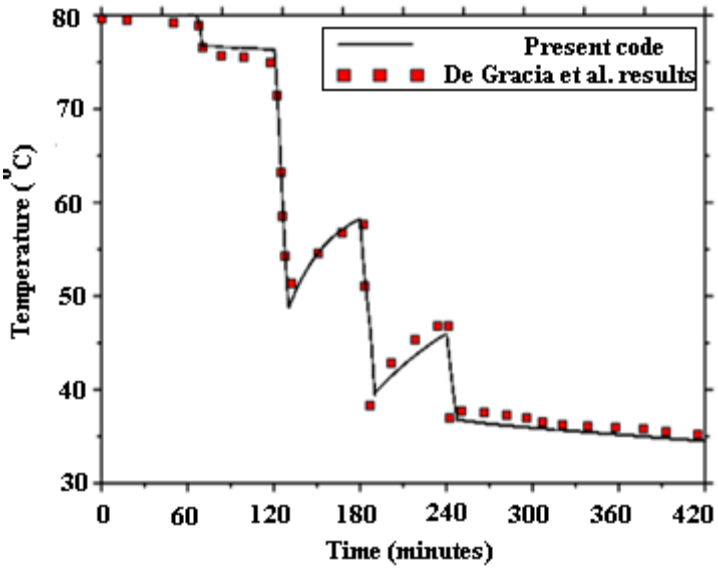

Figure 5.A.2: Comparison of the present code with (De Gracia et al., 2011) scenario 3 results.

Appendix B

Weather data and demand profile

Irradiation and ambient temperature were extracted from the Meteonorm database for Toronto location. Each season of the year is represented by a typical day which occurs frequently throughout the season. Figure 5.B.1 shows the irradiation and ambient temperature profiles for those days. The profiles used in the code are approximated with the dotted polynomial curve fit. The dispersed consumption profile for typical Canadian families was chosen based on the reported results by (Edward et al., 2015). The profile is shown in Figure 5.B.2. . . The mains temperature in each season is listed in Table 5.B.1.

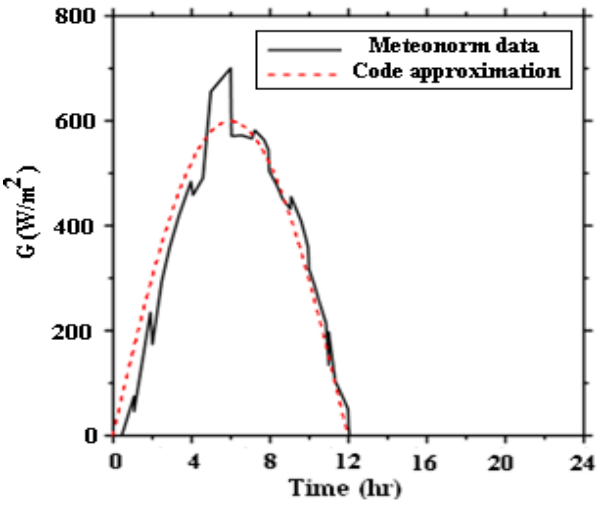

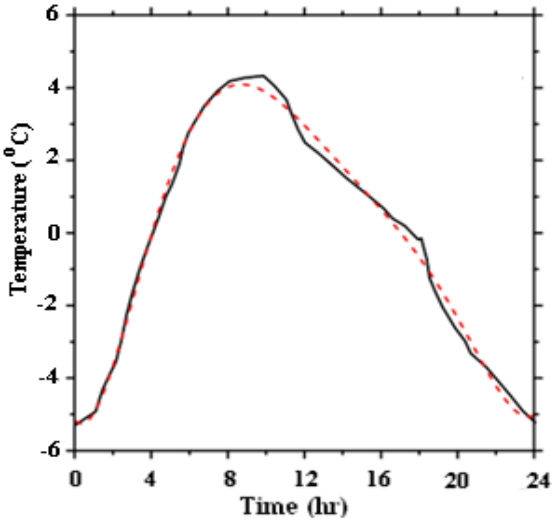

a) Irradiation profile on the horizontal b) Ambient temperature

i) Typical spring day data

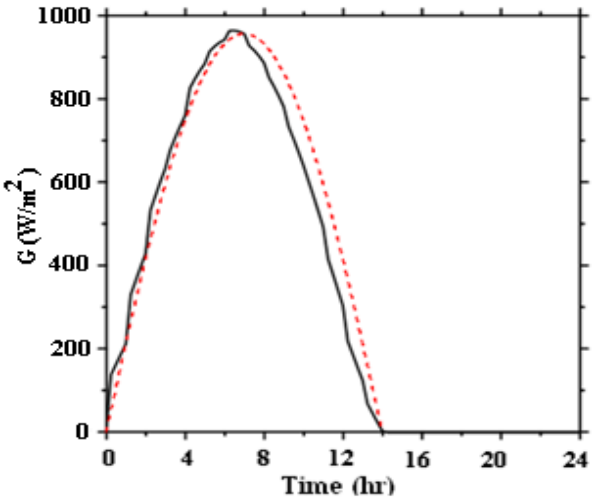

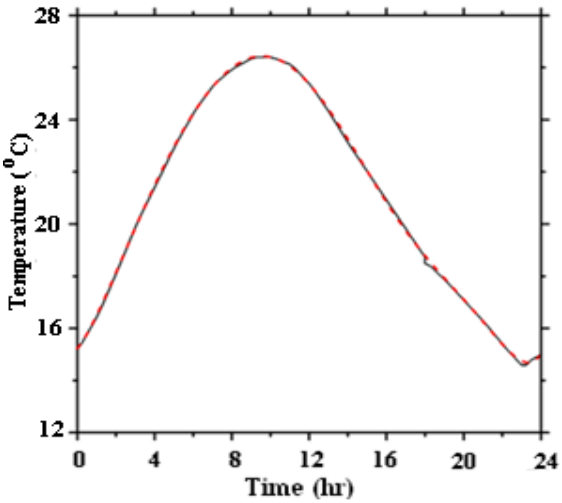

a) Irradiation profile on the horizontal b) Ambient temperature

ii) Typical summer day data

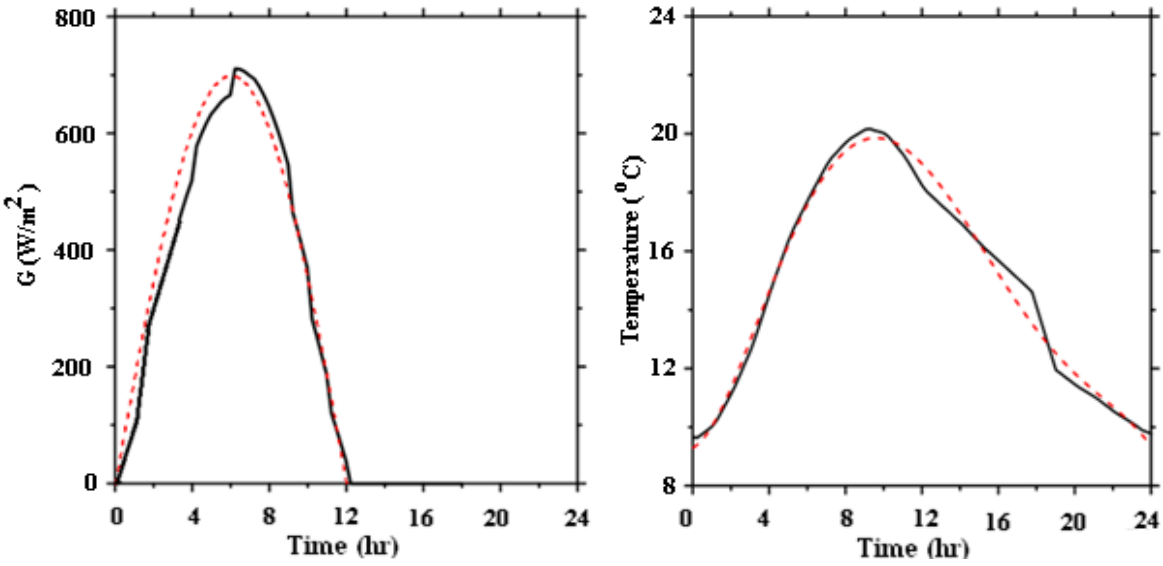

a) Irradiation profile on the horizontal b) Ambient temperature

iii) Typical autumn day data

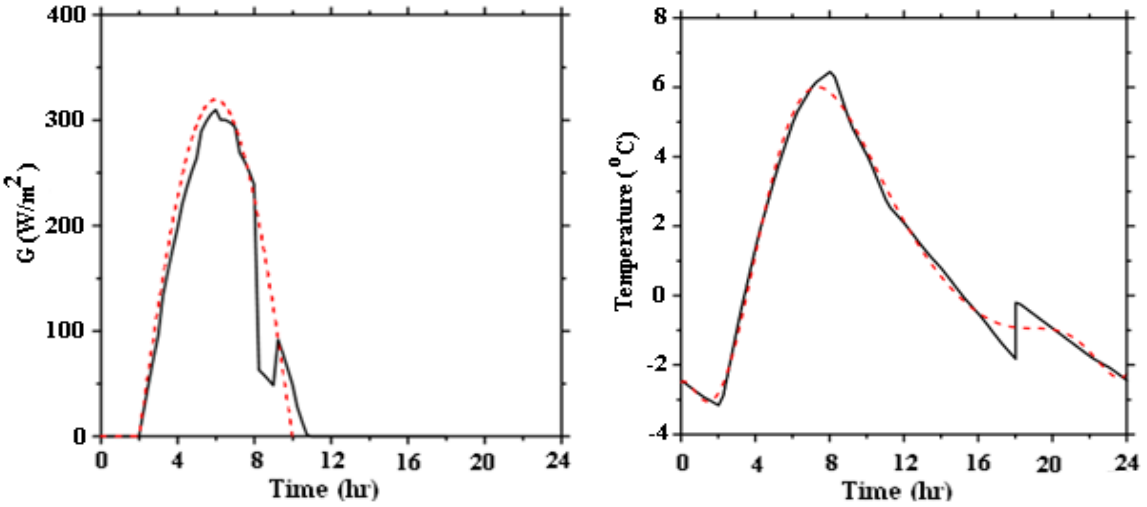

a) Irradiation profile on the horizontal b) Ambient temperature

iv) Typical winter day data

Figure 5.B.1: Typical radiation data for the four seasons.

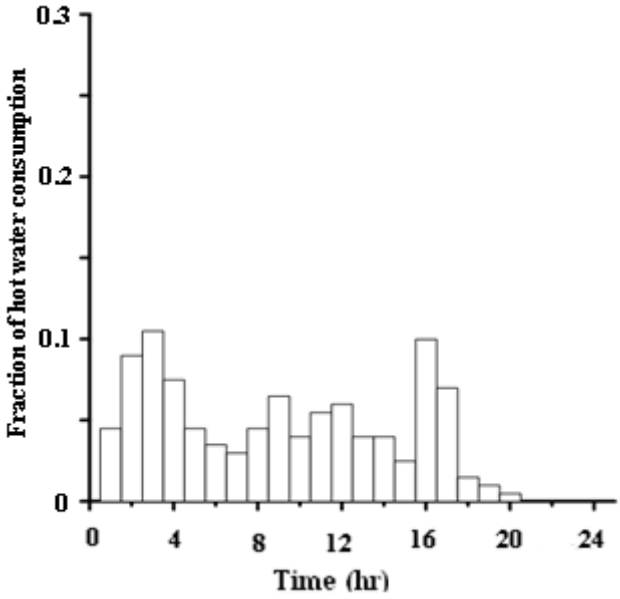

Figure 5.B.2: Dispersed draw profile tested in the code (Edwards et al., 2015).

Table 5.B.1: Mains temperature in different seasons (Meteonorm [software]).

Spring	summer	autumn	Winter
8^{o}C	18^{o}C	11^{o}C	2^{o}C

CHAPTER 6

Conclusions and Recommendations for Future Work

6.1. Conclusions

The current work presented a study of the dynamic performance of a multi-tank hybrid water/PCM system suitable for multi-residential solar domestic hot water applications. In comparison to a single large tank, a multi-tank configuration is more economical when a large storage volume is required. Phase change materials have the potential to reduce the size of thermal storage systems owing to their high latent heat of fusion. They also offer a temperature modulation effect in the system. However, innovative design of the systems containing these materials is necessary due to the poor sensible properties of these materials compared to liquid water. The poor conductivity of PCM requires an

encapsulation geometry with large surface area to volume ratio in order to reduce their imposed thermal resistance on the system. Also, the poor specific heat capacity is problematic since thermal storage systems usually have a wide operating temperature range. The solution proposed in the current research is to use a multi-tank system in series, each of which contains a specific type of PCM with cascading melt temperatures. This way, each tank in a multi-tank system works in a specific narrow temperature range and hence maximum benefit of latent heat can be achieved.

The considered hybrid tank in the study is a cylindrical tank with PCM enclosed in cylindrical containers. An in-house Fortran code was developed to model the phase change process inside the cylinders. The code was thoroughly verified and validated with predictions in a very good agreement with results from the literature (<5% deviation). The melting model was expanded to account for the heat exchange between water in the tank shell and PCM cylinders.

Component level analysis was conducted to understand the dynamic performance of a hybrid water/PCM tank. The evolution of temperatures inside the hybrid tank were compared to the water-only tank. PCM was found to modulate the system temperature around its melt temperature. The benefit of PCM inclusion in the system was judged by calculating the energy storage gain. The gain was computed as the energy storage enhancement relative to the water only system. Gains can reach as high as 179% by using 50% packing ratio and 10^{o}C operating temperature range in water tanks. The gains are

very sensitive to the design parameters and operating conditions of the system. Smaller diameter PCM modules increase the expected gains because of the higher heat transfer area and reduced internal PCM heat transfer resistance. Higher mass flow rates reduce the melting times non-linearly because of the higher heat transfer coefficient. Including PCM in a tank modulates the tank outlet temperature around its melting point due to the high heat transfer occurring during phase change. When the charging period of the system is between the tank turnover times of the hybrid system and the water-only system, incorporation of PCM yields negative gain. The gains are directly related to the temporal variation of temperatures inside the tanks. When sufficient charging period is available, the hybrid system shows significant gains relative to the water only system.

All the reported works on hybrid system focused on the energy storage enhancement and temperature modulation effect introduced by PCM inclusion. All those studies considered a certain configuration with certain dimensions, operating conditions, charging and discharging profiles. However, there is a lack of a unified platform to evaluate the performance of the integrated systems. This motivated the current work to develop a non-dimensional map for the gain as a function of various key parameters. The gain was found to be well correlated in terms of the two non-dimensional numbers ($FoRe_c^{0.8}\theta_m$) and $\widetilde{Ste}/(\rho C_P)^*$. The maps applicability was tested for the ranges of $0.1<\widetilde{Ste}<0.4$, $0<Fo<600$, $20<Re<4000$, $0.2 < (\rho C_P)^* < 0.8$ and $0.2 < \theta_m < 0.8$ with maximum deviation of 5.9% from the raw data.

The hybrid tank was studied in the solar domestic hot water system context. The main goal was to clarify the mixed research results on the value of PCMs in enhancing system performance. Some researchers have found an enhancement of solar fraction when PCM is introduced into the thermal storage tank whereas others have found a negligible impact. The present work has shown that storage volume plays a key role in influencing the collector performance. It is also demonstrated that PCMs provide a benefit only in comparison to an undersized water based storage system relative to the demand. As the tank volume is increased, the benefit of PCM diminishes and the two systems eventually converge to the same performance. This work has shown that the benefit of PCM is in reducing the required storage tank volume. The system energy balance revealed that the benefit of PCM at low tank volumes is due to:

- Reduction in the collector inlet temperature which reduced collector loss and increased collector efficiency.
- Increased pump run time due to cooler tank bottom.
- Increased water delivery temperature to load during early morning and late afternoon which is reflected on solar fraction enhancement.

A parametric analysis has been conducted on the hybrid tank using different packing ratios and PCM module diameters. Different design parameters including the collector areas and loss coefficient were considered as well. The results of this parametric study were found not to alter our previous conclusion on the effect of PCM on system performance enhancement.

The single hybrid tank model was extended to model the proposed multi-tank system. PCMs of different melt temperatures were placed in the tanks in a descending order from the solar supply to the load. Tank-to-tank stratification was predicted. The cascading of PCMs with different melting temperatures maintained a cooler returning water to the solar collector relative to a single PCM hybrid tank. This results in reduced collector losses and extension of the pump activation time. These two effects resulted in an increase in solar fraction relative to undersized water-only thermal storage system.

6.2. Recommendations for Future Work

The current work presented a numerical analysis of the dynamic performance of a multi-tank hybrid system. It considered a conduction dominated enthalpy porosity model to predict the PCM melting performance. Heat transfer correlations accounted for the heat exchange between water and PCM modules. The recommendations for future work can be summarized as follows:

1. The presented results are computational. Although the code was tested, verified and validated, still there is a need for experimental validations within a SDHW context.
2. The implemented solution of phase change process is conduction dominated. The addition of the effect of convection in the later melting stages is a recommendation.

3. Although the current work focusses on solar domestic hot water systems, a system energy balance is a recommended approach for the future studies on the incorporation of PCM in different application. This analysis helps to clearly understand the role played by PCM in the considered configuration.
4. In the current work, cylindrical PCM encapsulations were considered. Different PCM encapsulation configuration is an interesting aspect to explore including the rectangular slabs and spherical encapsulations. The impact of extended surfaces as a mean of heat transfer enhancement needs to be assessed as well.
5. Organic PCMs suitable for low temperature applications are characterized by their low thermal conductivity. This limits the charging and discharging rates for a prescribed period. Recent research Nakhla et al (2015) shows electro-hydrodynamics show a promising potential in enhancing PCM melting rate. The application of this technique on the studied system is expected to enhance the performance.
6. The present work considered several typical days as a representation for the whole year due to the high computational cost of the simulations. It will be worthy of investigation if simplified models of lower computational cost give accurate presentation of the whole year.

7. References

Abdelsalam, M.Y., "Comprehensive Research Proposal", McMaster University (2014).

Abhat, A.: Low Temperature Latent Heat Thermal Energy Storage: Heat Storage Materials. **Solar Energy, Vol. 30, Iss (4),** 313-332 (1983).

Agyenim, F., Hewitt, N., Eames, P. and Smyth, M.: A review of materials, heat transfer and phase change problem formulation for latent heat thermal energy storage systems (LHTESS). **Renewable and Sustainable Energy Reviews, Vol. 14, Iss(2),** 615–628 (2010).

Al-Hinti, I., Al-Ghandoor, A., Maaly, A., Abu Naqeera, I., Al-Khateeb, Z., and Al-Sheikh, O.: Experimental investigation on the use of water-phase change material storage in conventional solar water heating systems. **Energy Conversion and Management, Vol. 51,** 1735-1740 (2010).

Alkan, C., and Sari, A.: Fatty acid/poly (methyl methacrylate) (PMMA) blends as form-stable phase change materials for latent heat thermal energy storage. **Solar Energy, Vol. 82,** 118-124 (2008).

Baetens, R., Jelle, B., and Gustavsen, A.: Phase change materials for building applications: A state-of-the-art review. **Energy and Buildings, Vol. 42,** 1361-1368 (2010).

Bergles, A. E.: Recent developments in enhanced heat transfer. **International Journal of Heat and Mass Transfer, Vol. 47, Iss (8),** 1001-1008 (2011).

Cristofari, C., Notton, G., Poggi, P. and Louche, A.: Influence of the Flow rate and the Tank Stratification Degree on the Performances of a Solar Flat-plate Collector. **International Journal of Thermal Sciences, Vol. 42**, 455-469 (2003).

Cruickshank, C.A. and Harrison, S.J.: Characterization of a Thermosyphon Heat Exchanger for Solar Domestic Hot Water Systems. **Journal of Solar Energy Engineering, Vol. 131, Iss (2).** (2009a).

Desgrosseillier, L., Murray, R., Safatli, A., Marin, G., Stewart, J., Osbourne, N., White, M.A., Groulx, D.: Phase Change Material Selection in the Design of a Latent Heat Energy Storage System Coupled with a Domestic Hot Water Solar Thermal System. **ASHRAE Annual Conference,** Montreal, Canada (2011).

Dickinson, R. M., Cruickshank, C. A. and Harrison., S. J.: The Effect of Discharge Configurations on the Thermal Behavior of a Multi-tank Storage System. **Energy Procedia, Vol. 30,** 215-224 (2012).

Dincer, I. and Rosen, M.A.: **Thermal Energy Storage: Systems and Applications**. John Wiley & Sons York, N.Y. (2002).

Duffie, J.A. and Beckman, W.A.: **Solar Engineering of Thermal Processes**. John Wiley & Sons York, N.Y. (2006).

Esen, M., and Ayhan, T.: Development of a model compatible with solar assisted cylindrical energy storage tank and variation of stored energy with time for different phase change materials", **Energy Conversion and Management, Vol. 37, Iss(12),** 1775-1785 (1996).

Fazilati, M. A., and Alemrajabi, A. A.: Phase change material for enhancing solar water heater, an experimental approach. **Energy Conversion and Management, Vol. 71,** 138-145 (2013).

Feldman, D., Banu, D., and Hawes, D.: Development and application of organic phase change mixtures in thermal storage gypsum wallboard. **Solar Energy Materials and Solar Cells, Vol. 36,** 147-157 (1995).

Feldman, D., Banu, D., and Hawes, D.: Low chain esters of stearic acid as phase change materials for thermal energy storage in buildings. **Solar Energy Materials and Solar Cells, Vol. 36,** 311-322 (1995).

Hollands, K.G.T., and Lightstone, M.F.: A Review of Low-Flow, Stratified-Tank Solar Water Heating Systems. **Solar Energy, Vol. 43, Iss(2),** 97-105 (1989).

Ismail, K. A. R., Moraes, R. I. R.: A Numerical and Experimental Investigation of Different Containers and PCM Options for Cold Storage Modular Units for Domestic Applications. **International Journal of Heat and Mass Transfer, Vol. 52,** 4195-4202 (2009).

Jegadheeswaran, S., and Pohekar, S. D.: Performance enhancement in latent heat thermal storage system: A review. **Renewable and Sustainable Energy Reviews, Vol. 13, Iss(9),** 2225–2244 (2009).

Kousksou, T., Jamil, A., Eirhafiki, T., and Zeraouli, Y.: Paraffin wax mixtures as phase change materials. **Solar Energy Materials and Solar Cells, Vol. 94,** 2158-2165 (2010).

Kousksou, T., Bruel, P., Cherreau, G., Leoussoff, V. and El Rhafiki, T.: PCM storage for solar DHW: From an unfulfilled promise to a real benefit. **Solar Energy, Vol. 85, Iss(9),** 2033-2040 (2011).

Lacroix, M. and Benmadda, M.: Numerical Simulation of Natural Convection-Dominated Melting and Solidification From a Finned Vertical Wall. **Numerical Heat Transfer, Part A: Applications, Vol. 31, Iss(1),** 71-86 (1997).

Lane, G. A.: Solar heat storage: latent heat materials. **Vol. I. Boca Raton, FL: CRC Press, Inc** (1983).

Lavan, Z. and Thompson, J.: Experimental Study of Thermally Stratified Hot Water Storage Tanks. **Solar Energy, Vol. 19 (5)**, 519-524 (1977).

Mather, D.W., Hollands, K.G.T. and Wright, J.L.: Single- and Multi-tank Energy Storage for Solar Heating Systems: Fundamentals. **Solar Energy, Vol. 73 (1)**, 3–13 (2002).

Mehling, H., Cabeza, L.F., Hippeli, S., and Hiebler, S.: PCM-module to improve hot water heat stores with stratification. **Renewable Energy, Vol. 28,** 699-711 (2003).

Michels, H., Pitz-Paal, R.: Cascaded latent heat storage for parabolic trough solar power plants. **Solar Energy, Vol. 81, Iss(6),** Pages 829-837 (2007).

Nabavitabatabayi, M., Haghighat, F., Moreau, A., and Sra, P.: Numerical analysis of a thermally enhanced domestic hot water tank. **Applied Energy, Vol. 129,** 253-260 (2014).

Nakhla, D., Sadek, H., and Cotton, J. S.: Melting performance enhancement in latent heat storage module using solid extraction electrohydrodynamics (EHD). **International Journal of Heat and Mass Transfer, Vol. 81,** 695-704 (2015).

Nallusamy, N. N., and Velraj, R. R.: Numerical and experimental investigation of a combined sensible and latent heat storage unit integrated with solar water heating system. **Journal of Solar Energy engineering, Vol. 131,** 41002-41002-8 (2009).

NRCan. "Energy Use Data Handbook - 1990 to 2009." Technical report, Office of Energy Efficiency, Natural Resources Canada, Ottawa, ON, Canada. [Online] http://oee.nrcan.gc.ca/Publications/statistics/handbook11/ (2012).

Nkwetta, D. N., Vouillamoz, P., Haghighat, F., El Mankibi, M., Moreau, A., and Desai, K.: Phase change materials in hot water tank for shifting peak power demand. **Solar Energy, Vol. 107,** 628-635 (2014).

Phillips, W.F. and Dave, R.N.: Effects of Stratification on the Performance of Liquid based Solar Heating Systems. **Solar Energy, Vol. 29**, 111-120 (1982).

Pokhrel, R., Gonzalez, J. E., Hight, T., and Adalsteinsonn,T.: Analysis and Design of a Paraffin/Graphite Composite PCM Integrated in a Thermal Storage Unit. **ASME J. Sol. Energy Eng., Vol. 132, Iss(4),** 041006 (2010).

Sanusi, O., Warzoha, R., and Fleischer, A. S.: Energy storage and solidification of paraffin phase change material embedded with graphite nano-fibers. **International Journal of Heat and Mass Transfer, Vol. 54, Iss(19),** 4429–4436 (2011).

Sarafraz, P.: Thermal optimization of flat plate PCM capsules in natural convection solar water heating systems. **M.Sc. Thesis, McMaster University** (2013).

Sari, A., and Kaygusuz, K.: Thermal and heat transfer characteristics in a latent heat storage system using lauric acid", **Energy Conversion and Management, Vol. 43**, 2493-2507 (2002).

Sari, A., and Kaygusuz, K.: Some fatty acids used for latent heat storage: thermal stability and corrosion of metals with respect to thermal cycling. **Renewable Energy, Vol. 28,** 939-948 (2003).

Sari, A., and Karaipekli, A.: Preparation, thermal properties and thermal reliability of palmitic acid/expanded graphite composite as form-stable PCM for thermal energy storage. **Solar Energy Materials and Solar Cells, Vol. 93,** 571-576 (2009).

Seeniraj, R.V., Narasimhan, N.L.: Performance enhancement of a solar dynamic LHTS module having both fins and multiple PCMs. **Solar Energy, Vol. 82, Iss(6),** 535-542 (2008).

Sharma, A., Tyagi, V.V., Chen, C.R. and Buddhi, D.: Review on Thermal Energy Storage with Phase Change Materials and Applications. **Renewable and Sustainable Energy** Reviews (2008) doi:10.1016/j.rser.2007.10.005.

Stritih, U.: An experimental study of enhanced heat transfer in rectangular PCM thermal storage. **International Journal of Heat and Mass Transfer, Vol. 47, Iss(12),** 2841–2847 (2004).

Talmatsky, E., and Kribus, A.: PCM storage for solar DHW: an unfulfilled promise. **Solar energy, Vol. 82,** 861-869 (2008).

Tian, Y., and Zhao, C.Y.: Thermal and exergetic analysis of Metal Foam-enhanced Cascaded Thermal Energy Storage (MF-CTES). **International Journal of Heat and Mass Transfer, Vol. 58, Iss(1–2),** 86-96 (2013).

Velraj, R., Seeniraj, R. V., Hafner, B., Faber, C., and Schwarzer, K.: Heat Transfer Enhancement in a Latent Heat Storage System. **Solar Energy, Vol. 65, Iss(3),** 171–180 (1999).

Yingqiu, Z.,Yinping, Z., Yi, J., and Yanbing, K.: Thermal Storage and Heat Transfer in Phase Change Material Outside a Circular Tube with Axial Variation of the Heat Transfer Fluid Temperature. **ASME J. Sol. Energy Eng., Vol. 121, Iss(3),** pp. 145-149 (1999).

Wang, Z., Qiu, F., Yang, W., and Zhao, X.: Applications of solar water heating system with phase change material. **Renewable and Sustainable Energy Reviews, Vol. 52,** 645-652 (2015).

Watanabe, T., and Kanzawa, A.: Second law optimization of a latent heat storage system with PCMs having different melting points. **Heat Recovery Systems & CHP, Vol. 15, Iss(7),** 641-653 (1995).

Zalba, B., Marin, J.M., Cabeza, L.F. and Mehling, H.: Review on Thermal Energy Storage with Phase Change: Materials, Heat Transfer Analysis and Applications. **Applied Thermal Engineering, Vol. 23**, 251-283 (2003).

Zhang, Z.G., and Fang, X.M.: Study on paraffin/expanded graphite composite phase change thermal energy storage material. **Energy Conversion and Management, Vol. 47**, 303-310 (2006).

Appendix A

Parametric analysis results for single hybrid tank in SDHW system context

Introduction

This section presents a parametric analysis for the hybrid single tank in the SDHW context. The case described in chapter 4 is taken as a base case. For convenience, the parameters of the base case are listed here in Table A.1. The effect of various design and operating parameters are investigated. The results are divided into two subsections: 1) parameters affecting the performance of the hybrid system, and 2) parameters affecting the performance of both hybrid and water-only systems.

Table A.1: Parameters for the base case

Parameter	Value
Collector area	6 m^2
Collector slope	45^o
Azimuth	0^o
Collector loss coefficient	5 W/m^2K
Collector mass flow rate	0.05 kg/s
Storage tank loss coefficient	0.55 W/m^2K
Tank aspect ratio	2
PCM packing ratio	50%
PCM melting temperature	32^oC
PCM module diameter	2 cm
Daily drawn volume of hot water	160 liters
Discharging flow rate	0.19 kg/s

A.1. Parameters affecting hybrid system

Amongst the parameters affecting the hybrid system performance are: PCM melting temperature, packing ratio and module diameter. Their effects are explained in the context of the energy balance presented in detail in chapter four.

A.1.1 Effect of PCM melting point choice

PCM melting point choice is crucial for different climatic conditions and demand profiles. The melt temperature was chosen to be 32^{o}C in the case study presented in chapter 4. The expected solar fraction versus volume is shown in Figure A.1. It is seen that PCM of 42^{o}C melting point behaves slightly better compared to the 32^{o}C (base case). But when the melting temperature increases to 54^{o}C, the predicted solar fraction is worse relative to the base case. This is a result of the molten fraction of PCM only reaching 64% in the studied days. The trend in this curve can be easily explained by considering the energy exiting and entering the system shown in Figure A.2. The slight increase in solar input and decrease in collector loss causes the slight improvement for the (T_m=42^{o}C) case relative to the base case. For the 54^{o}C case there is an increase in the collector loss and slight reduction in solar irradiation. This result in a degraded solar fraction compared to the other two cases. The temperature directed to the load in the four studied days (Figure A.3).

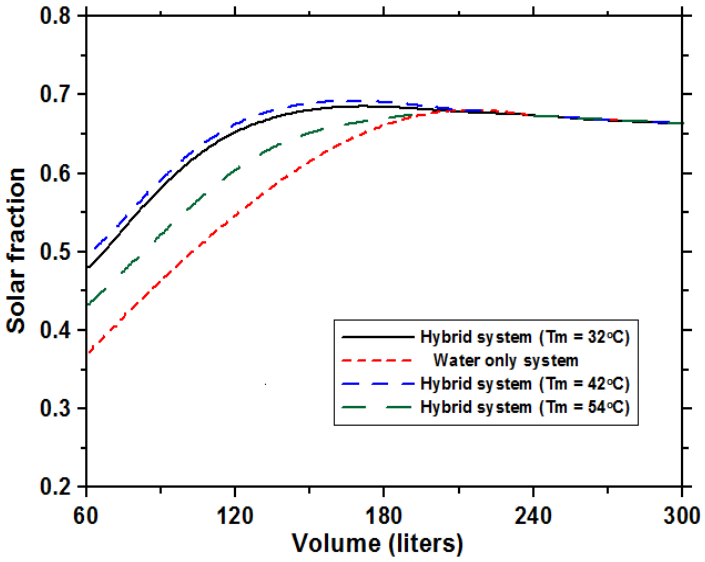

Figure A.1: Solar fraction versus volume for different PCM melting temperatures.

By inspecting temperature profiles in Figure A.3. The hybrid system is found to extend the period of supplying hot water to the load during the evening hours. This results from the latent heat of fusion that was absorbed in the day time being released at night. But for the case of Tm=54^{o}C, it is seen that PCM was not fully molten in the spring and autumn days. Moreover, it did not melt at all in winter. This caused the predicted solar fraction versus volume curve to degrade compared to the Tm=32^{o}C and Tm=42^{o}C cases (Figure A.1).

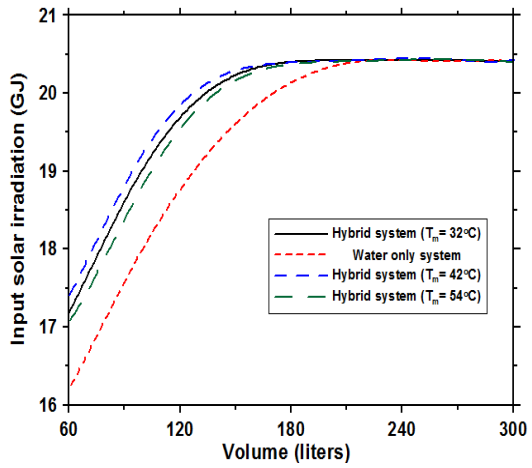

a) Input solar irradiation for different PCM melt temperatures

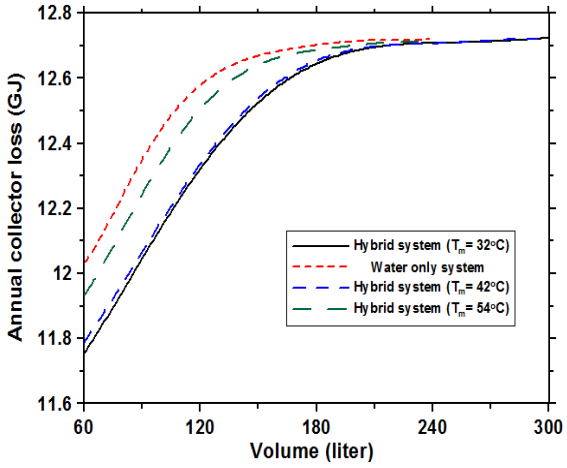

b) Annual collector loss for different PCM melt temperatures

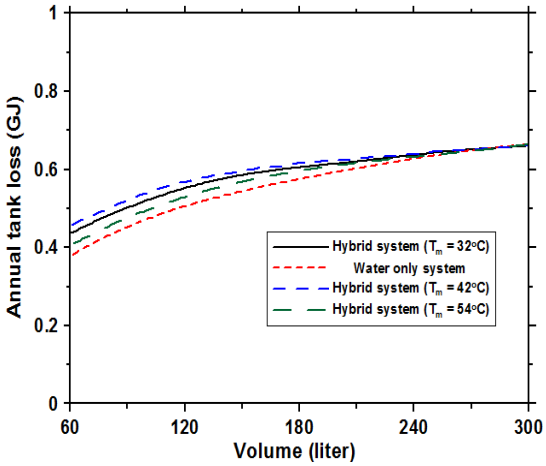

c) Annual tank loss for different PCM melt temperatures

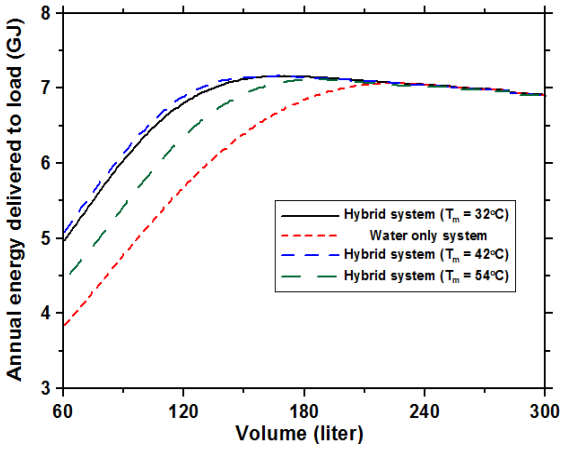

d) Annual delivered energy for different PCM melt temperatures

Figure A.2: Energy breakdown for different PCM melting points

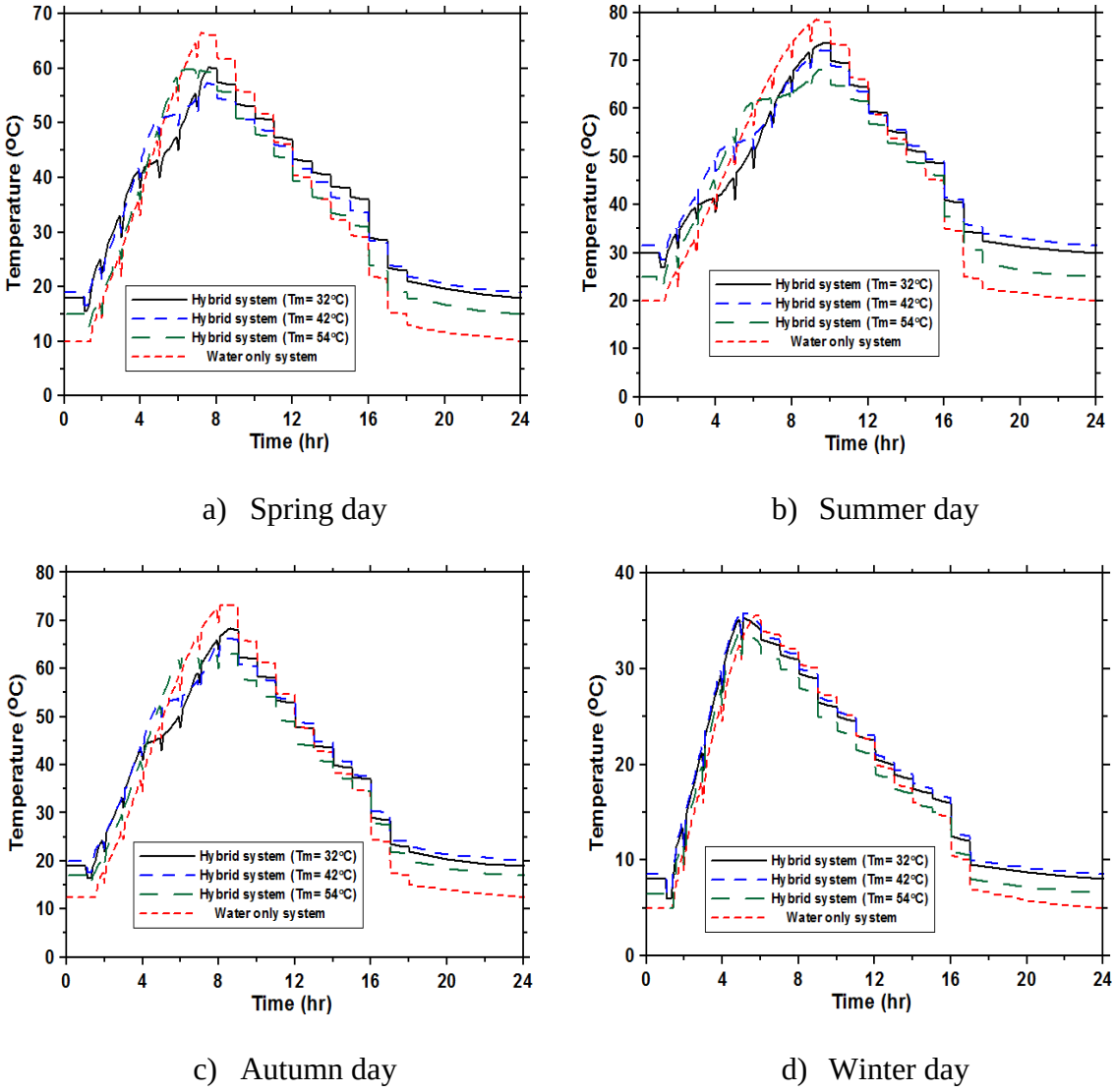

a) Spring day

b) Summer day

c) Autumn day

d) Winter day

Figure A.3: Temperature delivered to load for different PCM melting temperatures.

A.1.2. Effect of PCM packing ratio

The optimum PCM packing ratio varies according to the system operating conditions. The higher the packing ratio, the higher the temperature modulation effect around the PCM melting point. The expected solar fraction increases as the PCM packing ratio

increases as shown in Figure A.4. Based on the energy crossing the system boundaries (Figure A.5) it is seen that as packing ratio increases, input solar irradiation increases and collector losses decrease (70% packing ratio relative to the base case). This is mainly a result of cooler fluid at the bottom of the tank for a longer period. Those combined effects are manifested on the temperature delivered to the load (Figure A.6).

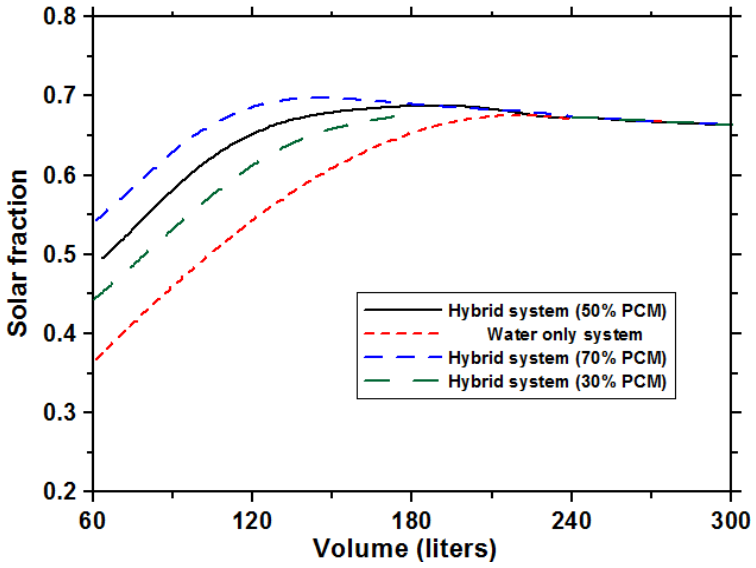

Figure A.4: Solar fraction versus volume for different PCM packing ratios.

By inspecting temperature profiles in Figure A.6., it is seen that the hybrid system extends the period in which hot water is supplied to the load in evening hours. Higher packing ratios of PCM, increases the modulation effect around the melting point. This causes the water supplied to the load to be hotter in the evening and reduces the need for auxiliary heating for an extended period.

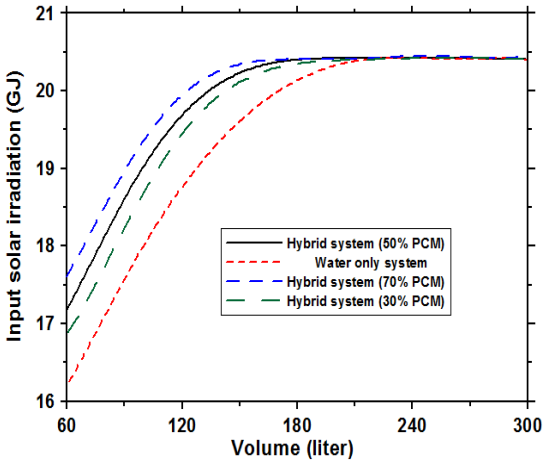

a) Input solar irradiation for different PCM melt temperatures

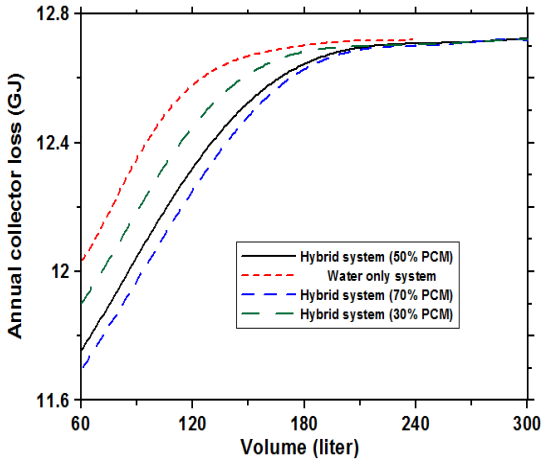

b) Annual collector loss for different PCM melt temperatures

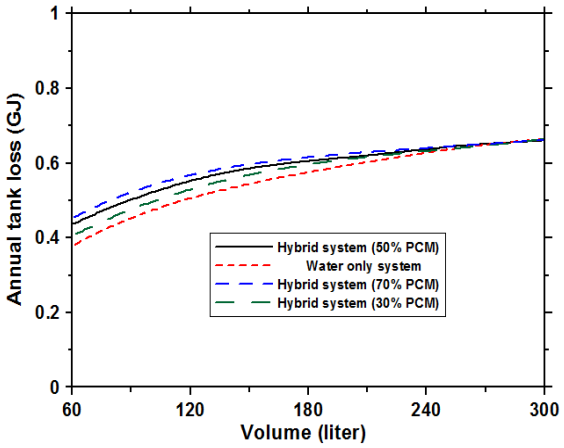

c) Annual tank loss for different PCM melt temperatures

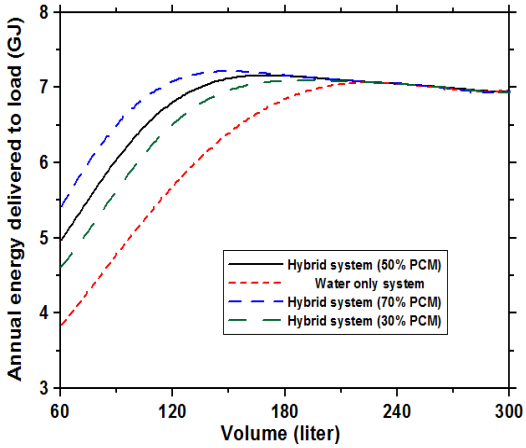

d) Annual delivered energy for different PCM melt temperatures

Figure A.5: Energy breakdown for different PCM packing ratios.

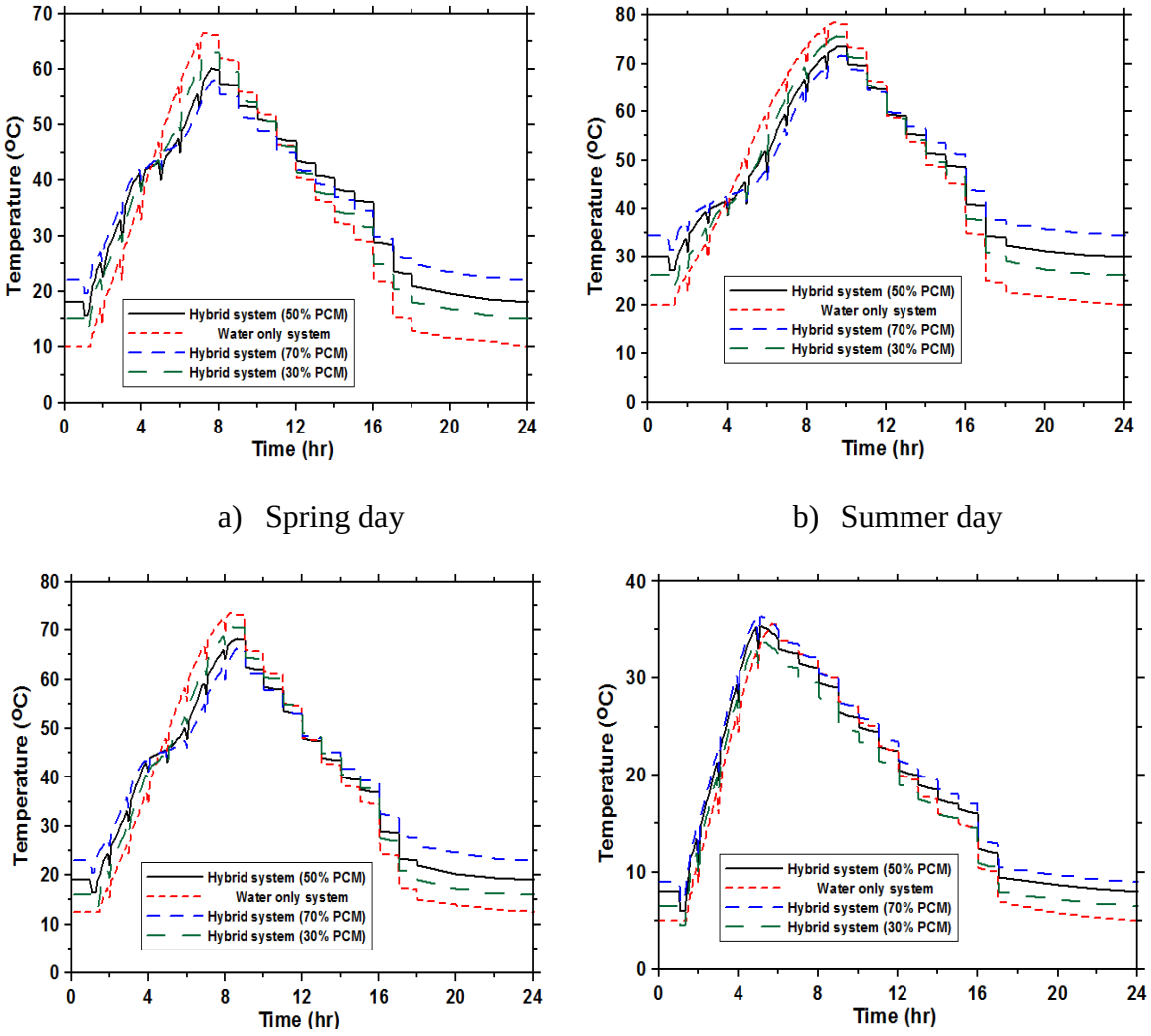

a) Spring day

b) Summer day

c) Autumn day

d) Winter day

Figure A.6: Temperature delivered to load for different PCM packing ratios.

A.1.3 Effect of PCM module diameter

Larger diameter PCM modules impose higher thermal resistance on the system which limits solar fraction for a prescribed charging period. This is mainly because of a

reduction of the PCM average molten fraction that leads to less utilization of its latent heat. Figure A.7 shows the expected solar fraction for three different studied diameters: 2 cm, 4 cm and 8 cm. The 4 cm case shows a slight reduction compared to the 2 cm case as the molten fraction difference is only 4% for the studied typical days. The 8 cm case shows an obvious reduction in solar fraction compared with the 2 cm base case. This attributed to the reduction in PCM molten fraction by 18% in the studied days. This highlights that PCM module diameter must be carefully chosen for the maximum possible utilization of PCM latent heat. The breakdown of energies is shown in Figure A.8. The temperature of water delivered to the load for the four typical days is given in Figure A.9.

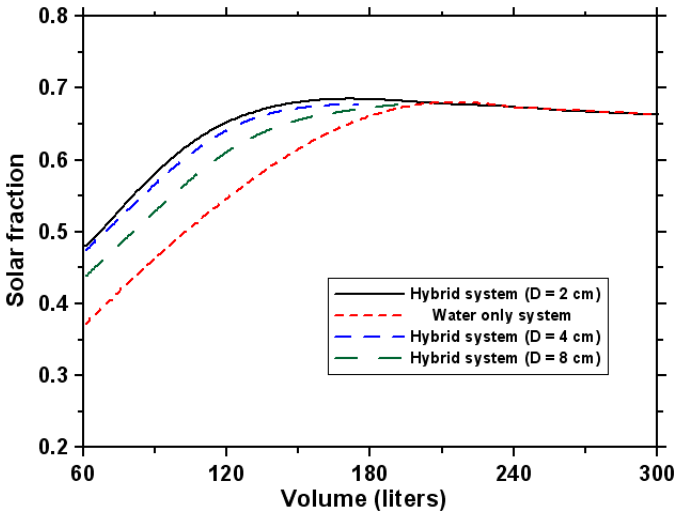

Figure A.7: Solar fraction versus volume for different PCM module diameters.

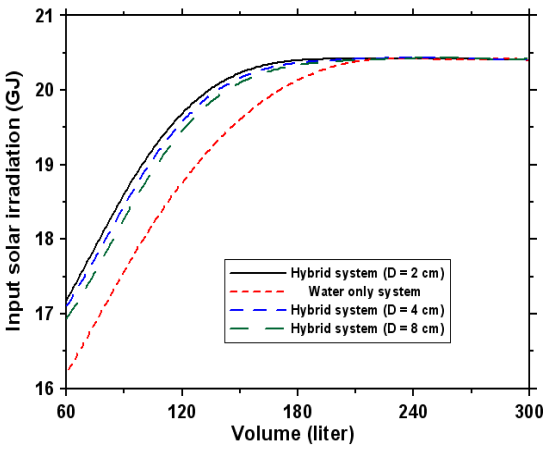

a) Input solar irradiation for different PCM melt temperatures

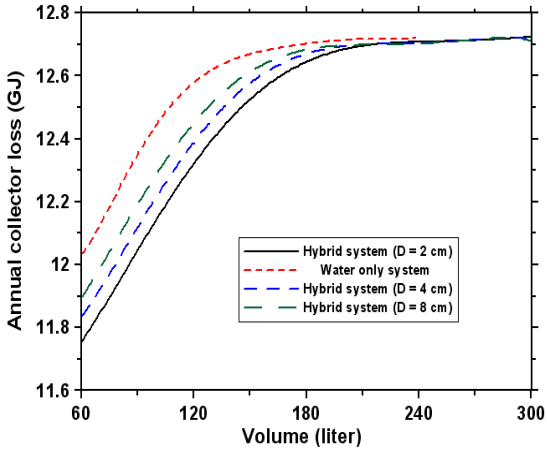

b) Annual collector loss for different PCM melt temperatures

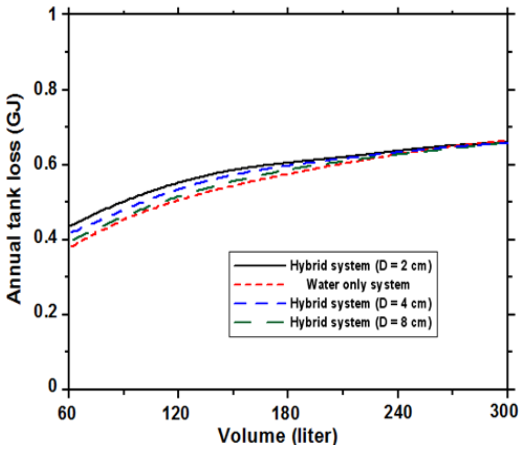

c) Annual tank loss for different PCM melt temperatures

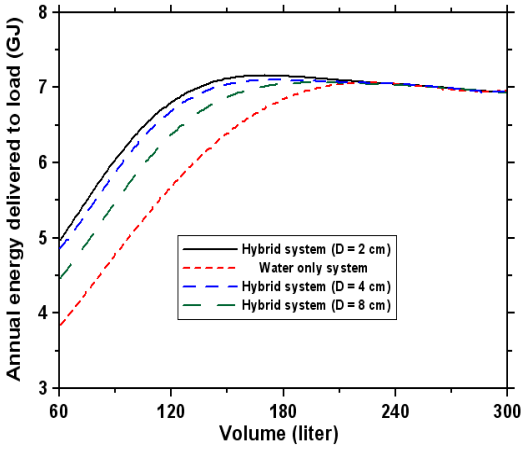

d) Annual delivered energy for different PCM melt temperatures

Figure A.8: Energy breakdown for different PCM module diameters.

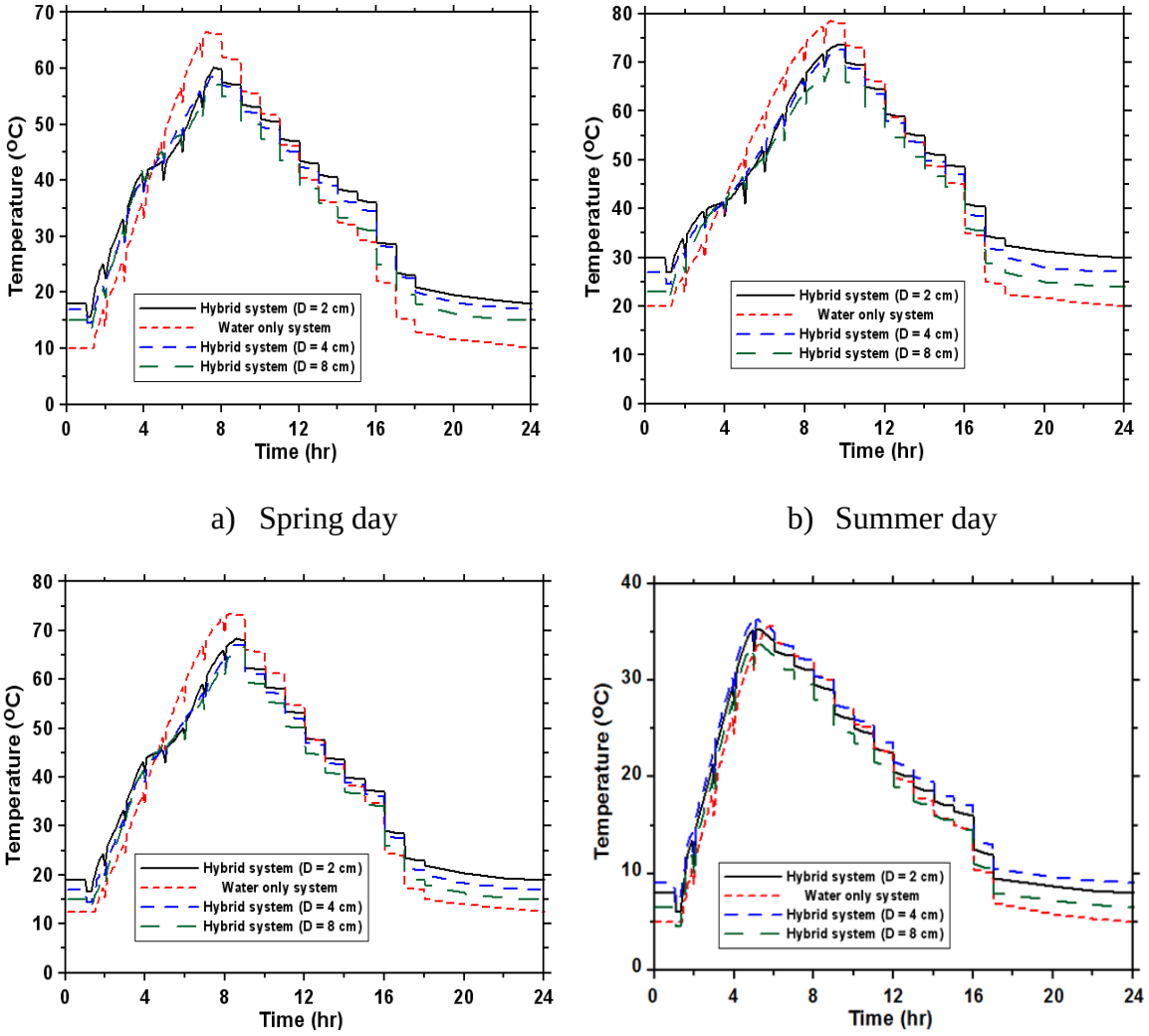

a) Spring day

b) Summer day

c) Autumn day

d) Winter day

Figure A.9: Temperature delivered to load for different PCM module diameters.

A.2. Parameters affecting both the hybrid and water-only systems

Amongst the parameters affecting both the hybrid and water-only systems performance are: the demand profile, the collector heat loss coefficient, area of the collector and mass flowrate through the system. All the presented results can be explained in terms of energy balance on the system as previously explained.

A.2.1. Effect of the demand profile

Consumption profiles differ from country to country and even between the people of a country itself. A number of researchers have performed a statistical analysis on different modes of consumption. Edwards et al. (2015) presented the dominant consumption patterns for families in Canada. The four reported modes are shown in figure A.10. The dispersed consumption profile constitutes a nearly steady demand throughout the day with a slight peak in the morning and late after noon (Figure A.10.a). Those peaks coincide with the times when people get up and return from their work. Some families are shown to be active in the early morning where the demand peak happens in the beginning of the day (Figure A.10.b). Others have their demand concentrated in the early evening hours when they come back from work or school (Figure A.10.c). In the last category, most of the consumption is in the late night hours (Figure A.10.d).

Demand profiles affect the predicted solar fraction of both hybrid and water-only systems (Figure A.11). The same benefit of PCM inclusion in undersized tanks is manifested in all demand profiles. However, the peak solar fraction is achieved at different volumes when the consumption profiles differ. Generally, the steadier the demand is throughout the day, the less storage volume is needed for both systems. This can be seen by comparing Figure A.11.a to Figures A.11.(b-d). The peak solar fraction for the hybrid system when dispersed profile is considered occurs at a volume of 140 liters. If a predominant morning consumption is considered, this peak occurs at a volume of 160 liters.

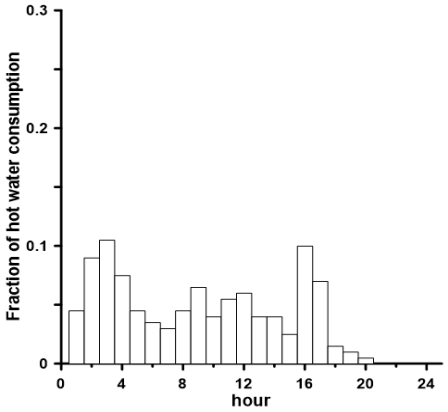

a) Dispersed consumption profile

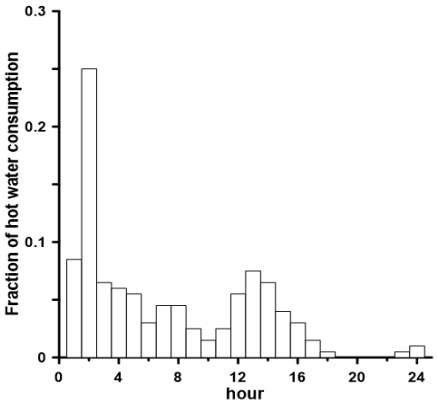

b) Predominant morning consumption profile

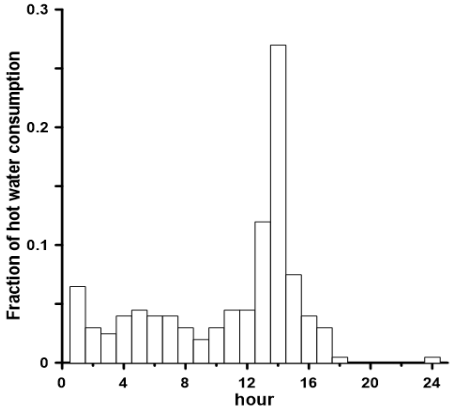

c) Predominant evening consumption profile

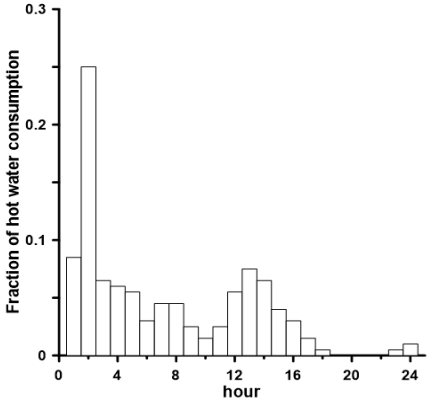

d) Predominant late night consumption profile

Figure A.10: Different consumption profiles.

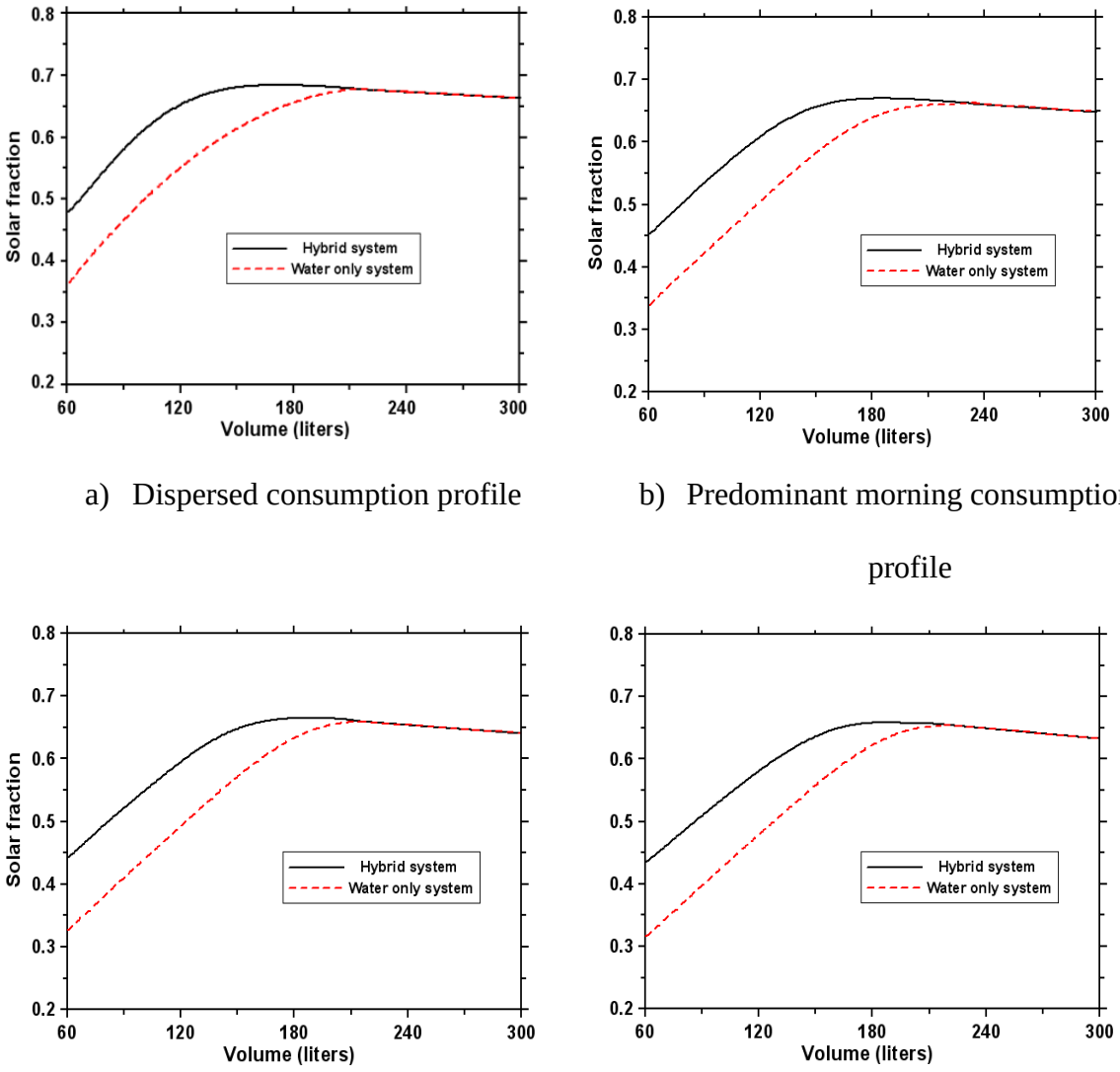

a) Dispersed consumption profile

b) Predominant morning consumption profile

c) Predominant evening consumption profile

d) Predominant late night consumption profile

Figure A.11: Solar fraction versus volume for different consumption profiles.

A.2.2 Effect of collector heat loss coefficient

The losses from the collector constitute an important component in the system energy balance. It is dominant in comparison to the losses from the tank since the face of the collector isn't insulated. As expected, a higher loss coefficient leads to a lower overall

solar fraction. Decreasing the loss coefficient to U_L= 3 W/m^{2}K, auguments the solar fraction of both systems (Figure A.12b). Increasing the loss coefficient to U_L= 7 W/m^{2}K, decreases the predicted solar fraction of both systems (Figure A.12c). The curves essentially shift up and down when the loss coefficient is changed but they have the same shape. By inspecting the volume of the hybrid tank and the water-only tanks to obtain the highest solar fraction, it is found that volume reduction capability is arround 40% for the three cases.

A.2.3. Effect of collector surface area

The Larger the surface area of the collector, the greater solar radiation input to the system. As shown from Figure A.13 increasing the collector area from 6 m^2 to 7.5 m^2 increases the predicted solar fraction from both systems by ~ 8% relative to the base case (Figure A.13a and A.13b). Also, decreasing the collector area from 6 m^2 to 4.5 m^2 decreases the predicted solar fraction from both systems by ~ 7% relative to the base case (Figure A.13a and A.13c). The curves are shifted up and down relative to the base case.

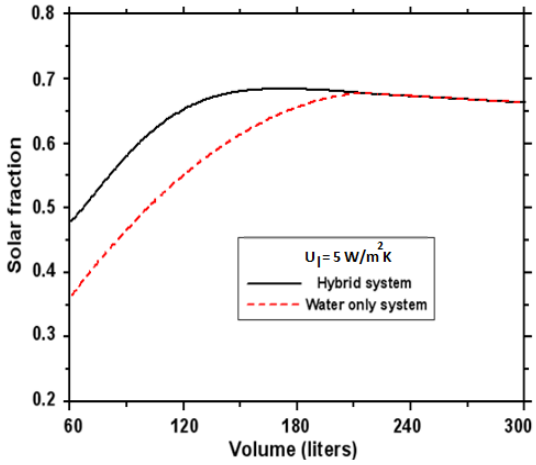

a) Base case (U_L= 5 W/m^{2}K).

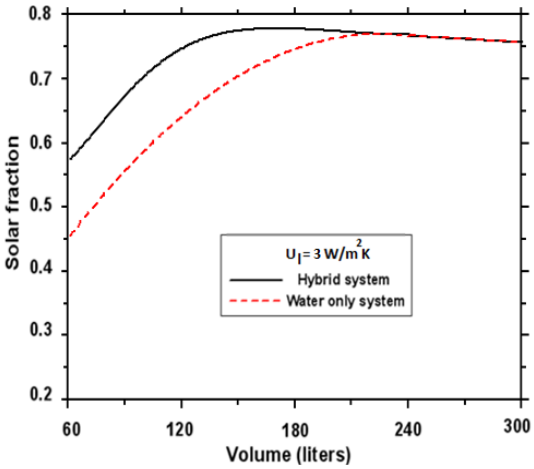

b) U_L= 3 W/m^{2}K

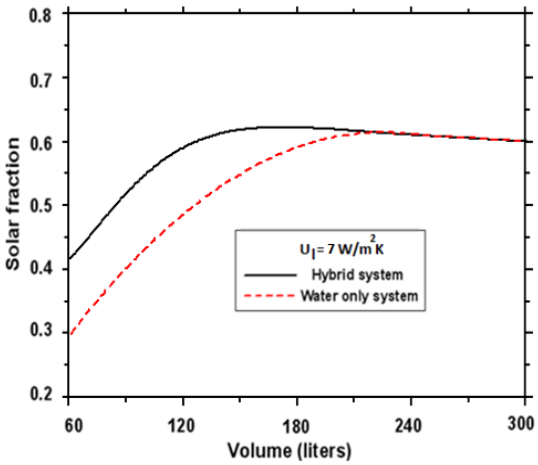

c) U_L= 7 W/m^{2}K

Figure A.12: Predicted solar fraction versus volume for different collector loss coefficient.

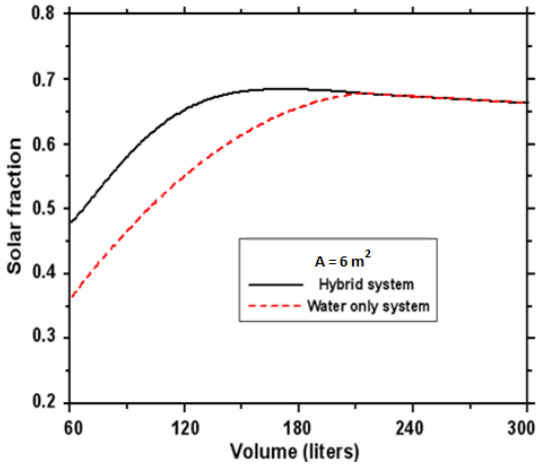

a) Base case (A= 6 m^2).

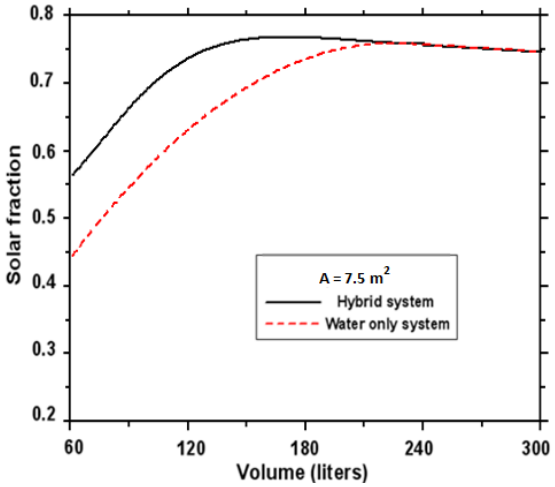

b) A= 7.5 m^2

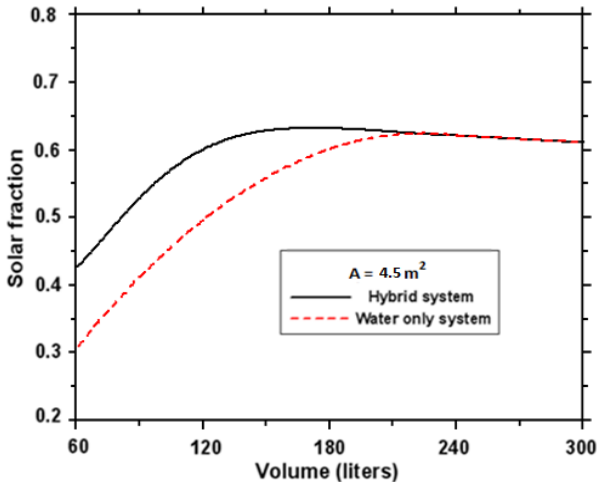

c) A= 4.5 m^2

Figure A.13: Predicted solar fraction versus volume for different collector surface areas.

A.2.4. Effect of collector mass flow rate

According to the reported literature on stratification (Hollands and Lightstone 1989), lower mass flowrate enhances the predicted solar fraction of the system. It extends the period on which the storage tank has a cooler bottom and promotes stratification. This is reflected on the extended period on which hot water is available to meet the load. Figure A.14 shows the predicted solar fraction for different mass flow rates. As seen from the Figure the lower flowrate shifts the curve to the left relative to the base case (Figure A.14a and A.14b). The best solar fraction can be obtained by a tank of volume 140 liters instead of 160 liters for the hybrid system. It is also obtained by a tank of volume 210 liters instead of 230 liters for the water-only system. The inverse trend happens when mass flowrate decreases as shown in Figure A.14c.

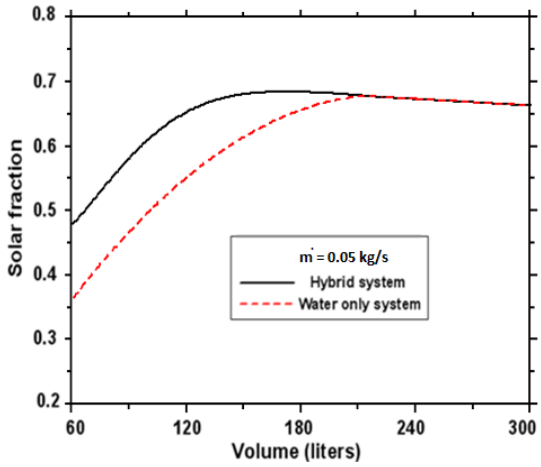

a) Base case ($\dot{m}$ = 0.05 kg/s).

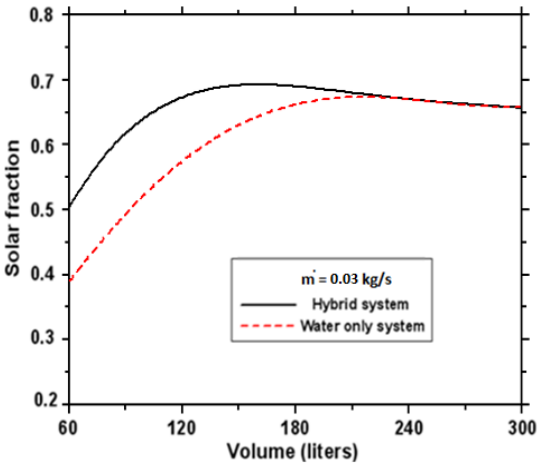

b) $\dot{m}$ = 0.03 kg/s

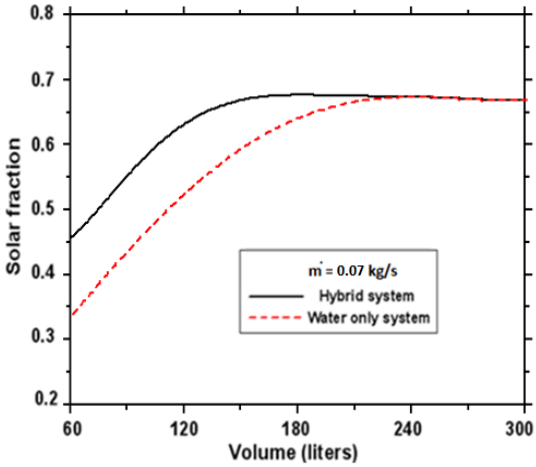

c) $\dot{m}$ = 0.07 kg/s

Figure A.14: Predicted solar fraction versus volume for different collector mass flowrates.

Appendix B

Parametric analysis results for multi-tank hybrid SDHW system

Introduction

This section presents a parametric analysis for the hybrid multi-tank in the SDHW system context. The case described in chapter 5 is taken as a base case. For convenience, the parameters of the base case are listed again in Table B.1. The effect of various design and operating parameters are investigated as previously assessed in the single tank. The chosen PCM cascading in the tanks is the same in chapter 5 and it is listed herein in Table B.2. The results are divided into the same two subsections:

1) parameters affecting the performance of the hybrid system:
    a) PCM packing ratio.
    b) PCM module diameter.

2) parameters affecting the performance of both hybrid and water-only systems.
   a) Demand profile.
   b) Collector heat loss coefficient.
   c) Collector surface area.
   d) Collector mass flow rate.

Table B.1: Parameters for the studied case

Parameter	Value
Collector area	16 m^2
Collector slope	45^o
Azimuth	0^o
Collector loss coefficient	5 W/m^2K
Collector mass flow rate	0.05 kg/s
Storage tank loss coefficient	0.55 W/m^2K
Tank aspect ratio	2
PCM packing ratio	50%
PCM melting temperature	32^oC
PCM module diameter	2 cm
Daily drawn volume of hot water	480 liters
Discharging flow rate	0.19 kg/s

Table B.2: PCM melting temperatures

Number of tanks	PCM melt temperatures [^{o}C]
1	32
2	42, 16
3	42, 32, 16
4	54, 42, 32, 16

B.1. Parameters affecting hybrid system

Amongst the parameters affecting the hybrid system performance are: PCM packing ratio and module diameter. Their effects are explained based on the energy balance stated in detail in chapter 5.

B.1.1. Effect of PCM packing ratio

The optimum PCM packing ratio varies according to the system operating conditions. The higher the packing ratio, the higher the temperature modulation effect around PCM melting point. The predicted solar fraction increases as the PCM packing ratio increases. Although not shown, the system energy balance reveals that as the packing ratio increases, solar input increases and collector losses decrease. This increases the energy delivered to the load. The effect is pronounced in the undersized storages (Figure B.1.a) . For example, a system employing three 75 liter tanks (i.e. total volume of 225 liters) gives solar fraction of 0.549, 0.563 and 0.583 for the 30%, 50% and 70% packing ratios respectively. For the cascaded 300 liter tanks there is a bit of enhancement in solar

fraction when only one tank is considered but when the storage is oversized the solar fraction of the hybrid and water-only systems are the same.

B.1.2 Effect of PCM module diameter

Thicker PCM modules impose higher thermal resistance on the system which limits solar fraction for a prescribed charging period. It causes a reduction of molten fraction of PCM that implies less utilization of its latent heat. Figure B.2 shows the expected solar fraction for three different studied diameters: 2 cm, 4 cm and 8 cm. For example, considering 3 cascaded 75 liters tanks give solar fraction of 0.563, 0.554 and 0.549 for the D=2 cm, D=4 cm and D=8 cm module diameters respectively. For the cascaded 300 liter tanks there is a bit of enhancement in solar fraction when only one tank is considered then both systems converge to the same behaviour when the storage is oversized (Volumes>600 liters in Figure B.2.b).

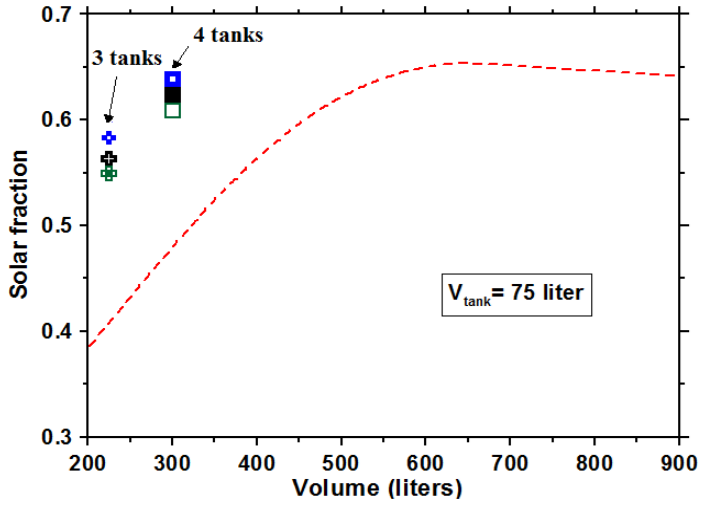

a) Effect of PCM packing ratio on solar fraction (V_{tank} = 75 liter). Dashed lines are water-only system. Symbols are: ✣ 3 tanks (70% PCM); ◘ 4 tanks (70% PCM); ✣ 3 tanks (50% PCM); ■4 tanks (50% PCM); ✣3 tanks (30% PCM); □ 4 tanks (30% PCM).

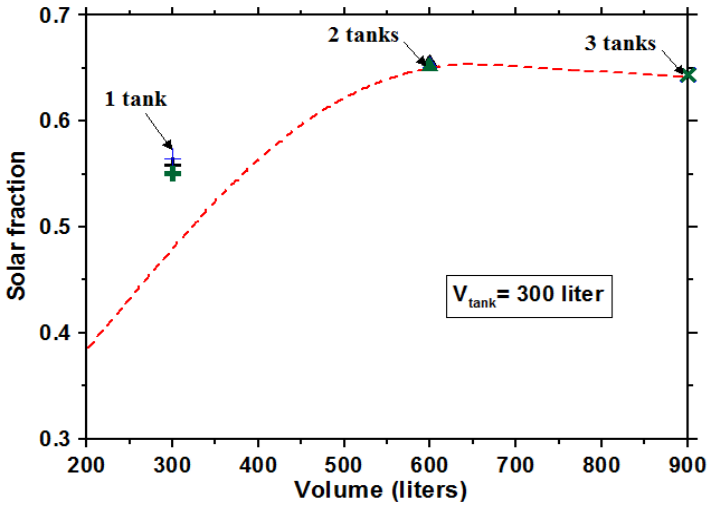

b) Effect of PCM packing ratio on solar fraction (V_{tank} = 300 liter) Dashed lines are water-only system. Symbols are: +1 tank (70% PCM); △2 tanks (70% PCM); × 3 tanks (70% PCM); + 1 tank (50% PCM); ▲ 2 tanks (50% PCM); ✕ 3 tanks (50% PCM); + 1 tank (30% PCM); ▲ 2 tanks (30% PCM); ✕3 tanks (30% PCM).

Figure B.1: Effect of PCM packing ratio on solar fraction

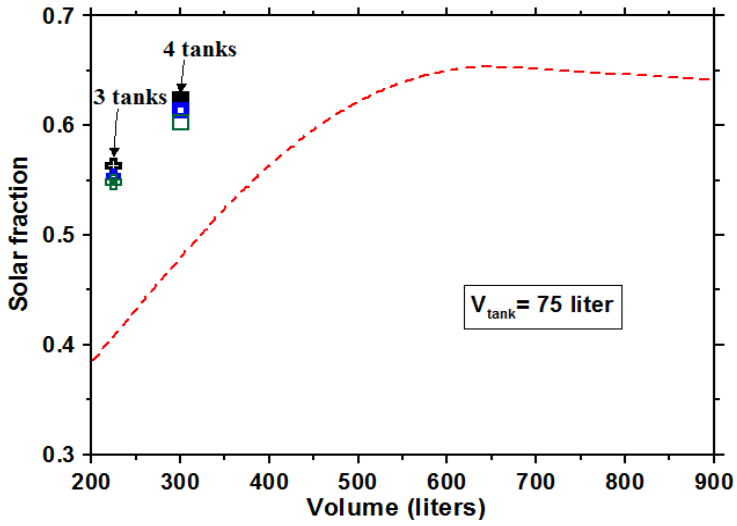

a) Effect of PCM module diameter on solar fraction (V_{tank} = 75 liter). Dashed lines are water-only system. Symbols are: ✣ 3 tanks (D= 4 cm); ◘ 4 tanks (D= 4 cm); ✣ 3 tanks (D= 2 cm); ■4 tanks (D= 2 cm); ✣3 tanks (D= 8 cm); □ 4 tanks (D= 8 cm).

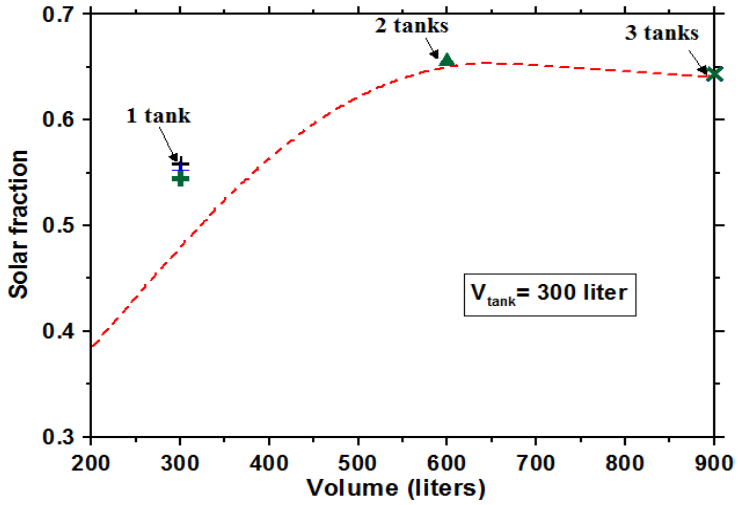

a) Effect of PCM module diameter on solar fraction (V_{tank} = 300 liter). Dashed lines are water-only system. Symbols are: +1 tank (D= 4 cm); △2 tanks (D= 4 cm); ×3 tanks (D= 4 cm); ✚ 1 tank (D= 2 cm); ▲ 2 tanks (D= 2 cm); ✕ 3 tanks (D= 2 cm); ✚ 1 tank (D= 8 cm); ▲ 2 tanks (D= 8 cm); ✕3 tanks (D= 8 cm).

Figure B.2: Effect of PCM module diameter on solar fraction

B.2. Parameters affecting both the hybrid and water-only systems

As mentioned before in Appendix A, the demand profile, the collector heat loss coefficient, area of the collector and mass flow rate through the system affect both hybrid and water-only systems. All the presented results can be explained in terms of energy balance on the system as explained in detail in chapter 4 and 5.

B.2.1. Effect of the demand profile

Different consumption profiles were found to affect solar fraction as concluded in the single tank system analysis (Appendix A). The same profiles adopted by Edwards et al. 2015 (Figure A.10) were applied on the base case considered here. Demand profiles affect the predicted solar fraction of both hybrid and water-only systems (Figure B.3). As load use is more aligned with supply (i.e. dispersed load), curves shift left compared to the other profiles.The same benefit of PCM inclusion in undersized tanks is manifested in all demand profiles when the cascaded 75 liter system (Figure B.3.a) and a 300 liter tank (Figure B.3.b) are considered. When the storage is over sized (volume of 600 liters and 900 liters), both hybrid and water-only systems exhibit the same behavior regardless of the draw profile (Figure B.3.b). As previously stated in the single tank analysis, the peak solar fraction is achieved at different volumes when the consumption profiles differ.

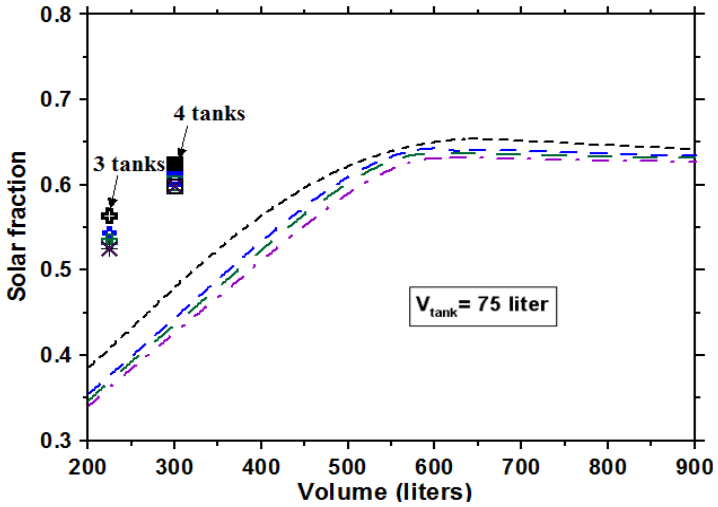

a) Effect of demand profile on solar fraction (V_{tank} = 75 liter). Dashed lines are: water-only (Dispersed); water-only (Morning); water-only (evening); water-only (late night). Symbols are: 3 tanks (Dispersed); 4 tanks (Dispersed); 3 tanks (Morning); 4 tanks (Morning); 3 tanks (evening); 4 tanks (evening); 3 tanks (late night); 4 tanks (late night).

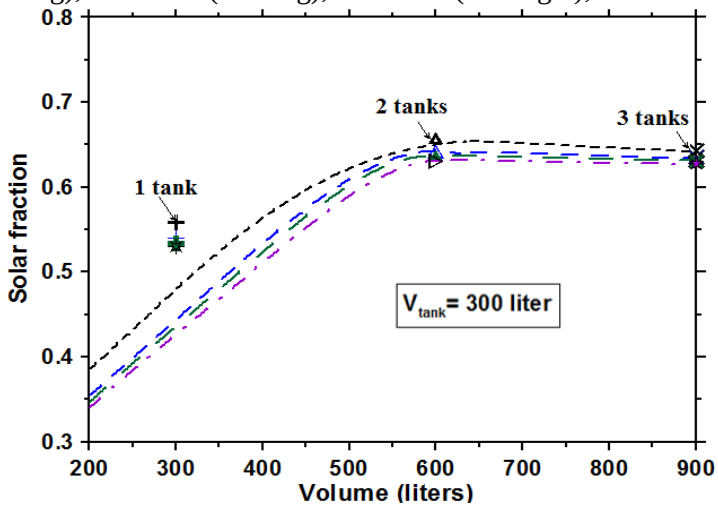

b) Effect of demand profile on solar fraction (V_{tank} = 300 liter Dashed lines are: water-only (Dispersed); water-only (Morning); water-only (evening); water-only (late night). Symbols are: 1 tank (Dispersed); 2 tanks (Dispersed); 3 tanks (Dispersed); 1 tank (Morning); 2 tanks (Morning); 3 tanks (Morning); 1 tank (evening); 2 tanks (evening); 3 tanks (evening); 1 tank (late night); 2 tanks (late night); 3 tanks (late night).

Figure B.3: Effect of demand profiles on solar fraction.

B.2.2 Effect of collector heat loss coefficient

Heat losses from the solar collector represent the dominant heat loss in the system. As such, changes to the collector heat loss coefficient significantly impact solar fraction. Figure B.4 shows the influence of changing the heat loss coefficients U_L to 3 W/m^{2}K, 5 W/m^{2}K and 7 W/m^{2}K. As expected solar fraction is increased with decreasing U_L. This is true for both the water only and the cascaded multi-tank systems.

B.2.3. Effect of collector surface area

Increasing collector area collects more energy. Simulations were performed for three different areas A_c= 13, 16 and 19 m^2. Solar fraction increases as area increases. As expected, figure B.5 shows that increasing the collector area from 16 m^2 to 19 m^2, increases the predicted solar fraction by 8% relative to the base case. Typically when the collector area increases, curves shift up.

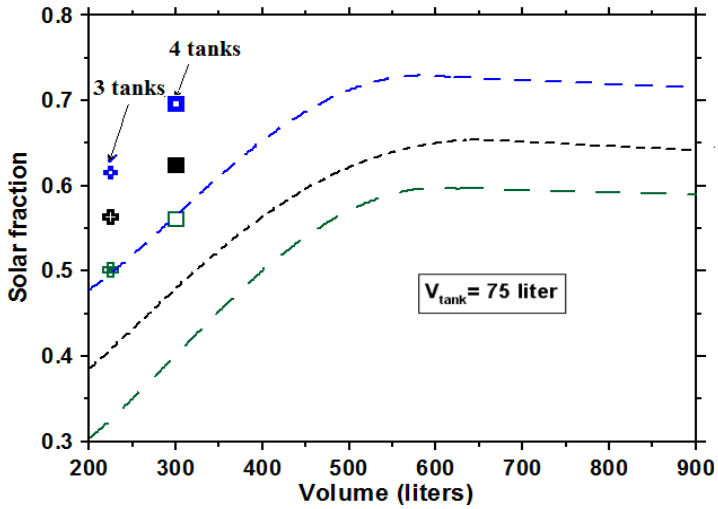

a) Effect of collector loss coefficient on solar fraction (V_{tank} = 75 liter). Dashed lines are water-only system. Symbols are: ✣ 3 tanks (U_L = 3 W/m^{2}K); ◘ 4 tanks (U_L = 3 W/m^{2}K);✣ 3 tanks (U_L = 5 W/m^{2}K); ■4 tanks (U_L = 5 W/m^{2}K); ✣3 tanks (U_L = 7 W/m^{2}K); □ 4 tanks (U_L = 7 W/m^{2}K).

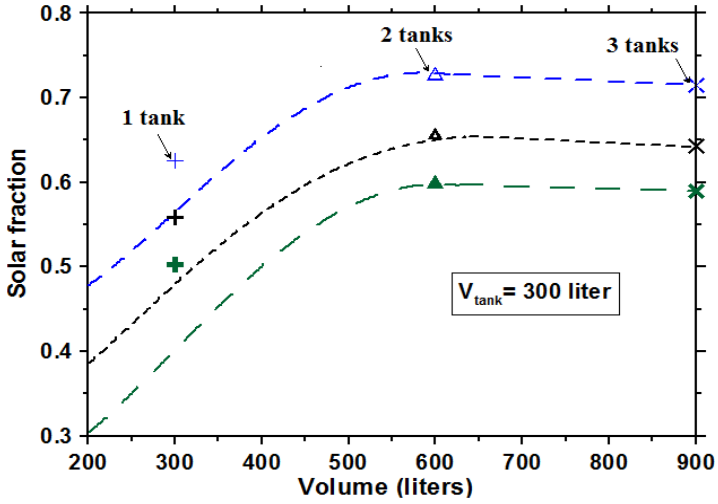

a) Effect of collector loss coefficient on solar fraction (V_{tank} = 300 liter)). Dashed lines are water-only system. Symbols are: +1 tank (U_L = 3 W/m^{2}K); △2 tanks (U_L = 3 W/m^{2}K); ×3 tanks (U_L = 3 W/m^{2}K); ✦ 1 tank (U_L = 5 W/m^{2}K); ▲ 2 tanks (U_L = 5 W/m^{2}K); ✕ 3 tanks (U_L = 5 W/m^{2}K); ✚ 1 tank (U_L = 7 W/m^{2}K); ▲ 2 tanks (U_L = 7 W/m^{2}K); ✖3 tanks (U_L = 7 W/m^{2}K).

Figure B.4: Effect of collector loss coefficient on solar fraction

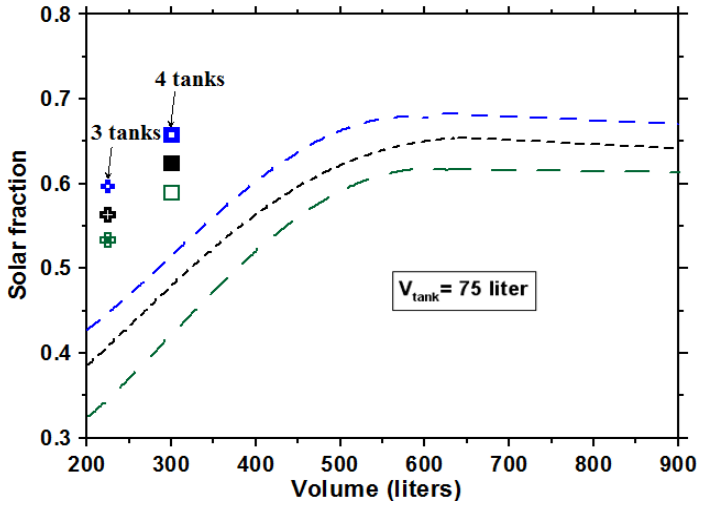

a) Effect of collector surface area on solar fraction (V_{tank} = 75 liter) Dashed lines are water-only system. Symbols are: ✣ 3 tanks (A = 19 m^2); ◘ 4 tanks (A = 19 m^2); ✣ 3 tanks (A = 16 m^2); ■4 tanks (A = 16 m^2); ✣3 tanks (A = 13 m^2); ◻ 4 tanks (A = 13 m^2).

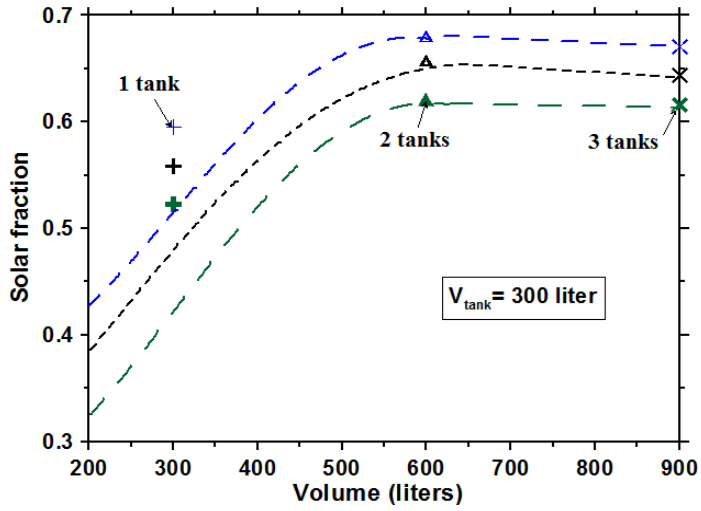

b) Effect of collector surface area on solar fraction (V_{tank} = 300 liter) Dashed lines are water-only system. Symbols are: +1 tank (A = 19 m^2); △2 tanks (A = 19 m^2); ×3 tanks (A = 19 m^2); ✚ 1 tank (A = 16 m^2); ▲ 2 tanks (A = 16 m^2); ✕ 3 tanks (A = 16 m^2); ✚ 1 tank (A = 13 m^2); ▲ 2 tanks (A = 13 m^2); ✖3 tanks (A = 13 m^2).

Figure B.5: Effect of collector surface area on solar fraction

B.2.4. Effect of collector mass flow rate

As mentioned in the literature, lower mass flow rate was found to enhance the predicted solar fraction of the system (Hollands and Lightstone, 1989). It promotes stratification which extends the period on which hot water is available to meet the load. Figure B.6 shows the predicted solar fraction for different mass flow rates. As seen from the Figure the lower flow rate shifts the curve to the left relative to the base case and vice versa (Figure B.6). This trend is similar to that explained in the single tank analysis.

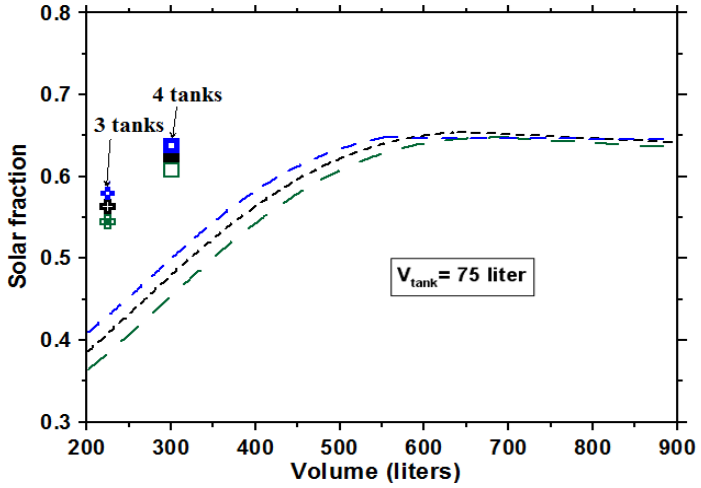

a) Effect of collector mass flowrate on solar fraction (V_{tank} = 75 liter). Dashed lines are water-only system. Symbols are: ❖ 3 tanks ($\dot{m}$ = 0.03 kg/s); ◘ 4 tanks ($\dot{m}$ = 0.03 kg/s); ✥ 3 tanks ($\dot{m}$ = 0.05 kg/s); ■4 tanks ($\dot{m}$ = 0.05 kg/s); ✠3 tanks ($\dot{m}$ = 0.07 kg/s); □ 4 tanks ($\dot{m}$ = 0.07 kg/s).

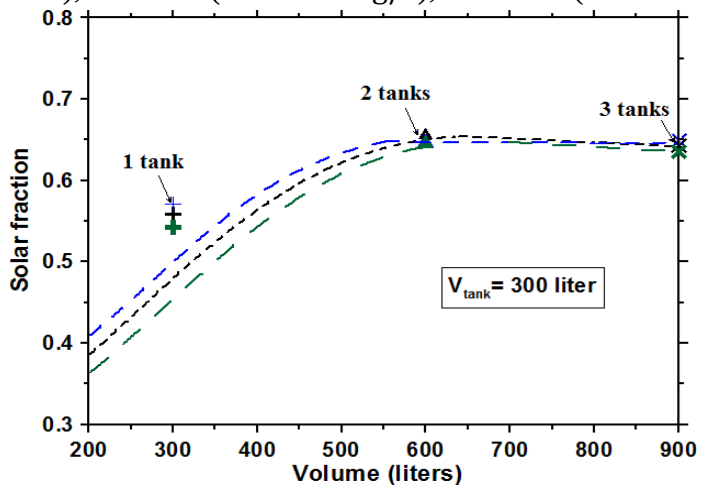

b) Effect of collector mass flowrate on solar fraction (V_{tank} = 300 liter). Dashed lines are water-only system. Symbols are: +1 tank ($\dot{m}$ = 0.03 kg/s); △2 tanks ($\dot{m}$ = 0.03 kg/s); ×3 tanks ($\dot{m}$ = 0.03 kg/s); ✦ 1 tank ($\dot{m}$ = 0.05 kg/s); ▲ 2 tanks ($\dot{m}$ = 0.05 kg/s); ✕ 3 tanks ($\dot{m}$ = 0.05 kg/s); ✚ 1 tank ($\dot{m}$ = 0.07 kg/s); ▲ 2 tanks ($\dot{m}$ = 0.07 kg/s); ✖3 tanks ($\dot{m}$ = 0.07 kg/s).

Figure B.6: Effect of mass flow rate on solar fraction

Appendix C

Pumping power

Pumping power

Hydraulic loss:

For hybrid tank, the tank dimensions are;

$V_{tank} = 0.2\ m^3,\ L = 0.76\ m$

$total\ cross\ section\ area = \frac{0.2}{0.76} = 0.263\ m^2$

PCM modules (50% by volume), then the number of tubes are calculated from the following equation.

$n = \frac{0.1}{\frac{\pi}{4} * 0.02^2 * 0.76} = 418$ tubes

$flow\ area = 0.263 - \ 418 * \frac{\pi}{4} * 0.02^2 = 0.132\ m^2$

Applying the continuity equation.

$$D_{h,c} = \frac{2}{\pi}\frac{V_{tank}}{N_c R_{c,out} L} - 2R_{c,out} = \frac{2}{\pi}\frac{0.2}{418 * 0.01 * 0.76} - 2 * 0.01 = 0.02\ \text{m}$$

$$U_{f,m} = \frac{\dot{m}}{\rho_f\left({V_{tank}}/{L} - \pi N_c R_{c,out}^2\right)} = 3.8 * 10^{-4}\ m/s$$

From Rohsenow et al 1985, assuming that the hydraulic loss in fittings and the whole piping system is equivalent to 5 m which is an extreme case.

$h_l = h_{l,\ friction} + h_{l,\ minor=} 6.8\ m$

Power=$0.05 * 10 * 6.8 = 3.4\ w$

On yearly basis if the pump operates 8 hours each day, the energy consumed in pumping is equal to **0.03 GJ** which is order of magnitude lower than the tank loss reported in chapter 4.

Appendix D

Effect of natural convection

The effect of natural convection on melting

Natural convection acts to enhance melting (Jones et al. 2006, Voller et al. 1989, Dhaidan and Khodadadi 2015). The relevance of convection is determined by the Raleigh number. The Raleigh number in the simulations presented in this thesis is of an order of 10^6. According to the correlations presented by Rohsenow et al 1985, there is a mild effect of natural convection. The high aspect ratio of PCM cylinders decreases the strength of natural convection relative to low aspect ratio ones. Typically natural convection is taken into account by the effective thermal conductivity as reported by Dhaidan and Khodadadi 2015. To the author's knowledge, the effective thermal conductivity for the considered configuration has not been reported before. As a recommendation for future work, natural convection effect needs to be explored. Natural convection is expected to slightly change the contours of the non-dimensional map presented in chapter 3. It is also expected to decrease the volume of sized hybrid storage tank this leads to increase in the reduction in storage volume concluded in chapter 4 and 5. The results presented in this thesis were reported by considering a conservative approach. When natural convection is included, more promising results are expected.